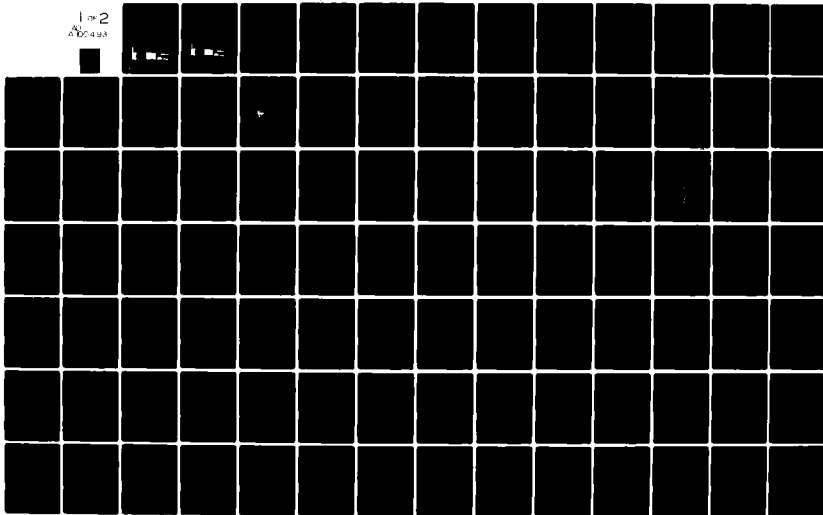AD-A100 493    LOCKHEED MISSILES AND SPACE CO INC PALO ALTO CA PALO --ETC  F/G 20/14
                THE ROLE OF ENERGETIC PARTICLE PRECIPITATION IN EXTREMELY LOW F--ETC(U)
                NOV 80   W L IMHOF, R C GUNTON, T R LARSEN      N00014-79-C-0175
UNCLASSIFIED     LMSC-D767238                                              NL

LMSC-D767238
24 NOVEMBER 1980

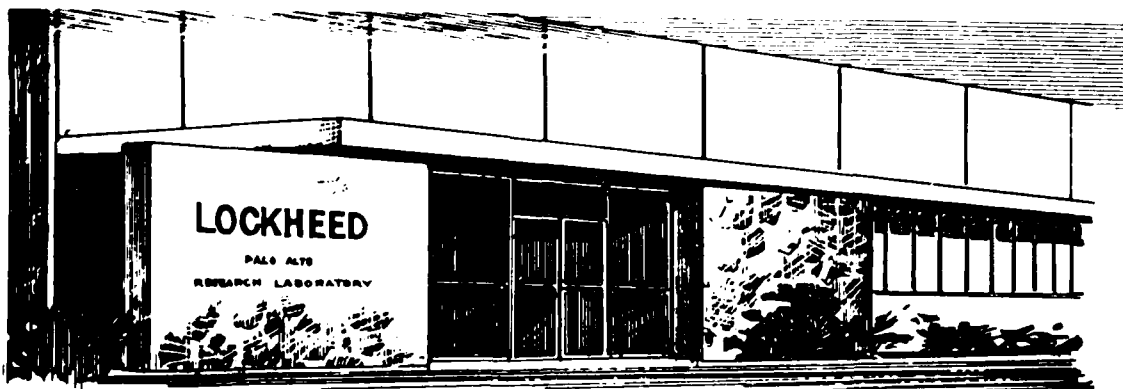# THE ROLE OF ENERGETIC PARTICLE PRECIPITATION IN EXTREMELY LOW FREQUENCY (ELF) PROPOGATION ANOMALIES

## FINAL TECHNICAL REPORT

Contract Number N00014-79-C-0175

W. L. Imhof
R. C. Gunton
T. R. Larsen
R. E. Meyerott
J. B. Reagan
E. E. Gaines

AD A100493

DTIC FILE COPY

LOCKHEED

PALO ALTO RESEARCH LABORATORY

LOCKHEED MISSILES & SPACE COMPANY. INC • A SUBSIDIARY OF LOCKHEED AIRCRAFT CORPORATION
PALO ALTO. CALIFORNIA

81 6 22 702

LMSC-D767238

24 NOV 80

# THE ROLE OF ENERGETIC PARTICLE PRECIPITATION IN EXTREMELY LOW FREQUENCY (ELF) PROPOGATION ANOMALIES.

## FINAL TECHNICAL REPORT.,

Contract Number N00014-79-C-0175

William L./Imhof
Robert C./Gunton
Trygve R./Larsen
Roland E./Meyerott
Joseph B./Reagan
E. E. Gaines

LOCKHEED

PALO ALTO RESEARCH LABORATORY

**LOCKHEED**

PALO ALTO RESEARCH LABORATORY

LOCKHEED MISSILES & SPACE COMPANY, INC • A SUBSIDIARY OF LOCKHEED AIRCRAFT CORPORATION
PALO ALTO, CALIFORNIA

| REPORT DOCUMENTATION PAGE | | READ INSTRUCTIONS BEFORE COMPLETING FORM |
|---|---|---|
| 1. REPORT NUMBER<br><br>LMSC-D767238 | 2. GOVT ACCESSION NO.<br><br>*AD-A100 493* | 3. RECIPIENT'S CATALOG NUMBER |
| 4. TITLE (and Subtitle)<br><br>STUDY OF ELF PROPAGATION ANOMALIES AS RELATED TO IMPROVED KNOWLEDGE OF ELECTRON DENSITY PROFILES PRODUCED BY ENERGETIC PARTICLE PRECIPITATION | | 5. TYPE OF REPORT & PERIOD COVERED<br>Final Technical Report for period ending 30 Sept, 1980 |
| | | 6. PERFORMING ORG. REPORT NUMBER<br>LMSC-D767238 |
| 7. AUTHOR(s)<br>William L. Imhof, Robert C. Gunton, Trygve R. Larsen, Roland E. Meyerott, Joseph B. Reagan, and Edward E. Gaines. | | 8. CONTRACT OR GRANT NUMBER(s)<br><br>N00014-79-C-0175 |
| 9. PERFORMING ORGANIZATION NAME AND ADDRESS<br>Space Sciences Laboratory<br>LOCKHEED PALO ALTO RESEARCH LABORATORY<br>3251 Hanover Street, Palo Alto, CA 94304 | | 10. PROGRAM ELEMENT. PROJECT, TASK AREA & WORK UNIT NUMBERS<br><br>NR-089-142 |
| 11. CONTROLLING OFFICE NAME AND ADDRESS<br>Department of the Navy<br>Office of Naval Research, Code 464<br>Arlington, VA 22217 | | 12. REPORT DATE<br>24 November 1980 |
| | | 13. NUMBER OF PAGES<br>147 |
| 14. MONITORING AGENCY NAME & ADDRESS(If different from Controlling Office) | | 15. SECURITY CLASS. (of this report)<br><br>UNCLASSIFIED |
| | | 15a. DECLASSIFICATION DOWNGRADING SCHEDULE |

16. DISTRIBUTION STATEMENT (of this Report)

This document has been approved for public release and sale; its distribution is unlimited.

17. DISTRIBUTION STATEMENT (of the abstract entered in Block 20, if different from Report)

Approved for public release and sale;
Distribution unlimited.

18. SUPPLEMENTARY NOTES

19. KEY WORDS (Continue on reverse side if necessary and identify by block number)

| | |
|---|---|
| ELF transmission anomalies | Free electron concentrations |
| Satellite energetic particle data | D-region electron densities |
| Precipitating electrons | Solar particle events |
| Ion-pair production rates | Polar cap absorption events |

20. ABSTRACT (Continue on reverse side if necessary and identify by block number)

The purpose of this report is to present further work on the influence of precipitating energetic particles on ELF propagation. The effort has principally involved the effects of solar particle events through changes in the conductivities at various altitudes.

The influence of precipitating energetic particles on ELF propagation has been investigated on the basis of satellite measurements of the particle inputs. The effects of solar particles have been calculated for three events
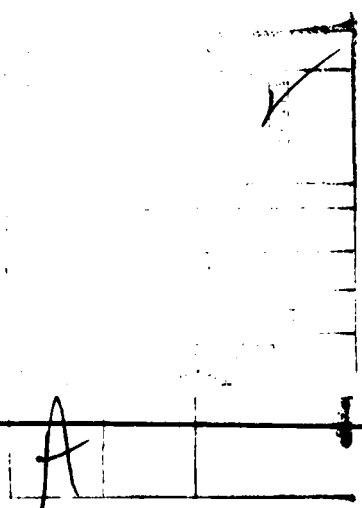
(12 Nov. 1960, 2 Nov. 1969 and 4 Aug. 1972) and it has been concluded that the ions formed by the high energy tail of the precipitating protons below 45-50 km are significant whereas above this altitude the ion contribution to the ionospheric conductivity decreases rapidly in comparison to the electron component. In the height range 20-45 km ions dominate as the cause for ELF wave attenuation through ohmic dissipation during disturbed conditions. Such ohmic losses may account for 50-60% of the total wave absorption, and they maximize around 30-40 km for the profiles analyzed. Relatively little ELF attenuation seems to occur below about 20 km. However, during very intense PCA daytime conditions the electron densities around 30 to 40 km may be 4-5 orders of magnitude above the ambient values. Field strength calculations were performed to establish the sensitivity to the detailed shape of such electron profiles and it was found that 1 dB changes can result from shifts of 5 km in the height of the profile.

A new standard ambient daytime altitude profile of electrons and ions is suggested for baseline calculations of ELF propagation. Taking into account recent measurements, electron densities are considerably higher than in the previous standard below 65 km, and are somewhat lower in the altitude range 70-100 km.

A study was made of new electron density data at 60 and 70 km measured by the SRI Chatanika radar during the solar particle event of 4 August 1972. A tentative conclusion was drawn that during sunset and sunrise the electron density time dependence is correlated with 0 atom density, suggesting that chemical detachment may be more important than photodetachment.

The mass distribution of ions in the troposphere was derived from mobility distributions measured by Hoppel at about 5 km altitude. It was found that over 50% of the ions have masses >440 amu and 20% have masses >800 amu. Implications of these results for stratospheric ion mass distributions are discussed.

The effects of solar particle events on the earth's electrical system have been modeled. For the 4 August 1972 SPE it has been found that the disturbed conductivity is slightly smaller than the undisturbed below ~12 km and is much larger than the disturbed for altitudes above 20 km due to the decrease in galactic cosmic ray flux at the time of the event. For the larger events the electrical current carried by the solar protons and electrons in the polar caps greatly exceeds the normal air-earth current that flows between the ionosphere and the ground at high altitudes. Since the proton current is larger than the air-earth current for altitudes above ~30 km the disturbed electric field becomes negative from ~30 km to ~55 km, the electron precipitation current exceeds the proton current and hence the electric field becomes positive above that altitude.

## TABLE OF CONTENTS

TABLE OF CONTENTS

## 1.0 INTRODUCTION

The transmissions of extremely low frequency (ELF) waves at nighttime are often subject to amplitude attenuations of several dB (Davis, 1974, 1976; Davis and Meyers, 1975; Larsen, 1974). A successful correlation between anomalous signal strengths and precipitating particles was established for the first time in 1976 (Imhof et al, 1976; Reagan et al, 1978 ). This preliminary finding, based primarily on the measured transmissions between the Wisconsin Test Facility (WTF) and the mid-latitude receiving site in Connecticut and direct satellite measurements of precipitating particles, has formed a basis for further more quantitative studies of the cause-and-effect relationship.

Subsequent studies of the effects of energetic particle precipitation on ELF transmission signal strength have been made at the Lockheed Palo Alto Research Laboratory (LPARL) based partly on data acquired with scientific payloads on the low altitude polar orbiting satellites 1971-089A and 1972-076B developed by the Space Sciences Laboratory of LPARL for the Office of Naval Research, the Defense Nuclear Agency, and the Defense Advanced Research Projects Agency. In these investigations, supported by the Office of Naval Research, ELF propagation data were obtained from Dr. John Davis of the Naval Research Laboratory, Washington, D.C., and P. R. Bannister of Naval Underwater Systems Center, New London, Connecticut. This large data set includes measurements taken during coordinated exercises involving ELF transmission between the U.S. Navy Wisconsin Test Facility and receiving stations in Connecticut, Maryland, Greenland, Norway, and Italy performed in March - April

1975 and March – April 1976. These studies have provided further verification of the importance of particle precipitation and have also demonstrated the influence of sporadic E-layers on ELF signal strength. Since the details of the horizontal and vertical distributions of the enhanced ionization are clearly very important, a large body of coordinated data is required to provide quantitative interpretations of the results and to assess the impact of important chemistry parameters on the transmitted ELF signal strength. Clearly, good chemistry models are also needed for a proper evaluation of the coordinated data. In this regard the satellite/Chatanika backscatter radar data acquired during the August 1972 solar particle event have been particularly useful.

In 1976 a qualitative correlation was established between anomalous ELF signal levels received at Connecticut and the precipitation of significant fluxes of electrons from the radiation belts as measured with the LPARL payloads on the low altitude polar-orbiting satellites 1971-089A and 1972-076B. However, a detailed quantitative correlation between the sign (signal enhancement versus degradation) and severity of the anomalies and particle characteristics such as intensities and spectra was not firmly established because of the limited data base used. Stimulated by these findings, special coordinated exercises were conducted in March – April 1976 involving satellite measurements of the precipitating particles and ELF transmissions between the U. S. Navy Wisconsin Test Facility and receiving stations in Maryland, Greenland, Norway, and Italy. Coordinated satellite/ELF transmission measurements were also made in March – April 1975 and July 1975.

From coordinated satellite and ELF attenuation measurements, it has been found that direct particle precipitation into the atmosphere can cause ELF

1-2

transmission anomalies. In these anomalies the signal strengths may be either

attenuated or enhanced depending upon the geometry and details of the ion and

electron density profiles resulting from the particle precipitation. Detailed

discussions of the investigations performed from the coordinated data sets

acquired in 1975 and 1976 are provided in the previous annual reports (Imhof,

et al., 1976, 1977, 1978) and by Reagan, et al. (1978).

The purpose of the present report is to present further work on the

influence of precipitating energetic particles on ELF propagation. The effort

principally involves the effects of solar particle events in enhancing the

conductivities of the earth's ionosphere wave guide. Calculations have been

made of the sensitivity of the ELF signal strength to changes in the conduc-

tivities over the transmitter that may occur during SPE conditions. In order

to be able to calculate more accurately the changes in ELF signal strength

associated with solar particle events and other disturbed conditions at twilight,

new electron density data measured in the 4 August 1972 event have been used to

provide increased knowledge of twilight behavior which will lead to improvements

in ion chemistry modelling. The effects of the charge deposition in the polar

caps on the earth's electric fields and current systems have been modeled.

More realistic ambient electron and ion density daytime profiles have been

proposed to provide accurate baseline signal strength calculations.

The changes in conductivity at times of SPE events discussed above have

all been based on calculations of the effects of the measured energetic

particle inputs. It has been recognized that these calculated effects should

be confirmed experimentally in a VLF-ELF field program. Accordingly, LPARL has

participated in appropriate planning discussions and further investigation

1 - 3

has been made of an acceptable criterion for deciding if a SPE event is suitable

for an ELF propagation field experiment based on satellite measurements of pre-

cipitating protons.

1- 4

## 2.0 PROPAGATION OF ELF WAVES - THEORETICAL APPROACHES TO THE CALCULATION OF FIELD STRENGTHS

The propagation of ELF waves is subject to anomalies, some of which are believed to be of ionospheric origin, but the causes and effects are not well understood at present. These anomalies result both from signal absorption and from changes in excitation of the waves into the propagation medium, a waveguide formed by the earth and the lower ionosphere. The conditions of the ionosphere are subject to major day/night differences and indeed the ELF signal strengths do display diurnal variations. Calculations of ELF transmissions have shown that the signal strengths may depend in a complex manner on the ionization profiles in the waveguide. The conductivity of the earth depends on whether the propagation is over rock, sea water, ice cap, etc. The conductivity of the atmosphere depends on the deposition of ionizing particles in the atmosphere and the absorption of ultra violet radiation from the sun. Below 40 km altitude, the conductivity of the atmosphere is produced by the deposition of energy from galactic cosmic rays during quiet times, and by the deposition of energy from solar cosmic ray protons during solar particle events. Unfortunately, there has been little experimental verification of the methods used to determine the conductivities. At altitudes above $\sim$ 50 km the electron conductivities are affected by electron precipitation but they can be predicted from the ion production rates with reasonable accuracy. In strong events the Bremsstrahlung x-rays produced by precipitating electrons may cause significant ionization at lower altitudes.

In this chapter we will briefly describe some of the approaches that have been used to calculate ELF field strengths.

## 2.1 The NOSC Model Computer Program

A waveguide model computer program extensively used over the last years and which is also being used by the present authors, was developed at Naval Ocean Systems Center (NOSC) and is well documented in the literature (see e.g. Sheddy, 1968; Pappert, 1970; Pappert and Moler, 1974).

The program is based upon the formalism developed by Budden (1961) and Budden and Daniell (1965) for electromagnetic wave propagation in the terrestrial waveguide. Special emphasis has been given to its applicability in the extremely low frequency (ELF) range.

The program allows for a terrestrial waveguide with the following characteristics:

- Arbitrary electron and ion density distributions with height

- Variable electron and ion collision frequency height profiles

- The lower boundary of the waveguide is assumed to be a smooth homogeneous earth with arbitrary conductivity and permittivity

- Allowance is made for the anisotropy of the ionosphere; arbitrary values for the strength and direction of the earth's magnetic field may be applied

- Horizontal inhomogeneties along the propagation path may be taken into account by segmenting the path into regions having different values for the waveguide characteristics listed above.

2-2

The computer program is thus capable of treating waveguides that are reasonable model representations of the actual complex terrestrial waveguide. The program does not allow for variation of the guide parameters perpendicular to the propagation path, therefore uniform conditions had to be assumed over distances extending a Fresnel Zone to either side of the path. This restriction has long been recognized as a major limitation of the model.

## 2.2 Recent Developments

In actual propagation cases both lateral and transverse variations can be expected to occur over most paths, especially at high latitudes. Recently, off-path effects have been considered and important steps have been taken in approaching formulations that address the real three-dimensional problems, at least in an approximate way (Pappert, 1980; Field and Joiner, 1979; Greifinger and Greifinger, 1978, 1979; Booker, 1980) as briefly described below.

Pappert (1980) treating localized disturbances in a surface propagation model coupled with a moments method, finds that a thick ionization patch at E-region heights can produce 6-8dB fades in signal strength for a 1.6Mm propagation path. Deepest fades occur when the disturbed area is well within the first Fresnel Zone, and a varying amount of fade is predicted depending on size and location of the disturbance area. When the center of the disturbance is located outside the second Fresnel Zone, he predicts that most of the amplitude fades are damped out.

Field and Joiner (1979) use an integral-equation approach for analyzing propagation in the earth-ionosphere waveguide where conditions change over distances comparable with a Fresnel Zone. They derive an expression for the

2-3

relative errors introduced by neglecting transverse ionospheric gradients over the path and find that full wave methods must be applied when the effective width of a localized disturbance is less than two-thirds of the width of the first Fresnel Zone. These authors also conclude that the WKB approximation significantly over-estimates the propagation anomaly when the disturbance is centered near the propagation path and underestimates the anomaly when the disturbance is centered far off path (c.f. also Field, 1978 ).

Further physical insights into ELF propagation and ionospheric parameters have been achieved by Greifinger and Greifinger (1978, 1979) in associating the eigenvalue solution mainly with ionospheric properties at two well defined altitudes where maximum ohmic heating occurs. Along with two scale heights at these altitudes, they derive an approximate solution for the ELF mode at high latitudes. They show that the lower altitude region of interest occurs where the conduction current parallel to the magnetic field becomes equal to the displacement current. At these heights the associated scale height is that of the parallel conductivity. At the other height regions the scale height in question is that of the refractive index. For daytime conditions the authors find that this upper height level is situated where the local wave number becomes equal to the reciprocal of the local scale height of the refractive index. With knowledge of these four parameters an approximate

wave solution may be found.  The authors conclude that the principal attenuation mechanisms are Joule heating by longitudinal currents in the vicinity of the lower altitudes and energy leakage of the whistler component of the ELF wave at the upper altitudes.

Booker (1980) presents an extensive survey of ELF propagation and outlines a theory for propagation in the earth-ionosphere transmission line based on the work of Greifinger and Greifinger (1979) and the earlier theory by Booker and Lefeuvre (1977).  His method greatly advances the physical understanding of the complex reflection and absorption processes.  Booker (1980) draws attention to several results important for understanding ELF propagation, among others:

- At ELF the transition from nearly horizontal phase propagation to nearly vertical propagation takes place in a refracting stratum at the bottom of the ionosphere.

- Between the bottom of the ionosphere and the level of ELF reflection, change of phase can as a first approximation be calculated on the basis of vertical propagation in free space.

- The reflecting stratum is located approximately at the level where the ionosphere fails to respond as a doubly refracting medium to the ELF waves.

- Thus, above the reflecting level the ionosphere is a slowly-varying, non-isotropic medium, whereas below it, the ionosphere behaves essentially as an isotropic medium.

In his theory Booker includes the magnetic field and derives a propagation model with worldwide application.

3.0  <u>ELF TRANSMITTER AND PROPAGATION PATH CHARACTERISTICS</u>

A thorough and comprehensive treatment of man-made ELF experiments
is given in a special issue of IEEE Transaction of Communications (April 1974).
Limited experimental activity has continued since 1974 using the US Navy's
experimental transmitter facility in Wisconsin.

3.1  <u>The US Navy ELF Transmitter (Wisconsin Test Facility - WTF)</u>

The Navy ELF Wisconsin Test Facility (WTF) is located in the Cheqeamegon
National Forest in north-central Wisconsin, USA, and consists of two 22.5 km
north-south antennas (one buried and one elevated) and one 22.5 km elevated
east-west antenna.  Each antenna is grounded at both ends.  The transmission
station is located at the mid-point intersection of the two antennas.  The
antenna array pattern can be steered to any particular receiving direction.

The transmitter has been operated in the 45 and 75 Hz bands with
antenna currents of 300 A.  The antenna radiation pattern and soil con-
ductivity ($\sigma_e$) under the antenna, have been measured by Bannister & Williams
(1974), for the EW antenna:

$$\sigma_e = 3.2 \ 10^{-4} \text{ mho/m at 75 Hz}$$

$$\sigma_e = 2.8 \ 10^{-4} \text{ mho/m at 45 Hz}$$

All ELF field strength values presented in this report have been
normalized to the above antenna characteristics, and the revised antenna
radiation pattern (Bannister, et al. 1974) is applied.

3.2  <u>The Ionospheric Conditions Near the Transmitter</u>

In Figure 3.1 is indicated the location of the transmitter as well
as positions of selected magnetic L-shells.  The Booker excitation circle
(Booker, 1973) is plotted for a frequency of 75 Hz (radius equals $\lambda_o/2\Pi$,

3-1
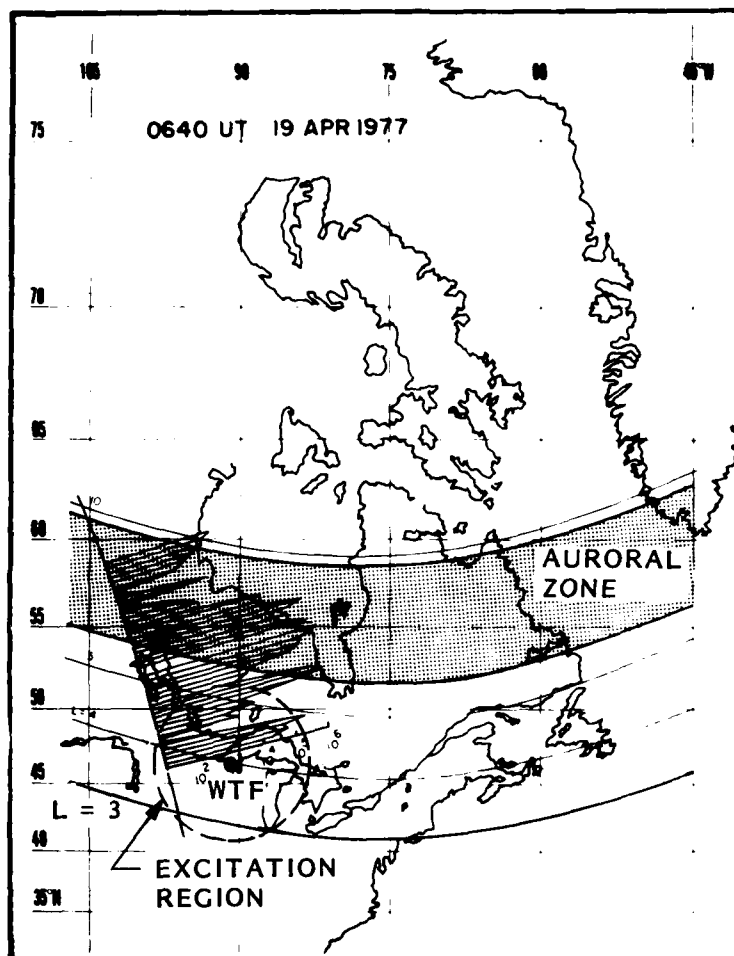
Figure 3.1 Location of the Wisconsin Test Facility (WTF) and positions of
the auroral zone and selected magnetic L-shells. The Booker
excitation region is also shown along with the intensity of
precipitating electrons measured on a satellite pass. See
text for further explanation.

3-2

where $\lambda_o$ is the free space ELF wavelength). Superposed on the figure is the counting rate of precipitating energetic electrons (> 150 keV) as measured on a pass by the 1972-076B satellite. Such latitude variations of the incoming fluxes are quite typical, and will cause marked local perturbations in the ionosphere below 100 km. Thus, in this case homogeneous ionospheric conditions do not exist over the whole excitation region of the transmitter. Experience from several years of satellite measurements indicate that precipitating electrons in the L range of 3-5 are probably present most of the time exhibiting dynamic time - and spatial variations.

Such findings complicate the ELF field prediction schemes, but this problem has not yet been attacked fully from a theoretical point of view. In model calculations homogeneous conditions over the transmitter area are assumed.

## 3.3 ELF Path Characteristics

The NOSC ELF computer code allows calculations to be made with the propagation path divided into a number of segments, within which the propagation medium and boundary conditions are kept constant. Table 3.1 lists for the path WTF to Tromso the segmentation and data for the various segments as used by the authors. Other paths have been segmented in a similar manner (Imhof et al., 1977).

Effects of changes in the ionospheric conditions due to different solar zenith angles along a propagation path (local time dependence) have also been considered and will be further discussed in section 7.

3-3

| Segment No. | Segment | Distance Range from WTF (km) | Conductivity (mho/m) | Rel. Perm. $E/E_o$ | Mag. Field (Wb/m²) | Co-dip (deg.) | Prop Direct. (azimuth in degrees) |
|---|---|---|---|---|---|---|---|
| 1 | Transmitter Area | 0-200 | $3.2 \times 10^{-4}$ | 15 | $5.94 \times 10^{-5}$ | $15.5°$ | $20°$ |
| 2 | Canada | 200-1000 | $1.0 \times 10^{-3}$ | 15 | $6.05 \times 10^{-5}$ | $11.6°$ | $27°$ |
| 3 | Hudson Bay | 1000-1800 | 4.0 | 81 | $6.00 \times 10^{-5}$ | 7.7 | $52°$ |
| 4 | North Canada | 1800-2900 | $1.0 \times 10^{-3}$ | 15 | $5.83 \times 10^{-5}$ | $6.4°$ | $89°$ |
| 5 | Davis Straight | 2900-3300 | 4.0 | 81 | $5.72 \times 10^{-5}$ | $6.6°$ | $102°$ |
| 6 | Greenland Ice Cap | 3300-4400 | $1.0 \times 10^{-5}$ | 5 | $5.50 \times 10^{-5}$ | $8.0°$ | $115°$ |
| 7 | Norwegian Sea | 4400-5800 | 4.0 | 81 | $5.26 \times 10^{-5}$ | $10.6°$ | $122°$ |
| 8 | Receiver Area (Tromso,Norway) | 5800-6000 | $1.0 \times 10^{-3}$ | 15 | $5.23 \times 10^{-5}$ | $12.2°$ | $128°$ |

Table 3.1 Data for segmented propagation path WTF to Tromso

3-4

## 3.4 Ambient Profiles and Collision Frequencies

For the ambient day- and nighttime ionsopheric conditions the following

electron and ion density profiles have been used by the present authors.

|  |  |
|---|---|
| 0 - 100 km | GE Tempo, RPT66TMP-82 <br> 1 March 1966 by W . Knapp |
| 100 - 200 km | Satellite Environment Handbook, Stanford University <br> Press, 1965, edited by F. S. Johnson |

These ambient profiles are reproduced in Figure 3.2 (from Pappert and

Moler, 1974).

The electron-neutral and ion-neutral collision frequencies used both for

ambient and disturbed conditions are likewise those listed by Pappert and Moler

(1974), cf Table 3.2.

Table 3.2 Collision Frequencies

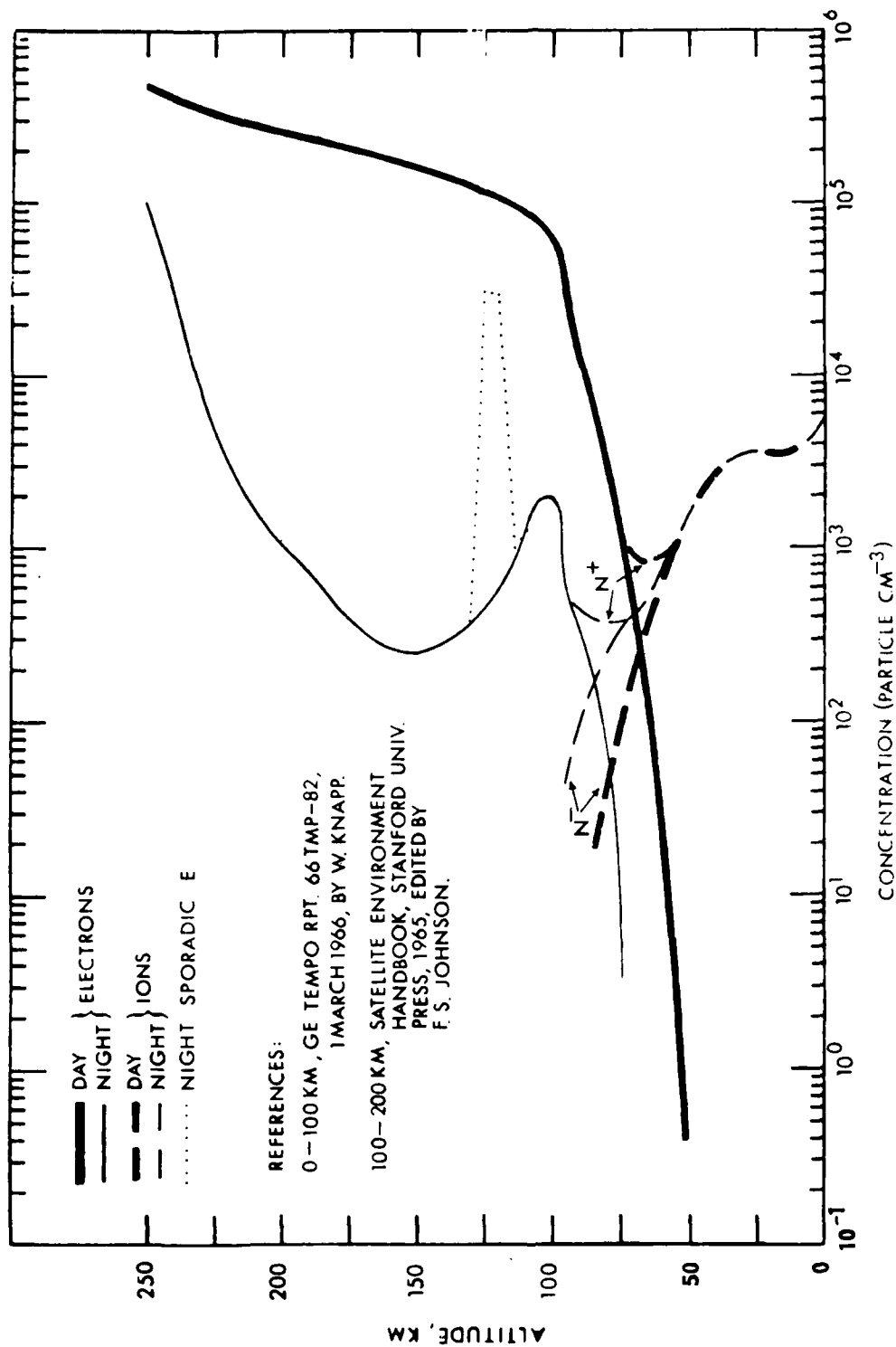| Altitude (km) | Nighttime Ionospheric Collision Frequency | | |
|---|---|---|---|
| | Electrons (sec$^{-1}$) | Positive Ions (sec$^{-1}$) | Negative Ions (sec$^{-1}$) |
| 250 | $1.05 \times 10^{2}$ | $4.50 \times 10^{-1}$ | $4.50 \times 10^{-1}$ |
| 225 | $3.50 \times 10^{1}$ | $9.00 \times 10^{-1}$ | $9.00 \times 10^{-1}$ |
| 220 | $3.00 \times 10^{1}$ | $1.00 \times 10^{0}$ | $1.00 \times 10^{0}$ |
| 210 | $3.30 \times 10^{1}$ | $1.30 \times 10^{0}$ | $1.30 \times 10^{0}$ |
| 200 | $4.50 \times 10^{1}$ | $2.00 \times 10^{0}$ | $2.00 \times 10^{0}$ |
| 150 | $1.60 \times 10^{3}$ | $4.50 \times 10^{1}$ | $4.50 \times 10^{1}$ |
| 120 | $1.00 \times 10^{4}$ | $3.00 \times 10^{2}$ | $3.00 \times 10^{2}$ |
| 100 | $3.90 \times 10^{4}$ | $8.00 \times 10^{3}$ | $8.00 \times 10^{3}$ |
| 0 | $4.30 \times 10^{11}$ | $1.07 \times 10^{10}$ | $1.07 \times 10^{10}$ |

Figure 3.2 Day and Night Ambient Profiles and Nighttime Sporadic E

While these electron and ion density profiles have been used in previous work on this project and throughout the present work, there are newer daytime data which permit a more suitable daytime profile to be suggested for future work. This is discussed in Section 10.

## 4.0 ELF PROPAGATION MEASUREMENTS AND PREDICTIONS

A number of reports present results from recordings of WTF signals propagated over different paths in the USA and to Europe (Bannister and Williams, 1974; Bannister 1974; Davis, 1976).

Data for paths such as:

- WTF to Connecticut, USA          (1.6 Mm path length)

- WTF to Greenland                 (3.6 Mm    "      "   )

- WTF to Tromso, Norway            (6.0 Mm    "      "   )

- WTF to Pisa, Italy               (7.5 Mm    "      "   )

have been collected indicating the diversity of different propagation media analyzed.

The measurements have yielded several general features of ELF propagation, viz:

- Seasonal changes in ionospheric characteristics influence ELF propagation, e.g. through variation in the attenuation rates and relative excitation factors.

- Daytime attenuation rates at 75 Hz are higher than nighttime values, due to higher electron densities below 80 km altitude resulting from electron detachment; typical ambient values are 1.1 - 1.3 dB/Mm during the day and 0.8 - 1.0 dB/Mm at night.

- Nighttime propagation is more variable than daytime propagation

- Polar cap and auroral zone effects are found in ELF propagation

Such findings, reported e.g. by Bannister (1974) are also reflected in

theoretical field strength predictions using propagation models with ambient

and disturbed ionospheres (Pappert and Moler, 1974; Pappert, 1980;

Field and Joiner, 1979; Imhof et al., 1976, 1977, 1978, 1980).


## 4.1 Short Path Propagation

Initially results of some short path measurements (< 2000 km path

length) are summarized. Field strengths have showed that anomalous signal

reductions of 3 dB and more may occur with a frequency of 30% of all nights.

It has been calculated that these signal strength reductions are caused by

precipitation of electrons from the radiation belts resulting in enhanced

ionization in the lower atmosphere. Attempts to correlate the anomalous

signal strength behavior with geomagnetic indicies indicating the degree

of disturbed magnetospheric conditions have met with limited success.

As an example, in Figure 4.1 values measured by Bannister and Williams

(1974) are reproduced over the years 1970-73 for the WTF to Connecticut path.

Seasonal variations are seen, but the average value of all observations

agree to within 0.1 dB of the predicted ambient night value as calculated

by LMSC. Furthermore, in Figure 4.2 is depicted an anomalous signal reduction

event occuring on 19 April 1973. The signal reduction lasting several

hours amounted to ≃ 5 dB as compared with night values before and after

the event. Such large signal attenuations have yet to be recorded at a

time when a discrete electron precipitation event in the same location was

measured from a satellite.

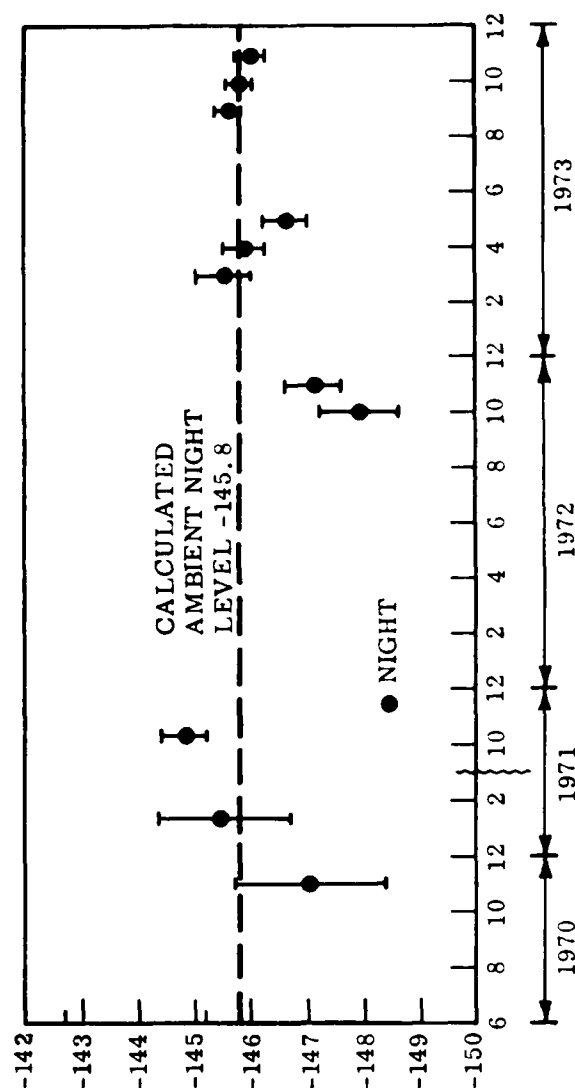Figure 4.1  75-Hz monthly nighttime field strength averages for 1970-73 for the path WTF to Connecticut (Bannister and Williams, 1974). The error bars mark the 80% confidence intervals. Also shown is the LMSC calculated ambient field strength level (see the text).
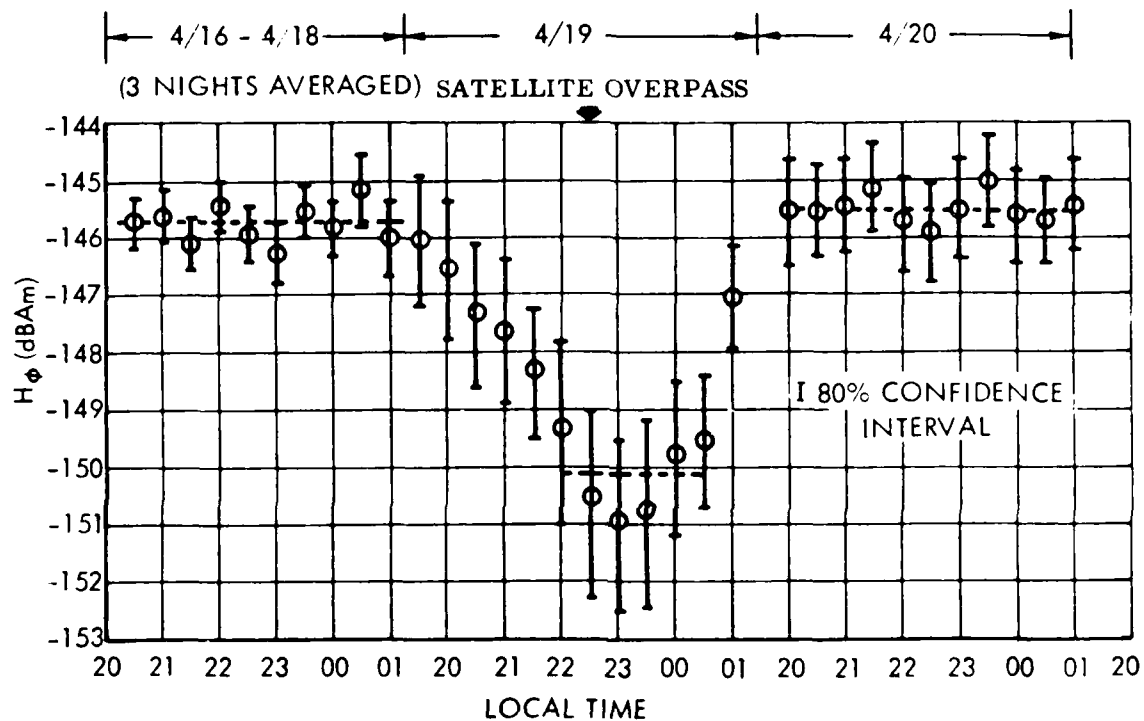
4-3

Figure 4.2  16-20 April 1973 Connecticut 76-Hz Nighttime Field Strengths
versus Local Time (Effective Integration Time = 30 min/sample
Bannister, 1973).

## 4.2 Long Distance Propagation

Long distance ELF propagation (>1600 km) also exhibits anomalous signal fades. Figures 4.3 and 4.4 show measurements over long and short paths by Davis (private communication, 1977) and Bannister (private communication, 1978), respectively, together with plots of the magnetic disturbance index Dst and energetic precipitating electron fluxes. However, no simple, systematic relationships appear to exist between signal fades and disturbed conditions.

## 4.3 Possible Influence of Sporadic E-Layers on ELF Propagation

Attempts, however, to explain the signal attenuation due to excessive losses in sporadic E-layers have resulted in predicted signal fades of the right magnitude (Pappert, 1978, 1980; Barr, 1977; Imhof et al., 1976, 1977, 1978, 1980) both for short and long paths.

Measured $E_S$ layers are very thin (3-4 km or thinner), but they may extend over large geographical areas, up to 1 $Mm^2$ and more (Whitehead, 1970). These layers do not reside at a constant height, but seem to move towards lower heights with time. One example of the observed shape of a sporadic E layer measured at Wallops Island is shown in Figure 4.5, (Smith and Miller, 1980). As noted in Appendix A, $E_S$ layers are observed in the altitude range 100 - 130 km. The $E_S$ layer has been placed at 118 km in contrast to the observed altitude of 105 km because it was found (Imhof, et. al., 1977) that such a layer produced a very small effect at 105 km and a large effect at 75 Hz at 118 km. See Appendix A for further general characteristics of $E_S$ layers.

Propagation characteristics at 75 Hz for such a profile indicate significant departures from ambient conditions, viz:

Ambient night : $\alpha$ = 1.07 dB/Mm; v/c = 0.85

$E_S$             : $\alpha$ = 1.83 dB/Mm; v/c = 0.75
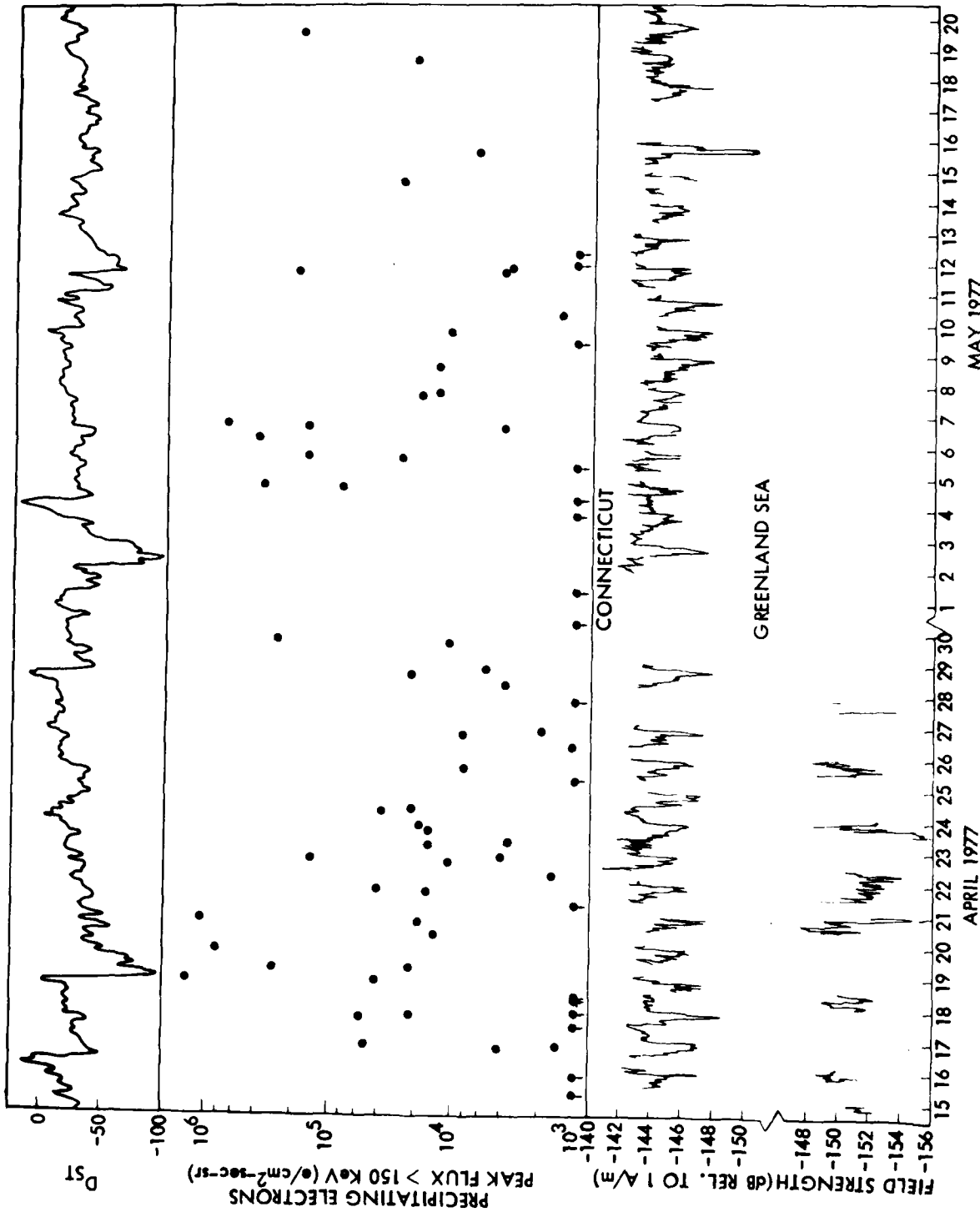
Figure 4.3  The ELF field strengths as measured in the Greenland Sea exercise and at the Connecticut receiving station. Also plotted are the fluxes of precipitating electrons >150 keV measured on the S72-1 satellite. The $D_{st}$ geomagnetic index is plotted in the upper section.

4-6
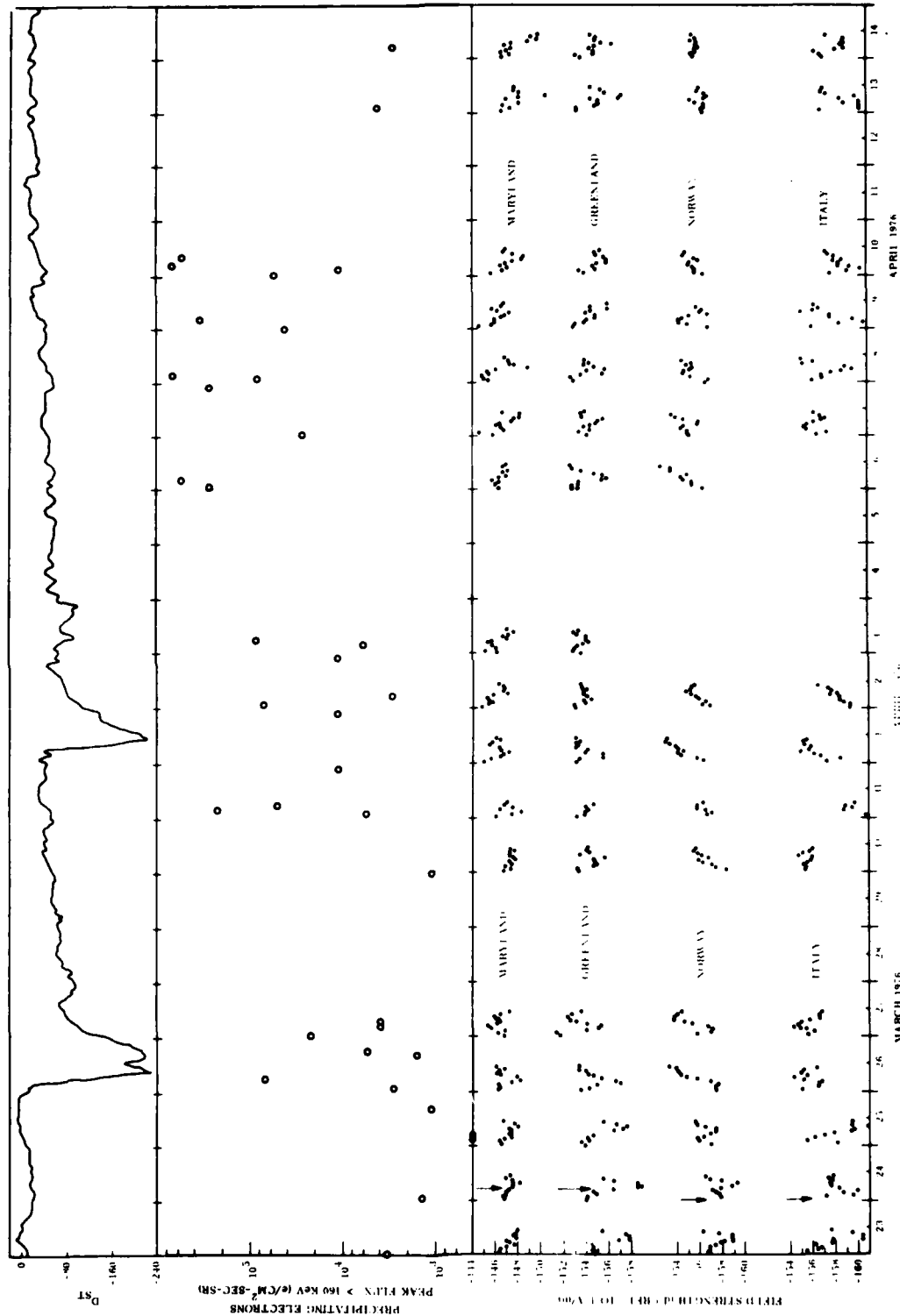
Figure 4.4 Plot of the precipitating electron flux >160 keV as measured from the satellite on coordinated passes and the ELF signal strengths as received at the various stations. For comparison the $D_{st}$ geomagnetic index is also plotted to indicate the general occurrence of magnetic storms.

**LOCKHEED PALO ALTO RESEARCH LABORATORY**

LOCKHEED    MISSILES    &    SPACE    COMPANY,    INC.
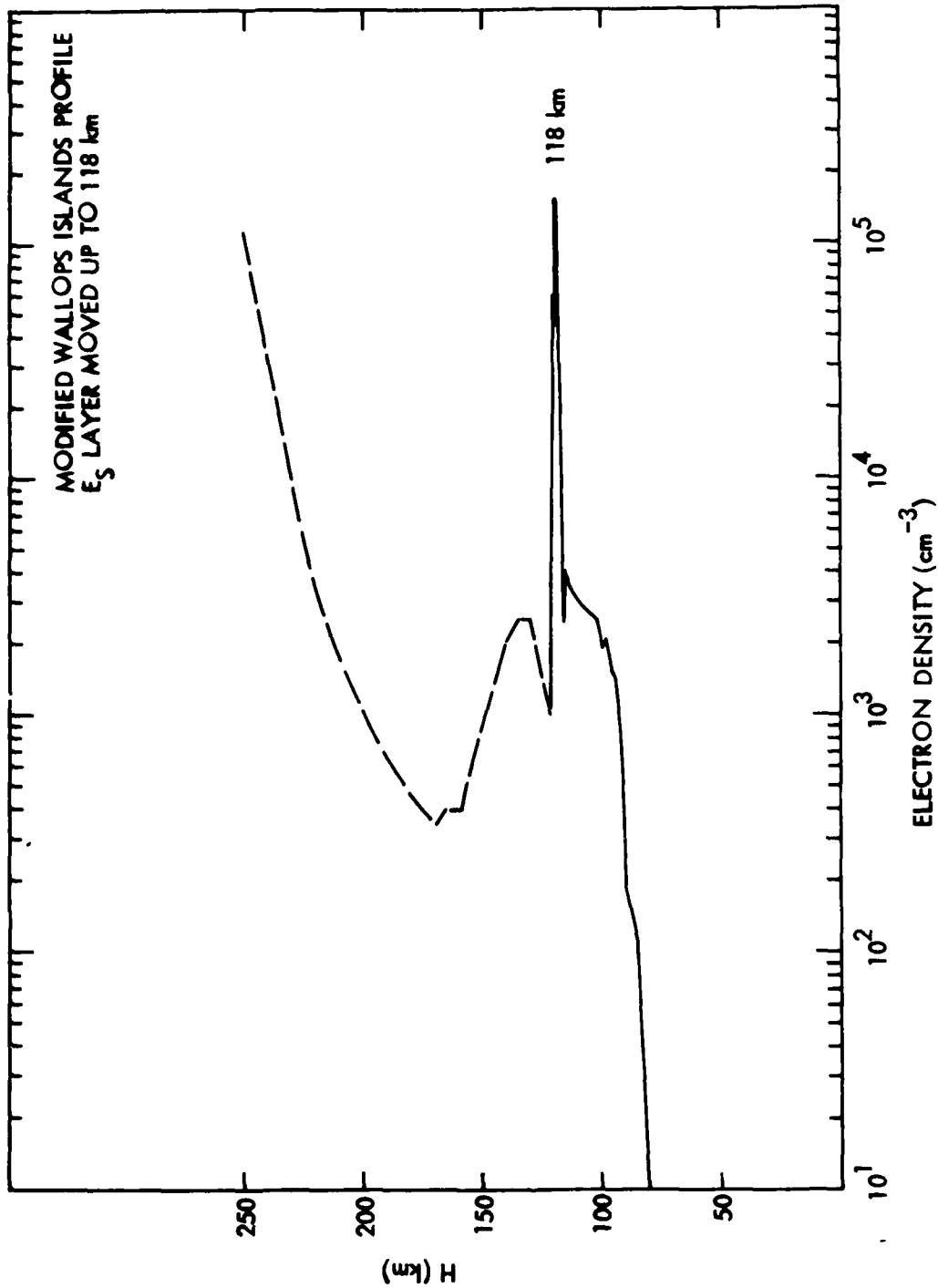
Figure 4.5  The standard nighttime ambient electron density profile with a superimposed experimental sporadic E layer profile taken from Smith and Miller (1980), but placed at 118 km.

For a thicker ionization ledge positioned at 123 km altitude Pappert (1980) obtained even much higher attenuation rates for a short path:

$\alpha$ = 9.83 dB/Mm; v/c = 0.68. In this case a resonant absorption seems to be present (cf also Imhof et al., 1976, 1977; Pappert, 1978). However, this resonance is strongly dependent upon thickness of the ionization ledge and its position in altitude (Imhof et al., 1977). Large values for the attenuation rates can also result from reflections at more than one level in the atmosphere (Barr, 1977).

Amplitude variations also on longer propagation paths may tentatively be explained by sporadic E layers, in as much as propagation characteristics for such profiles indicate attenuation effects, but the degree of attenuation depend on the position of the $E_S$ layer with respect to the propagation path. As an example, in Table 4.1 is shown some computed field strength values for $E_S$ conditions over three selected areas for the path WTF to Tromso, Norway. The values marked $E_S$ x 10 are calculated for an increase in the electron density of the $E_S$ layer (only) by a factor of 10. Apparently the geographic position of the $E_S$ layer with respect to the propagation path and its intensity must be known in order to predict ELF field strength values for comparison with measured values.

4-9

Table 4.1  Calculated field Strengths at 75 Hz for propagation WTF to Tromso.

|  | Field Strength (dB WRT 1A/m) * |
|---|---|
| Ambient Night | -154.7 |
| $E_s$ over receiver, ambient elsewhere | -155.5 |
| $E_s$ over Norwegian Sea, ambient elsewhere | -156.5 |
| $E_s$ x 10 over Norwegian Sea, ambient elsewhere | -165.9 |

* The field strength values in this table and in all other later LMSC
references in this report have been normalized to include the signal of the
WTF E-W antenna in addition to that of the N-S antenna which is computed
by the waveguide mode code:  The E-W antenna conditions are:  Current 300A;
length 22.5 km, conductivity of ground under antenna $3.2 \times 10^{-4}$ mho/m;
phasing between E-W and N-S antennas = $0^{\circ}$.

Table 4.2 shows in more detail examples of computed characteristics
at 75 Hz for propagation from WTF to Tromso for ambient and sporadic E
conditions.

Effects are predicted for an $E_S$ over Norwegian Sea area ($\sim$ 1400 km
in lateral size) amounting to 2 dB attenuation.  For the very enhanced
$E_S$ (Peak electron density of $1.5 \cdot 10^{6}$ el/cm$^3$) a major signal fade in
excess of 10 dB is predicted.

We may thus conclude that idealized $E_S$ disturbances have produced
severe ELF attenuation in model calculations, but actual measurements of
$E_S$ conditions have not been made during the operation of the Navy's ELF
transmitter.  Attempts to explain the observed ELF signal fades in terms
of absorption due to $E_S$ conditions, can therefore not be conclusive, but the

Table 4.2 Propagation Characteristics at 75 Hz calculated for ambient and sporadic E conditions for the WTF area ($\sigma = 3.10^{-4}$ mho/m), Greenland ice caps ($\sigma = 1.10^{-5}$ mho/m) and Norwegian Sea ($\sigma = 4$ mho/m).

| Conditions | Eigenangle (Degrees) | $S = \sin \theta$ | $\alpha$ | $v/c$ |
|---|---|---|---|---|
| Ambient (day) | (81.918 - i 38.061) | (1.22 - i 0.10) | 1.37 | 0.82 |
| Ambient (night) | (82.795 - i 34.328) | (1.18 - i 0.08) | 1.09 | 0.85 |
| $E_s$ ($\sigma=3.10^{-4}$) | (82.158 - i 46.395) | (1.33 - i 0.12) | 1.68 | 0.75 |
| $E_s$ ($\sigma=1.10^{-5}$) | (79.549 -i 49.804) | 1.38 -i 0.18 | 2.43 | 0.73 |
| $E_s$ ($\sigma=4$) | (80.191 -i 46.935) | 1.33 -i 016) | 2.13 | 0.75 |
| $E_s$ x 10 ($\sigma=3.10^{-4}$) | (78.041 -i 58.076) | (1.52 -i 0.25) | 3.39 | 0.66 |
| $E_s$ x 10 ($\sigma=1.10^{-5}$) | (69.888 -i 62.374) | (1.55 - i 0.45) | 6.18 | 0.64 |
| $E_s$ x 10 ($\sigma=4$) | (59.926 - i 58.767) | (1.36 - i 0.61) | 8.54 | 0.73 |

theoretical efforts in this area point out the potential influences of $E_S$

on an ELF communication system.

## 4.4 Propagation During REP Conditions

Some electron precipitation events are classified as Relativistic

Electron Precipitation (REP) events since it is believed that electrons with

energies between 0.1 and 1 Mev are principally responsible. These events

cause significant ionization in the lower D region below about 70 km. The

events are observed to be strongest in the region below the edge of the

outer radiation belt during the daytime hours and are believed to result

from the scattering of trapped relativistic electrons by some particle

interaction. Substorm activity is believed to be a necessary condition for

REP events but not all substorms lead to internal relativistic electron

precipitation.

Relativistic electron precipitation events frequently cause excess

ionization in the ionospheric D-region to persist for one to several hours

over relatively large geographical areas. Larsen (1974, 1979) infers

that the disturbed area may extend over 2000 km in longitude. Satellite

measurements indicate that the precipitation area may cover several degrees

in latitude and one may therefore assume that the REPs may have such large

geographic extentions that they can influence ELF propagation.

Examples of precipitating electron energy spectra are shown in Figure

4.6. Note the "peaks" at energies between 800-1500 keV. Ion pair production

rates from such events, are high enough to give substantial increases

in the electron density down to 50-60 km in altitude, cf Figure 4.7. Assuming

that this precipitation occurred over segments of the propagation paths under
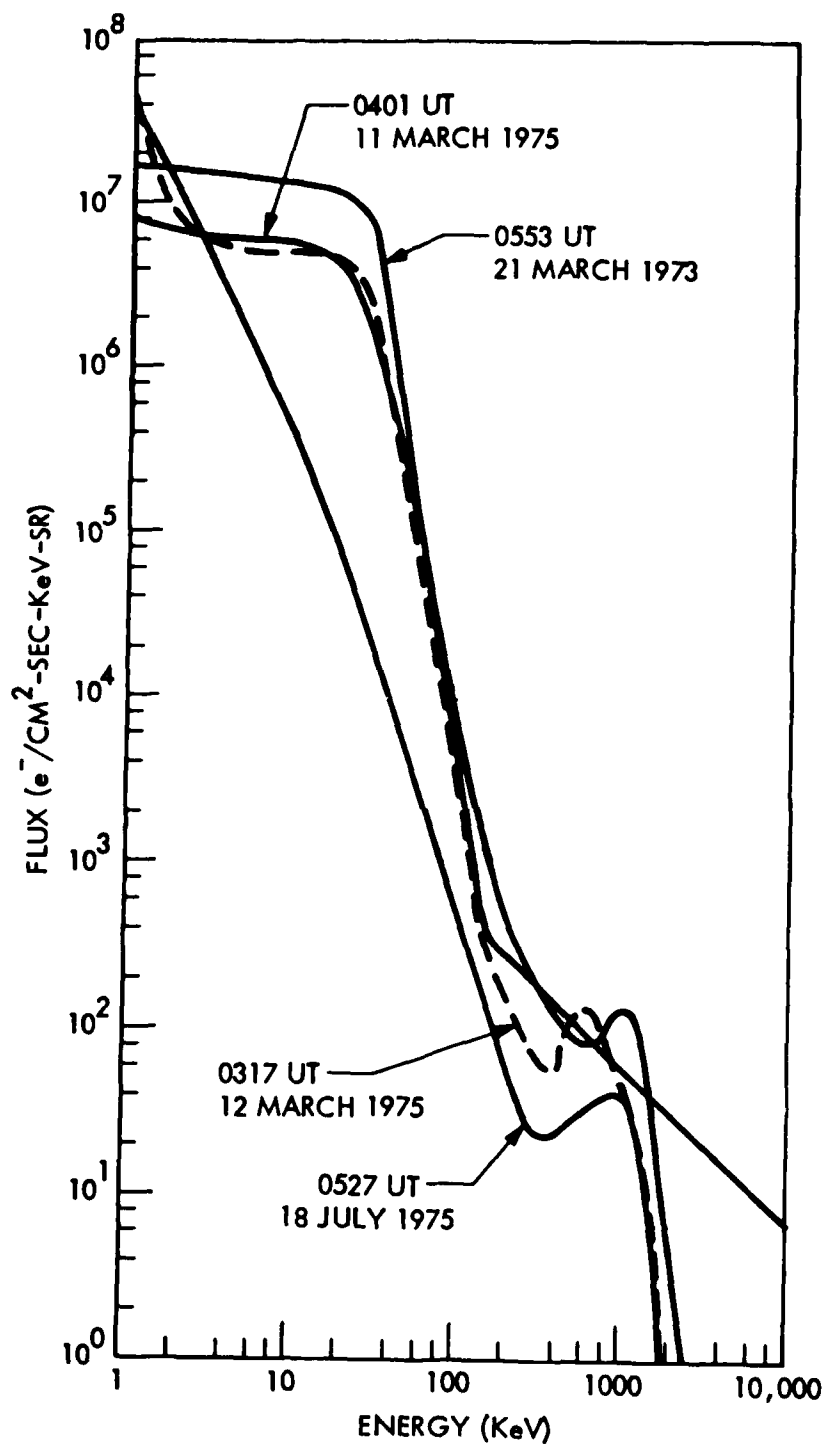
4-12

Figure 4.6 Examples of REP energy spectra measured during the coordinated exercises.
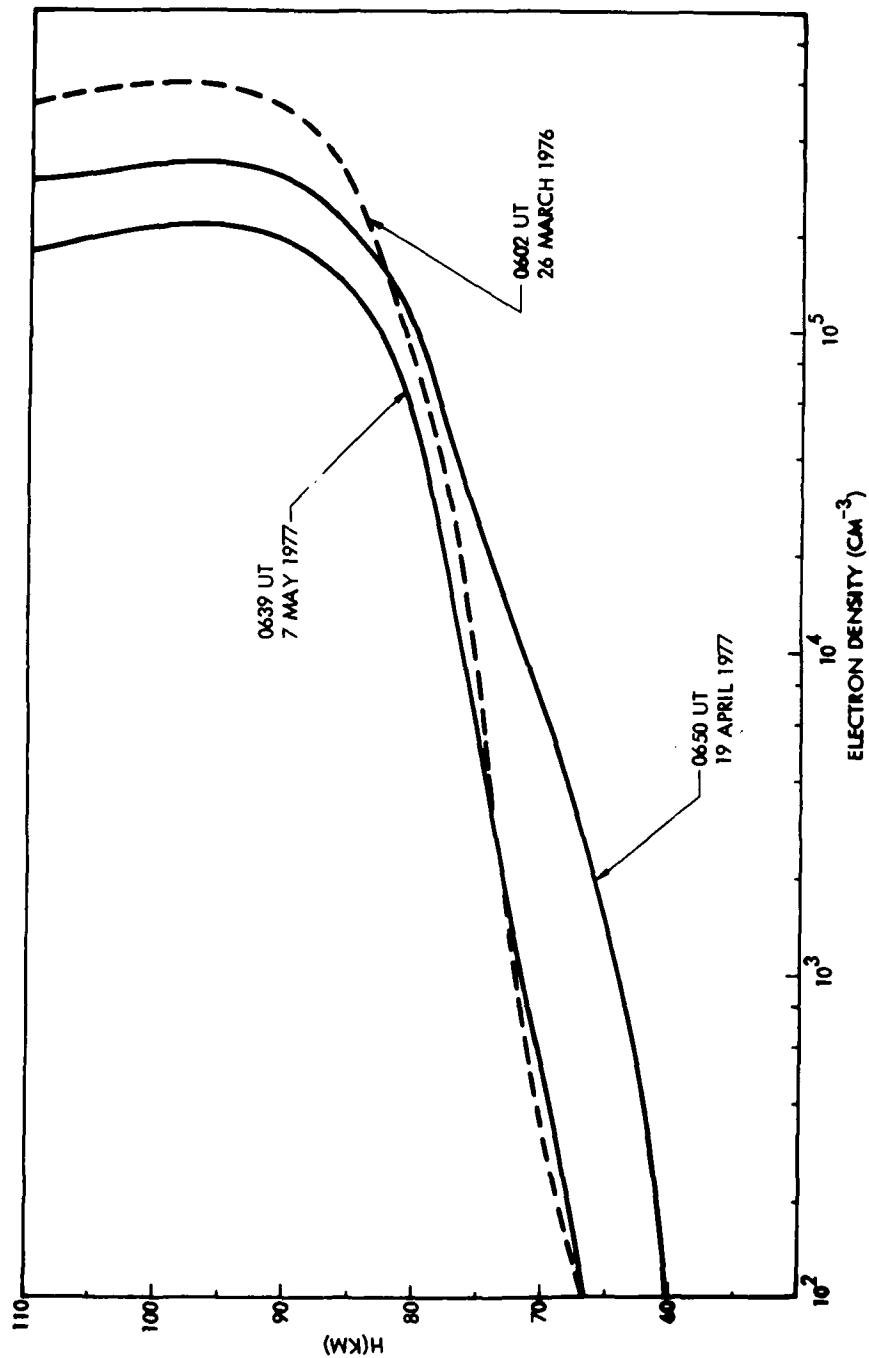
Figure 4.7  Electron density inferred from the satellite measurements of precipitating electrons during 3 different events.  Those of 19 April and 7 May were major REP events during the Greenland Sea exercise.

4-14

study, as indicated in Figure 4.8, it is possible to estimate the effects on propagation, as illustrated in Tables 4.3 and 4.4. It is seen that signal enhancements are predicted for all these nighttime REPs, by 1 dB or more when the effects occur over the transmitter (receiver) or tenths of dB when the effects are localized to areas over the paths. REP conditions over the complete path would markedly enhance the signal (by several dB).

Propagation characteristics calculated at 75 Hz for ambient conditions and for two of the REP events of Figure 4.7, in three segments of the WTF-Tromso path, are shown in Table 4.5.

In some cases REP ionization profiles have also resulted in predicted signal decreases depending upon the relative position between the disturbed area and the propagation path (Imhof et al. 1978).

In addition to direct ionization due to the electrons during an REP event, there is also some secondary ionization due to bremsstrahlung x-rays produced by the electrons. This contribution is usually neglected, but in some cases it should be considered. In Figure 4.9, it is shown that the x-rays may dominate as an ionization source between 40 and 60 km, filling in the "valley between the profiles of the ionization by electrons and that by galactic cosmic rays. Inclusion of the x-ray contribution resulted in a predicted field strength attenuated by 0.7 dB over the signal strength computed without the x-ray ionization (calculated for the 1.6 Mm path: WTF to Connecticut).

In summarizing, ELF measurements coordinated with satellite particle measurements and ELF computer code predictions, have given the following conclusions:

Figure 4.8 Plots of electron precipitation bands for the REP events of 19 April and 7 May 1977 during the Greenland Sea exercise. The bands are assumed to follow invariant magnetic latitude contours. Also shown are great circle paths from WTF to several ELF receiving stations with the segments used in ELF propagation calculations.

4-16

**LOCKHEED PALO ALTO RESEARCH LABORATORY**

LOCKHEED MISSILES & SPACE COMPANY INC

Table 4.3   Calculated Field Stre  ths for Electron Precipitation Events.
Transmissions from the Wisconsin Test Facility to the
Receiving Station at Tromso, Norway*

| Event Date | Observed Invariant Latitude Range of Precipitation | Path Segment for Precipitation | Calculated Field Strength at 75 Hz WTF - Tromso (dB wrt to 1A/m) |
|---|---|---|---|
| Ambient Night | - | - | - 154.7 |
| 26 Mar. 1976 | $57.7^{\circ} - 64.8^{\circ}$ | 0 - 900 km | - 153.6 |
| 19 Apr. 1977 | $61.5^{\circ} - 65.7^{\circ}$ | 0 - 900 | - 153.5 |
| | | 200 - 900 | - 154.6 |
| | | whole path | - 151.9 |
| 7 May 1977 | $65.2^{\circ} - 68.9^{\circ}$ | 0 - 1800 | - 153.4 |
| | | 1000 - 1800 | - 154.4 |
| | | whole path | - 151.9 |

*   The whole path length is 6000 km

Table 4.4   Calculated Field Strengths WTF - Greenland* for 19 April and 7 May 1977
Precipitating Electron Profiles

| Profile Date | Path Segments for Precipitation | Calculated Field Strength at 75 Hz (dB wrt 1 A/m) | Calculated Change from Ambient Night (dB wrt 1 A/m) |
|---|---|---|---|
| 19 April | 0 - 1200 km | - 152.1 | + 1.2 |
| | 300 - 1200 km | - 152.2 | + 0.1 |
| 7 May | 0 - 1200 km | - 151.2 | + 1.1 |
| | 300 - 1200 km | - 152.1 | + 0.2 |
| Ambient Night | | - 152.3 | |

*   Total path length 3500 km

**LOCKHEED PALO ALTO RESEARCH LABORATORY**
LOCKHEED   MISSILES   &   SPACE   COMPANY,   INC

Table 4.5  Propagation characteristics at 75 Hz calculated for ambient and REP conditions for the WT area ($\sigma = 3.10^{-4}$ mho/m), Greenland icecap ($\sigma = 1.10^{-5}$ mho/m) and Norwegian Sea ($\sigma = 4$ mho/m).

| Conditions | Eigenangle ($\theta$), Degrees | S = sin $\theta$ | $\alpha$ (db/Mm) | v/c |
|---|---|---|---|---|
| Ambient (day) | (81.918 $-$ i 38.061) | (1.22 $-$ i 0.10) | 1.37 | 0.82 |
| Ambient (night) | (82.795 $-$ i 34.328) | (1.18 $-$ i 0.08) | 1.09 | 0.85 |
| REP 26 Mar 76 ($\sigma=3.10^{-4}$) | (83.772 $-$ i 33.313) | (1.17 $-$ i 0.07) | 0.91 | 0.86 |
| REP ($\sigma=1.10^{-5}$) | (80.646 $-$ i 38.667) | (1.22 $-$ i 0.12) | 1.61 | 0.82 |
| REP ($\sigma=4$) | (84.729 $-$ i 31.896) | (1.15 $-$ i 0.05) | 0.74 | 0.87 |
| REP 19 Apr 77 ($\sigma=3.10^{-4}$) | (83.116 $-$ i 33.036) | (1.16 $-$ i 0.07) | 1.00 | 0.86 |
| REP ($\sigma-1.10^{-5}$) | (80.027 $-$ i 33.036) | (1.22 $-$ i 0.13) | 1.73 | 0.82 |
| REP ($\sigma=4$) | (84.054 $-$ i 31.401) | (1.15 $-$ i 0.06) | 0.81 | 0.87 |

"Soft" Spectrum (rows 3–5)
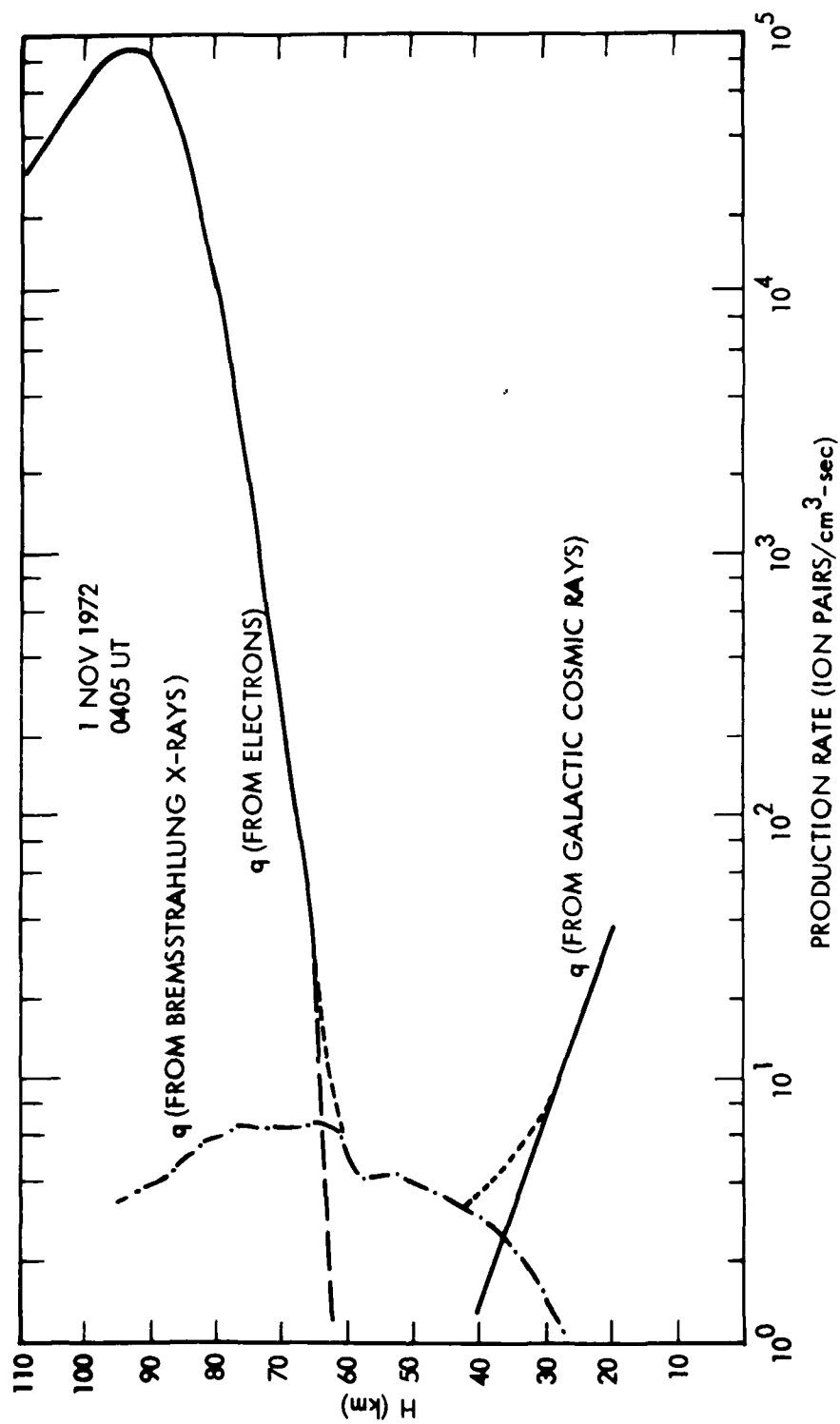
"Hard" Spectrum (rows 6–8)

Figure 4.9 Ion pair production rate profiles for the nighttime electron precipitation event of 0405 UT 1 November 1972

- From both the satellite and ELF station measurements it has
  been found that direct particle precipitation into the atmosphere
  can cause ELF transmission anomalies. In there anomalies the signal
  strengths may be either attenuated or enhanced depending upon the
  geometry and details of the ion-pair production profiles. Nighttime
  REP events may on the average improve ELF propagation conditions.

- Variations in the nighttime ELF signal strengths on a fine time scale
  are observed which may be due entirely to electron precipitation, but
  cannot be accounted for quantitatively due to present limitations in
  the measurements and computational techniques.

- The geometry for the effect of electron precipitation on nighttime
  ELF transmission is very complex and as a result the need for new
  techniques for mapping electron precipitation profiles simultaneously
  over a broad spatial region has become apparent.

## 5.0  CALCULATIONS FOR SIMULATED PCA CONDITIONS

There have been no actual measurements of signals from WTF during

a PCA event.  Calculations for simulated conditions, however, indicate

that significant signal strength reductions could occur.  The total amount

of signal absorption would depend on the extent of the disturbed area

and location of the ELF transmitter with respect to the PCA area.  Imhof

et al. (1980) summarized their findings as follows:

- Typical PCA nighttime conditions as observed during the August

  1972 event, will decrease the ELF signal at 75 Hz by several dB

  over a polar propagation path (WTF to Tromso) for uniform conditions

  along the whole path.

- The received ELF field strength for such a path is predicted to be

  reduced by an additional 1-3 dB when the WTF transmitter area is

  outside the PCA disturbed area.

- The ELF signal strength was found to be sensitive to changes in the

  ion densities at heights below 45-50 km.

## 5.1  PCA Simulations Using Data from the August 1972 PCA

In the following we present some additional work (including daytime

PCA simulations) on signal strength calculations during simulated PCA

conditions.  For reference the PCA profiles used* are reproduced in Figures

---

\*  These test cases are based on electron density measurements made by the SRI
Chatanika incoherent scatter radar.  As originally interpreted the
measurements yielded electron densities which are now known to be too
large by a factor which is altitude dependent and ranges in magnitude
from one to two.  Theory developed by Matthews (1978) and Fukuyama
and Kofman (1979) shows that when negative ions are taken into account
smaller electron densities result from the measurements as discussed
in Imhof et al. (1980). The positive ion densities inferred from the electron
densities are thus too small.  These test cases however have been used
frequently in our work and are retained as good examples of a very
intense PCA.

5.1 and 5.2 (cf Imhof et al.,1980 for further comments). Care has been taken to include ion densities at all heights commensurate with the electron densities.

The values for the positive ions above 40 km were obtained using the chemistry code of Gunton et al. (1977). At lower altitudes the values for the positive ion density $N_+$ are obtained using the formula

$$N_+ = \sqrt{q/\alpha_i\,(h,T)}$$

where height and temperature dependent values of the ion-ion recombination rate $\alpha_i$ are used, of Table 5.1

Table 5.1    Ion-ion Recombination Rates ($\alpha_i$) Calculated for 65°N, August

| Altitude (km) | P Pressure (Dynes/cm$^2$) | T Temperature (K) | $\alpha_i$ (cm$^3$ sec$^{-1}$) |
|---|---|---|---|
| 60 | $2.869\ 10^2$ | 261 | $5.16\ 10^{-8}$ |
| 55 | $5.366\ 10^2$ | 274 | $5.26\ 10^{-8}$ |
| 50 | $9.834\ 10^2$ | 278 | $5.46\ 10^{-8}$ |
| 45 | $1.801\ 10^3$ | 274 | $5.87\ 10^{-8}$ |
| 40 | $3.383\ 10^3$ | 261 | $6.84\ 10^{-8}$ |
| 35 | $6.571\ 10^3$ | 247 | $9.11\ 10^{-8}$ |
| 30 | $1.305\ 10^4$ | 236 | $1.41\ 10^{-7}$ |
| 25 | $2.800\ 10^4$ | 228 | $2.64\ 10^{-7}$ |
| 20 | $5.900\ 10^4$ | 225 | $5.16\ 10^{-7}$ |
| 15 | $1.260\ 10^5$ | 225 | $1.05\ 10^{-6}$ |
| 10 | $2.680\ 10^5$ | 225 | $2.17\ 10^{-6}$ |
| 5 | $5.410\ 10^5$ | 260 | $3.03\ 10^{-6}$ |
| 0 | $1.017\ 10^6$ | 289 | $4.35\ 10^{-6}$ |

Note: These values for $\alpha_i$ have been calculated using the formula

$$\alpha_i = 5 \times 10^{-8} + 6 \times 10^{-6}\ P\ T^{-5/2},$$

where P is pressure in dynes/cm$^2$ and T is temperature in degrees Kelvin.

   This formula is from Niles (1976) with the first term changed from $3 \times 10^{-8}$ to $5 \times 10^{-8}$ in light of the latest laboratory measurements by Smith and Church (1977).

   The model atmosphere is for August at 65°N latitude.

**LOCKHEED PALO ALTO RESEARCH LABORATORY**
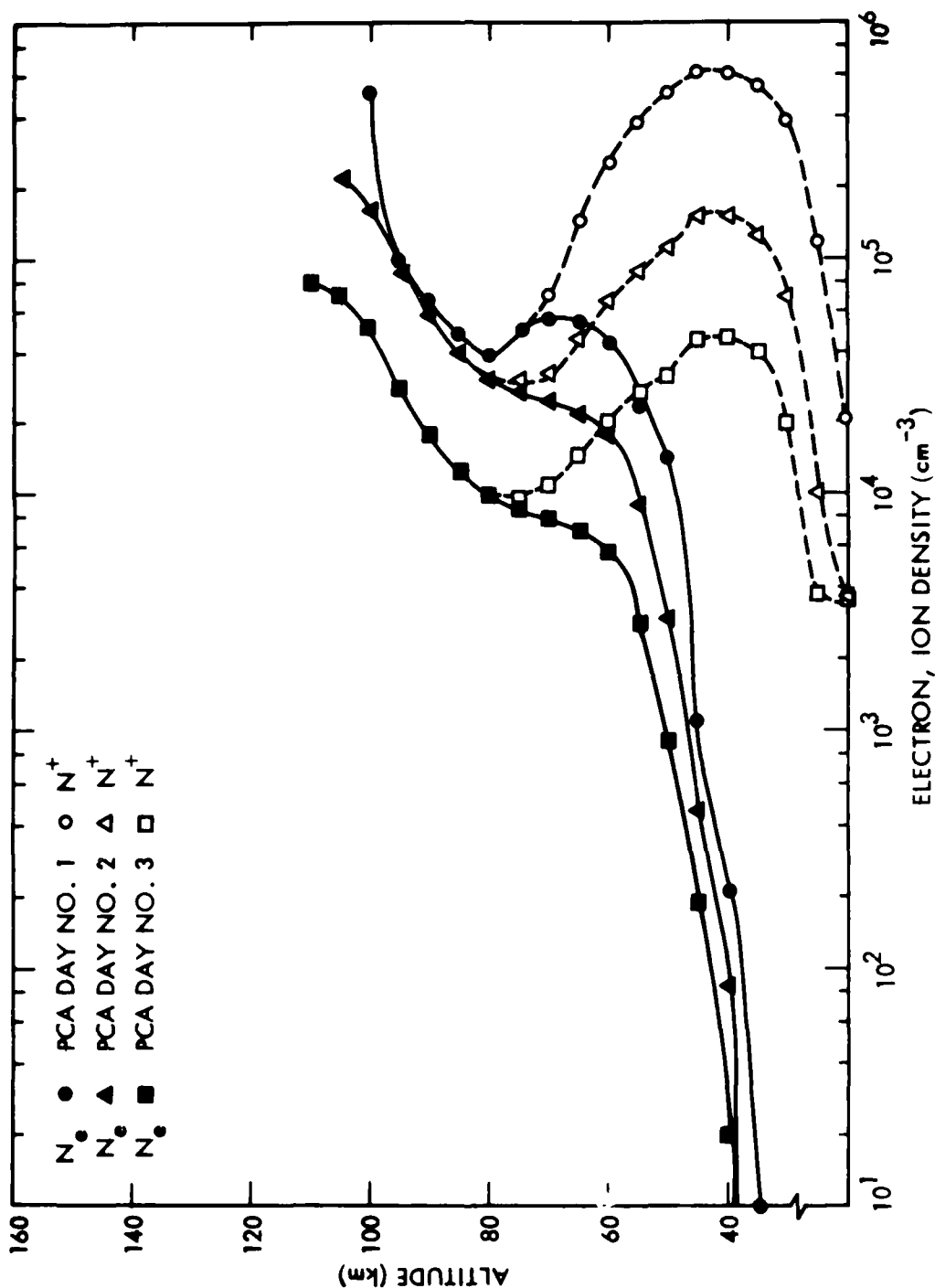LOCKHEED MISSILES & SPACE COMPANY, INC

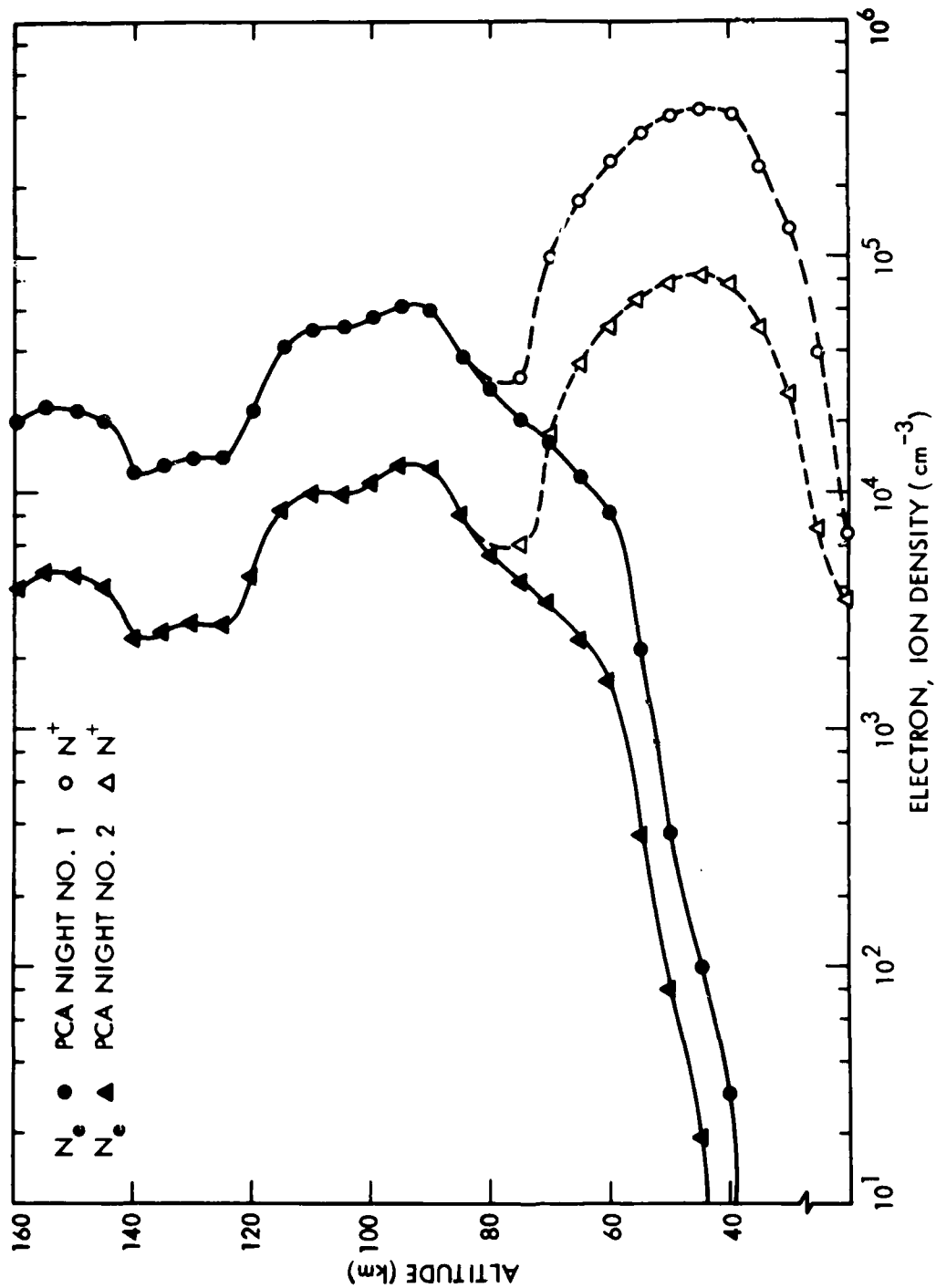Figure 5.1 Electron and ion density profiles for the PCA daytime test cases

Figure 5.2  Electron and ion density profiles for the PCA nighttime test cases

Table 5.2  Comparison between ELF absolute field strength calculations at 75 Hz for the path WTF to Tromso.

| Condition | LMSC dB/1A/m | Predicted Change (dB) |
|---|---|---|
| Day, ambient | -154.7 | - |
| Night, ambient | -154.7 | - |
| Day PCA #1 | -160.4 | -5.7 |
| Day PCA #2 | -157.5 | -2.8 |
| Day PCA #3 | -157.0 | -2.3 |
| Night PCA #1 | -161.1 | -6.4 |
| Night PCA #2 | -162.6 | -7.9 |

## 5.2  Sensitivity of ELF Field Strengths Using Other Simulated PCA Conditions

The earlier efforts (Imhof et al., 1976, 1977, 1978, 1980) have emphasized the importance of the conditions prevailing during the August 1972 event in absorbing energy from the ELF waves. The present work extends these efforts through use of data for three PCA events, having energy spectra of different spectral shapes and intensities, viz:

PCA of 12 Nov 1960        1930 UT

PCA of  2 Nov 1969        1448 CST

PCA of  4 Aug 1972        Daytime Test Case #1

The ion and electron density profiles for the PCA of 12 November 1960 were calculated using the ion pair production altitude profiles shown in Figure 5.3 together with electron and ion loss coefficients calculated during our modeling of the PCA of 4 August 1972 (Imhof et al. 1980).
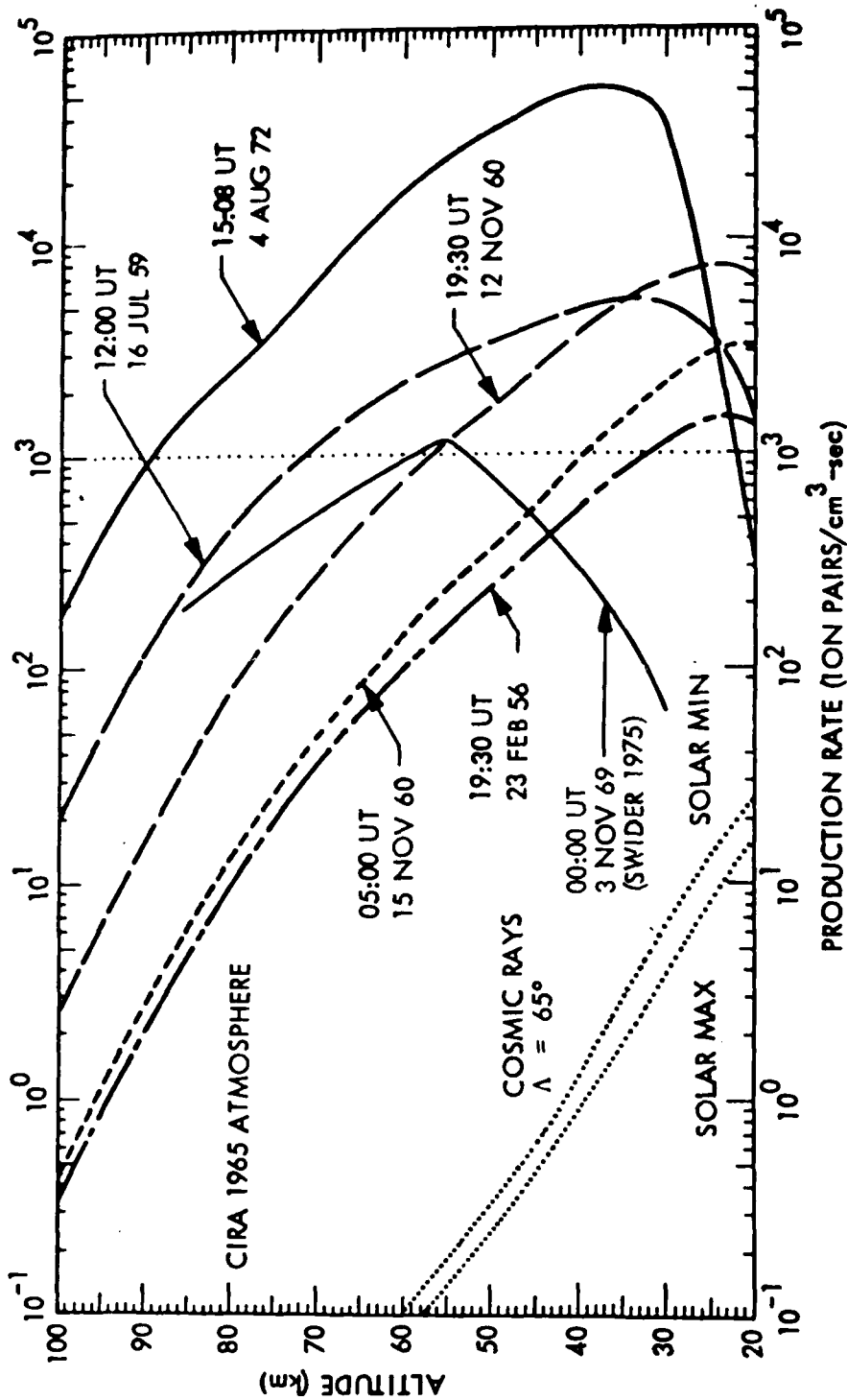
5-5

Figure 5.3    Solar proton induced ion production rates during the major solar particle events
in solar cycles 19 and 20 from Reagan et al. (1981) with the 3 Nov 69 curve added.
The cosmic ray ionization for solar maximum and minimum is shown for comparison. The
4 August 1972 SPE dominates in ion production rate over all of the other events in
cycles 19 and 20 at altitudes above 26 km.

The ion and electron density profiles for the PCA of 2 November 1969 were calculated with our ion chemistry model. The ion pair production altitude profile time dependence was derived from Swider (1975).

The deduced electron and positive ion densities for these cases are given in Table 5.3 and plotted in Figure 5.4. It may be noted in Figure 5.3 that the November 1960 event had a harder proton spectrum yielding higher $N^+$ densities below 30 km than the August 1972 PCA. Above 80 km, however, the ionization due to the protons during the 1960 and 1969 events was below the normal ionization levels of the solar radiation, and the daytime ambient $N_e$ and $N^+$ curves have been used from 80 to 160 km for these two cases.

We first present the calculated field strengths at 75 Hz for propagation from WTF to Tromso which are as follows:

| | | |
|---|---|---|
| PCA 12 Nov 1960 | −163.3 dB; | 8.6 dB below ambient |
| PCA  2 Nov 1969 | −155.7 dB; | 1.0 dB below ambient |
| PCA  4 Aug 1972 (Day test case #2) | −160.4 dB; | 5.7 dB below ambient |

For these simulated cases, ambient conditions were assumed over the WTF transmitter area. In the calculation for the PCA of 2 November 1969, the standard segmentation of the path into eight parts was used. The first five segments were assumed to be in daylight and the remainder in night. For the daylight segments beyond the WTF area, a daylight profile calculated for segment 3 under PCA conditions was used. The segments assumed to be in darkness were given a profile based on nighttime PCA calculations for segment 3. In the other two cases all of the segments beyond the WTF area

Table 5.3     Electron and Ion Densities for Selected PCA Events

| Altitude (km) | PCA 12 Nov 60 | | PCA 2 Nov 69 | | PCA 4 Aug 72 | |
|---|---|---|---|---|---|---|
| | $N_e(cm^{-3})$ | $N^+(cm^{-3})$ | $N_e(cm^{-3})$ | $N^+(cm^{-3})$ | $N_e(cm^{-3})$ | $N^+(cm^{-3})$ |
| 100 | 6.00(+4) | 6.00(+4) | 6.00(+4) | 6.00(+4) | 5.00(+5) | 5.00(+5) |
| 95 | 3.60(+4) | 3.60(+4) | 3.60(+4) | 3.60+4) | 1.00(+5) | 1.00(+5) |
| 90 | 1.50(+4) | 1.50(+4) | 2.00(+4) | 2.00(+4) | 6.50(+4) | 6.50(+4) |
| 85 | 7.00(+3) | 7.00(+3) | 1.57(+4) | 1.57(+4) | 4.80(+4) | 4.80(+4) |
| 80 | 5.36(+3) | 5.60(+3) | 1.74(+4) | 1.75(+4) | 3.80(+4) | 3.80(+4) |
| 75 | 6.40(+3) | 8.19(+3) | 1.06(+4) | 1.09(+4) | 5.00(+4) | 5.00(+4) |
| 70 | 6.46(+3) | 1.40(+4) | 1.01(+4) | 1.23(+4) | 5.50(+4) | 7.00(+4) |
| 65 | 5.72(+3) | 3.04(+4) | 9.22(+3) | 2.07(+4) | 5.40(+4) | 1.50(+5) |
| 60 | 3.84(+3) | 6.01(+4) | 7.32(+3) | 3.17(+4) | 4.50(+4) | 2.50(+5) |
| 55 | 2.18(+3) | 1.06(+5) | 3.81(+3) | 6.38(+4) | 2.30(+4) | 3.70(+5) |
| 50 | 8.50(+2) | 1.59(+5) | 1.68(+3) | 9.18(+4) | 1.40(+4) | 5.00(+5) |
| 45 | 5.46(+2) | 2.08(+5) | 2.39(+2) | 8.84(+4) | 1.10(+3) | 6.00(+5) |
| 40 | 1.11(+2) | 2.43(+5) | 2.18(+1) | 5.69(+4) | 2.15(+2) | 6.00(+5) |
| 35 | 2.10(+1) | 2.47(+5) | 9.20(-4) | 3.25(+3) | 1.00(+1) | 5.40(+5) |
| 30 | 1.10(+1) | 2.22(+5) | 3.00(-4) | 3.55(+3) | 1.67(-4) | 3.75(+5) |
| 25 | 5.00(-3) | 1.76(+5) | 1.00(-4) | 3.69(+3) | 7.70(-5) | 1.15(+5) |
| 20 | 1.00(-3) | 1.19(+5) | 3.43(-5) | 3.65(+3) | 3.43(-5) | 2.05(+4) |
| 15 | 3.00(-4) | 6.14(+4) | 1.50(-5) | 3.63(+3) | 1.50(-5) | 3.63(+3) |
| 10 | 6.58(-6) | 3.72(+3) | 6.58(-6) | 3.72(+3) | 6.58(-6) | 3.72(+3) |
| 5 | 3.43(-6) | 4.48(+3) | 3.43(-6) | 4.48(+3) | 3.43(-6) | 4.48(+3) |

NOTE: In the calculations the profiles for 12 Nov 60 and 2 Nov 69 were extended to 160 km with ambient daytime values above 80km and 100 km, respectively.  The profile for PCA 2 Nov 69 is for daytime conditions.
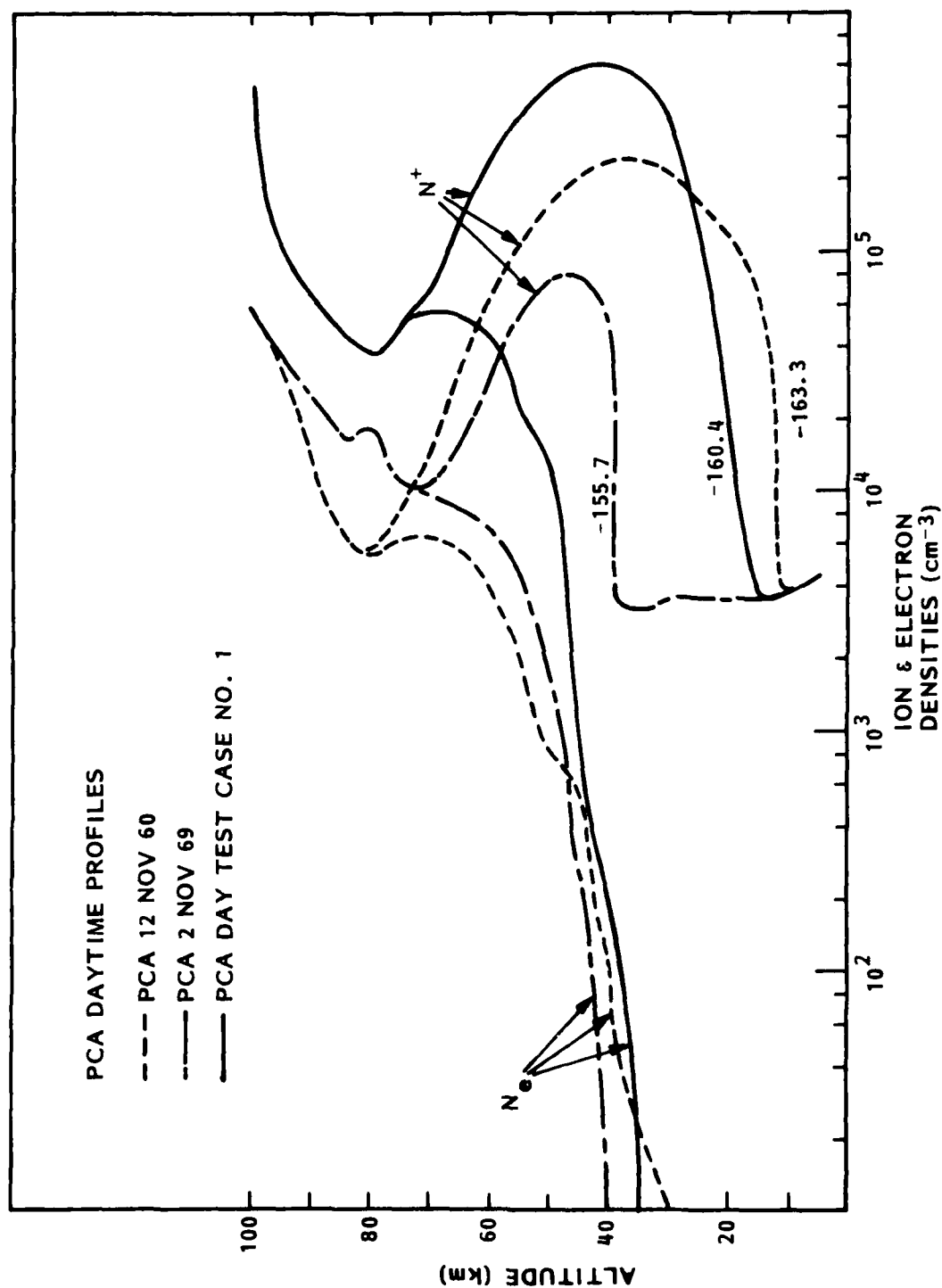
Figure 5.4  Electron and positive ion densities vs. altitude for three PCA test profiles. The numbers on the curves are the calculated signal strengths in dB at 75 Hz for the Tromso path.

used the profile specified in Figure 5.3.  In Table 5.4 are listed the S-values

(sin θ, the eigenangle solution) for three selected segments of the path,

representing a range in ground conductivity and different propagations with

respect to the earth's geomagnetic field.  For comparison a recent S-value

computed by Field et al. (1980) at 75 Hz for a "strong PCA" case is included.

Detailed information on the computed attenuation rates and phase

velocities are given in Table 5.5.

Figure 5.5 shows the variation of ELF field strengths as a function

of distance for these three cases.

Table 5.4  Computed values for S = sin θ at 75 Hz for various segments along
propagation path WTF to Tromso.  Also given is the value deduced by
Field et al. (1980) for a "strong PCA" case.

| Segment | PCA 12 Nov 60 | PCA 2 Nov 69 | PCA 4 Aug 72 (Day test case #1) |
|---|---|---|---|
| #6 Greenland Icecap $\sigma = 10^{-5}$ mho/m | 1.4526 − 0.3084 i | 1.3563 − 0.1916 i | 1.4308 − 0.2725 i |
| #7 Norwegian Sea $\sigma = 4$ mho/m | 1.3656 − 0.2139 i | 1.2681 − 0.1104 i | 1.3337 − 0.1725 i |
| #8 Tromso Area $\sigma = 10^{-3}$ mho/m | 1.3748 = 0.2252 i | 1.2767 − 0.1187 i | 1.3433 − 0.1830 i |

| | |
|---|---|
| Field et al (1980) Value for "strong PCA" | $S_1$ = 1.50 − 0.25 i |

Table 5.5    Propagation characteristics at 75 Hz for three PCA events of
different proton energy spectral shape.

| Segment # | PCA Nov 60 | | PCA Nov 69 | | PCA Aug 72 | |
|:---:|:---:|:---:|:---:|:---:|:---:|:---:|
| | α (db/Mm) | v/c | α (db/Mm) | v/c | α (db/Mm) | v/c |
| 1 | | | | | 2.614 | 0.7400 |
| 2 | 2.940 | 0.7321 | 1.641 | 0.7828 | 2.496 | 0.7445 |
| 3 | 2.811 | 0.7369 | 1.527 | 0.7882 | 2.354 | 0.7499 |
| 4 | 2.935 | 0.7318 | 1.637 | 0.7829 | 2.496 | 0.7444 |
| 5 | 2.801 | 0.7363 | 1.520 | 0.7884 | 2.353 | 0.7499 |
| 6 | 4.032 | 0.6912 | 2.6:2 | 0.7373 | 3.715 | 0.6989 |
| 7 | 2.782 | 0.7356 | 1.505 | 0.7886 | 2.352 | 0.7498 |
| 8 | 2.912 | 0.7306 | 1.618 | 0.7833 | 2.495 | 0.7444 |

## 5.3    Sensitivity of ELF Waves to Absorption by Ions at Low Altitudes

In this section we will briefly discuss the importance of ions below
45-50 km altitude in determining the absorption of ELF waves.  Calculations
were made at 75 Hz for the WTF to Tromso path.  Ambient day conditions were
assumed over the WTF area.

To achieve this we have modified the PCA 4 Aug 1972 and 12 Nov 1960
ion profiles at low altitudes, and calculated the effects.  Figures 5.6
and 5.7, respectively, show the modifications and the corresponding field
values.

It can be concluded    that    the    ions    formed by    the high
energy    tail    of the precipitating protons    below 45 - 50 km    are significant.
In the case of    PCA    Nov    1960    calculation shows that the ions below 40-45 km
would cause about 8 dB attenuation    over    the 6 megameter    path tc Tromso,
a very    large    effect.    The    region    20 - 45 km    seems    to    be    the    most
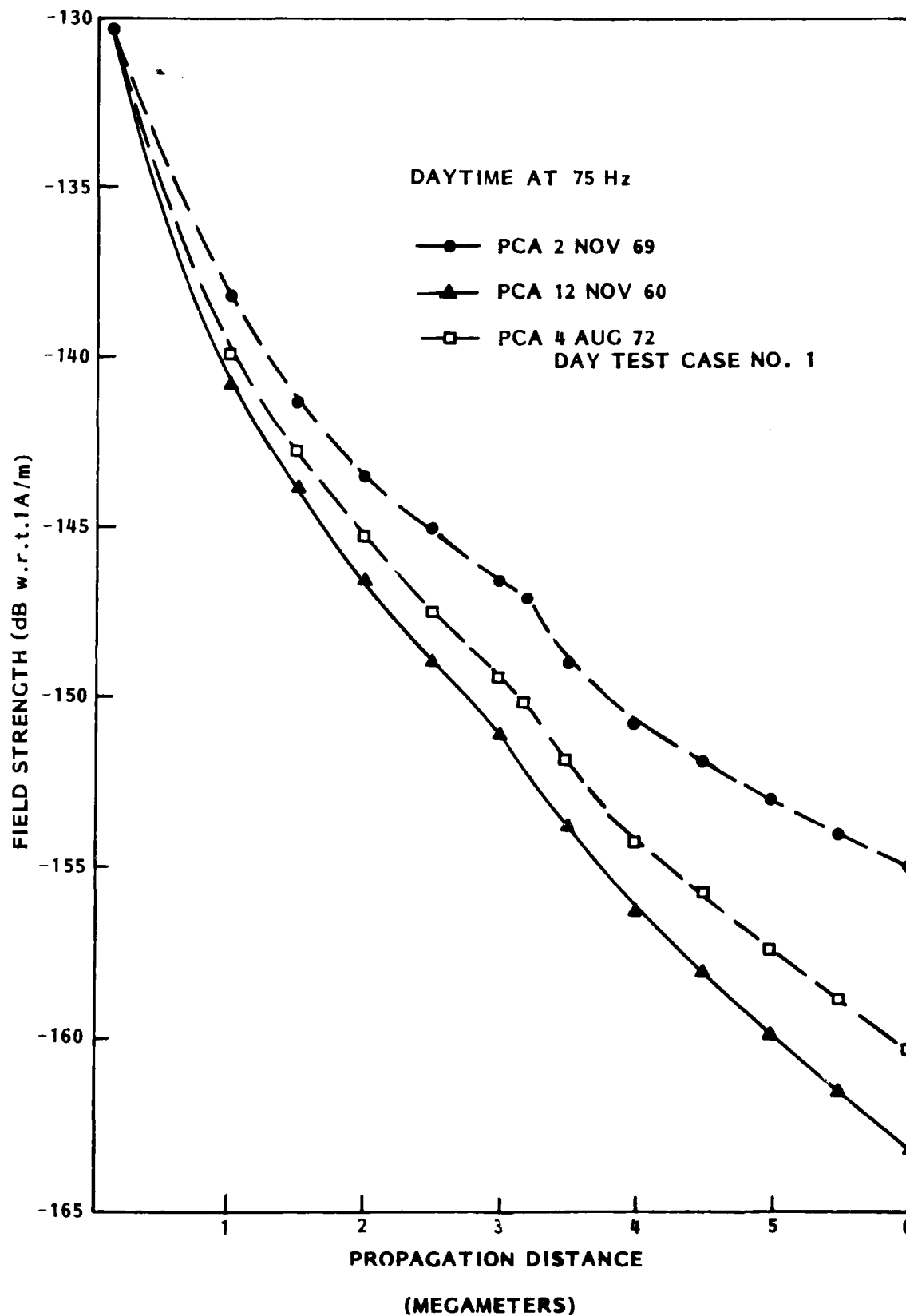
5-11

Figure 5.5  Variation of field strength over the WTF to Tromso path for three PCA profiles.
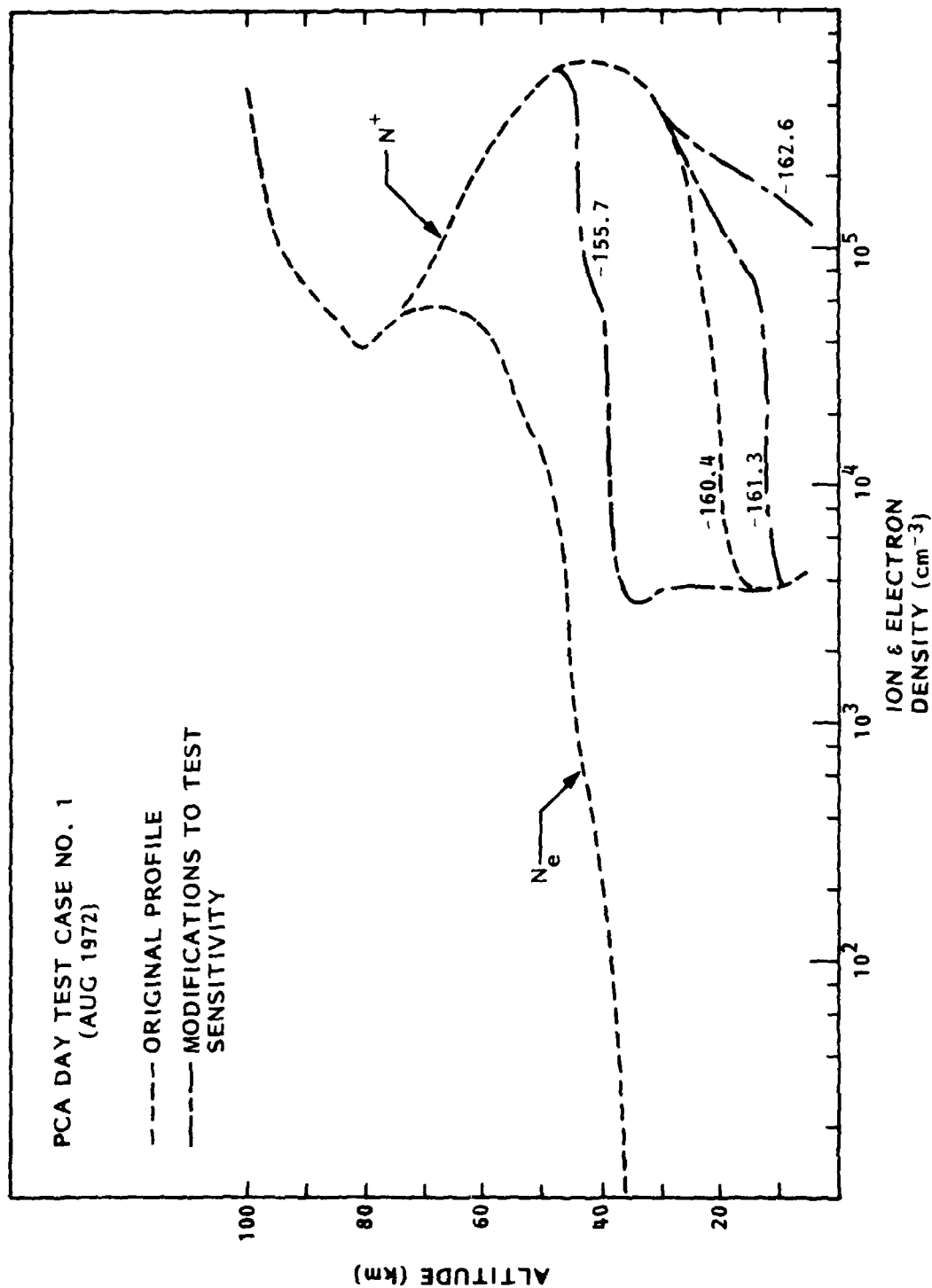
Figure 5.6  Electron and ion density profiles for the PCA Day Test Case #1 and modifications of the ion profile to test sensitivity of the signal strength over the WTF to Tromso path to such variations. The numbers on the curves are attenuations in db at 75 Hz

LOCKHEED PALO ALTO RESEARCH LABORATORY

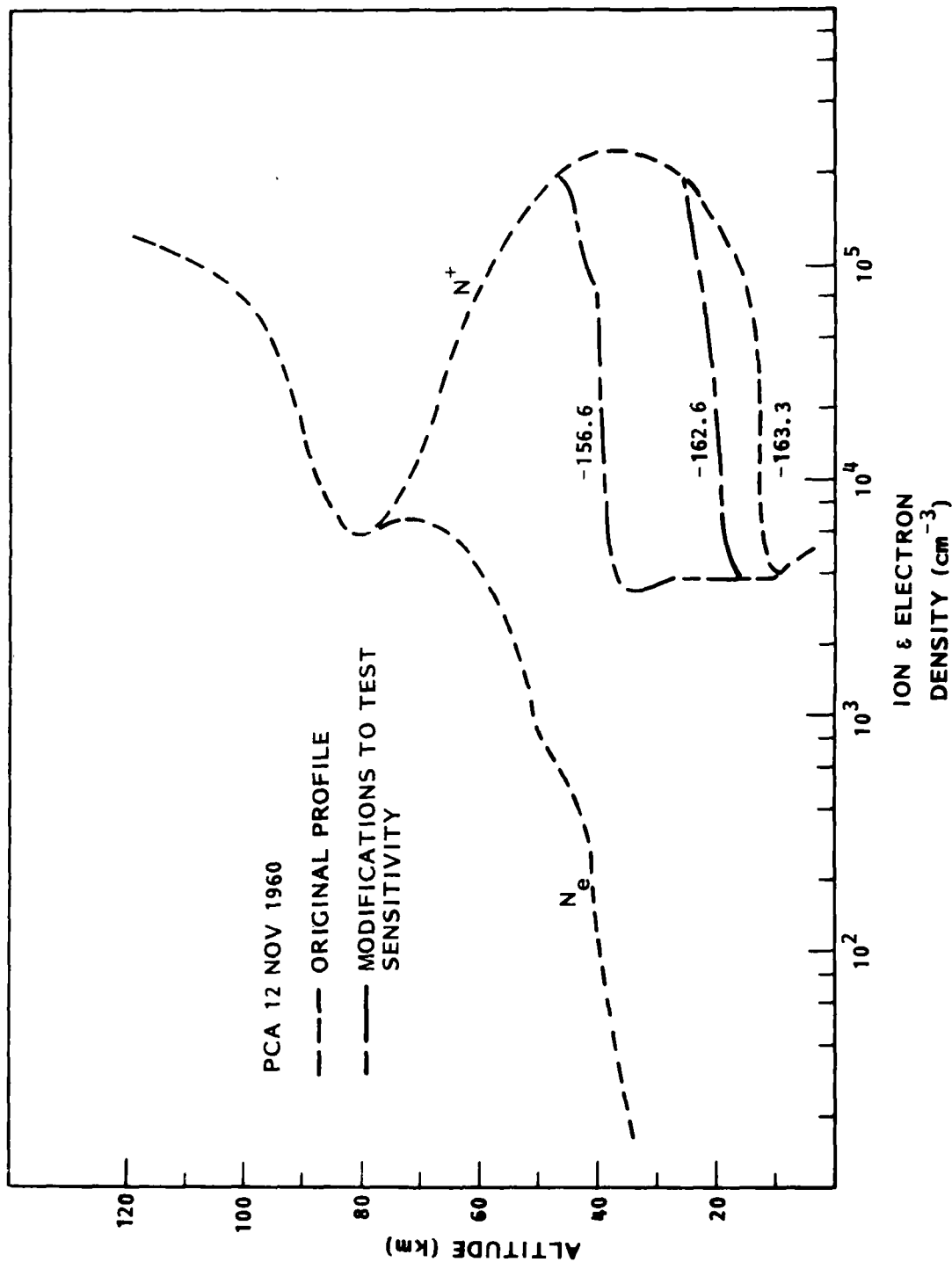LOCKHEED  MISSILES  &  SPACE  COMPANY,  INC

Figure 5.7 Electron and ion density profiles for the PCA of 12 November 1960 along with modifications in the positive ion portions to test sensitivity of the signal strength to such modifications. The numbers on the profiles are attenuations in dB at 75 Hz over the WTF to Tromso path.

important height range for this attenuation, but enhanced densities even

below 20 km cause some absorption

Figure 5.6 showing the modifications to the daytime 4 Aug 1972 PCA

(Test Case #1), also indicates effects due to a postulated "extreme" case

for ion densities below 20 km. Here the ion densities are almost two orders

of magnitude above ambient at the 20 km level. The amount of ohmic heating

that occurs at these altitudes is strongly reduced and only a minor ($\sim$ 1dB)

amount of excess absorption takes place. Detailed propagation characteristics

are listed in Tables 5.6 and 5.7.

From the present and earlier studies the following conclusions can

be drawn regarding importance of ions:

- Relatively little ELF attenuation seems to occur below about

    20 km. For extreme cases with high $N^+$ densities some ELF attenuation

    is predicted to occur even at these altitudes.

Table 5.6   Propagation Characteristics at 75 Hz for PCA day Test Case #1
(4 Aug 72) - Original and Modifications.

| Segment # | Original Profile | | Original to 30 km; below 30 km: PCA Nov 60 | | Original to 30 km; Very High Ion Densities | | Original to 45 km; Below 45 km: Sharp Transit. | |
|---|---|---|---|---|---|---|---|---|
| | $\alpha$(dB/Mm) | v/c | $\alpha$ | v/c | $\alpha$ | v/c | $\alpha$ | v/c |
| 1 | 2.614 | 0.7400 | | | | | | |
| 2 | 2.496 | 0.7445 | 2.644 | 0.7452 | 2.869 | 0.7460 | 1.141 | 0.8036 |
| 3 | 2.354 | 0.7499 | 2.501 | 0.7505 | 2.724 | 0.7513 | 1.018 | 0.8099 |
| 4 | 2.486 | 0.7444 | 2.644 | 0.7452 | 2.869 | 0.7460 | 1.141 | 0.8036 |
| 5 | 2.353 | 0.7499 | 2.500 | 0.7505 | 2.723 | 0.7513 | 1.018 | 0.8098 |
| 6 | 3.715 | 0.6989 | 3.873 | 0.6999 | 4.113 | 0.7011 | 2.185 | 0.7516 |
| 7 | 2.352 | 0.7498 | 2.499 | 0.7505 | 2.722 | 0.7513 | 1.017 | 0.8098 |
| 8 | 2.495 | 0.7444 | 2.643 | 0.7451 | 2.868 | 0.7460 | 1.140 | 0.8036 |

Table 5.7  Propagation characteristics at 75 Hz for PCA 12 Nov 60 profile (original and modifications).

| Segment # | Original Profile | | Original to 30 km below 30 km: PCA day test case #1 | | Original to 45 km below 45 km: Sharp transition | |
|---|---|---|---|---|---|---|
| | $\alpha$ (db/Mm) | v/c | $\alpha$ (db/Mm) | v/c | $\alpha$ (db/Mm) | v/c |
| 1 | 3.039 | 0.7278 | 2.908 | 0.7269 | | |
| 2 | 2.940 | 0.7321 | 2.810 | 0.7312 | 1.795 | 0.7584 |
| 3 | 2.811 | 0.7369 | 2.682 | 0.7360 | 1.678 | 0.7656 |
| 4 | 2.935 | 0.7318 | 2.804 | 0.7309 | 1.789 | 0.7581 |
| 5 | 2.861 | 0.7363 | 2.672 | 0.7354 | 1.668 | 0.7630 |
| 6 | 4.032 | 0.6912 | 3.895 | 0.6901 | 2.780 | 0.7142 |
| 7 | 2.782 | 0.7356 | 2.653 | 0.7347 | 1.648 | 0.7624 |
| 8 | 2.912 | 0.7306 | 2.782 | 0.7297 | 1.766 | 0.7569 |

- In the height range 20-45km ions dominate as the cause of ELF wave attenuation through ohmic dissipation during disturbed conditions. Such ohmic losses may account for 50-60% of the total wave absorption, and they maximize around 30-40 km for the profiles analyzed.

- At heights above 45-50 km the ion contribution to the ionospheric conductivity decreases fast relative to the electron component which rapidly becomes the dominant part at these and higher altitudes.

5.4 <u>Sensitivity of ELF Waves to Changes in Electron Densities at Low</u>
<u>Heights During PCA Conditions</u>

During PCA daytime conditions the electron densities around 40 to 50 km

may be 4-5 orders of magnitude above the ambient values. Clearly some

uncertainty will be connected with the deduced PCA densities due to changes

in reaction rate coefficients . A simple test on the sensitivity of

the ELF field strengths to $N_e$ changes at low heights can be made by moving

the lower part of the $N_e$ profile up and down, say 5 km, and

strength calculations for these cases.

As an example we have taken the PCA Day Test case #1 and modified it

below 60 km in the way suggested above. The $N^+$ curve was kept unchanged

as were the electron densities above 65-70 km (cf Figure 5.8).

Results for propagation at 75 Hz from WTF to Tromso were as follows:
PCA Daytest case #1

| Unchanged | Up 5 km | Down 5 km |
|-----------|---------|-----------|
| − 160.4 dB | − 161.3 dB | − 159.4 dB |

These calculations indicate that for a solar proton event like that

of Aug 72 an uncertainty in the lower part of the $N_e$ profile of $\pm$ 5 km,

would yield $\pm$ 1 dB uncertainty in the field strength value. In a real

situation the $N_e$ values would probably be known to a greater accuracy than

assumed in this example.

It may be noted that lowering the profile at low altitudes by 5 km

(making the ionosphere 5 km thicker) increases the expected signal level

essentially through a lower value for the attenuation constant. Conversely,

raising the $N_e$ profile by 5 km, resulted in increased attenuation rates by
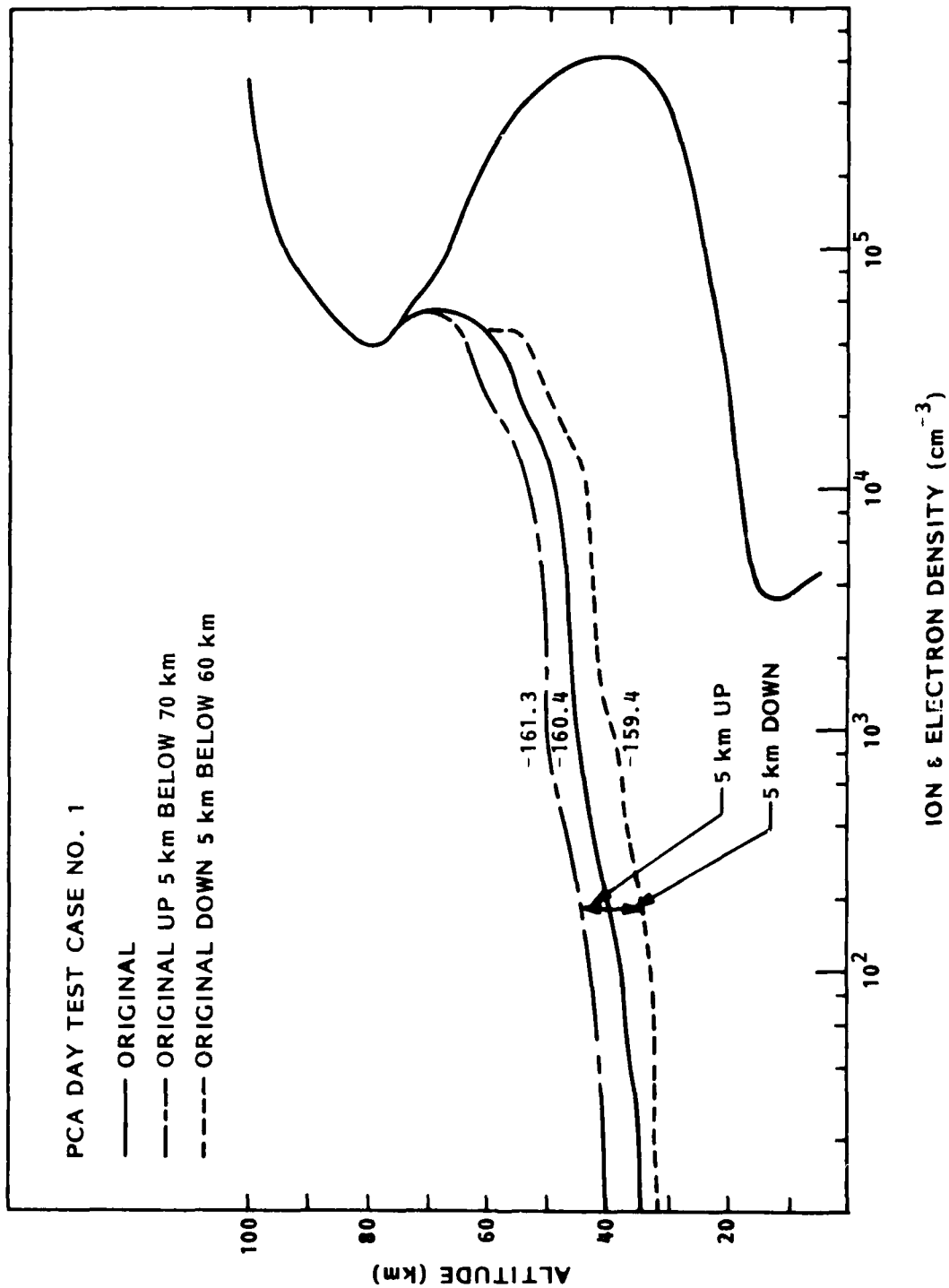
0.3-0.4 dB/Mm.

Figure 5.8  Electron and ion density profiles for the PCA Day Test Case #1 and modifications of the electron profile to test sensitivity of the signal strength over the WTF to Tromso path to such variations. The numbers on the curves are attenuations in db.

## 5.5 Criteria for ELF Field Program

Earlier results (Imhof et al., 1980) indicated that the predicted field strength at 75 Hz for WTF to Tromso decreased in approximately a logarithmic manner with the $N^+$ density at 30 km altitude. These results were for the PCA Aug 72 day time test profiles 1-3 (see section 5.1). When data for the PCA Nov 60 and PCA Nov 69, with energy spectra differing from the August 72 PCA, are included, this relation becomes more diffuse, cf Figure 5.9. Taking a variety of PCAs having differing spectral hardness, one can expect to observe or predict a range of field strengths for a given ion density at 30 km. This is qualitatively indicated in the figure by the shaded area. The unusually large signal attenuation for the PCA event of 12 November 1960 is due to the unusually large ion pair production below 30 km, shown in Figure 5.3, which led to enhanced effects by the resulting ions.
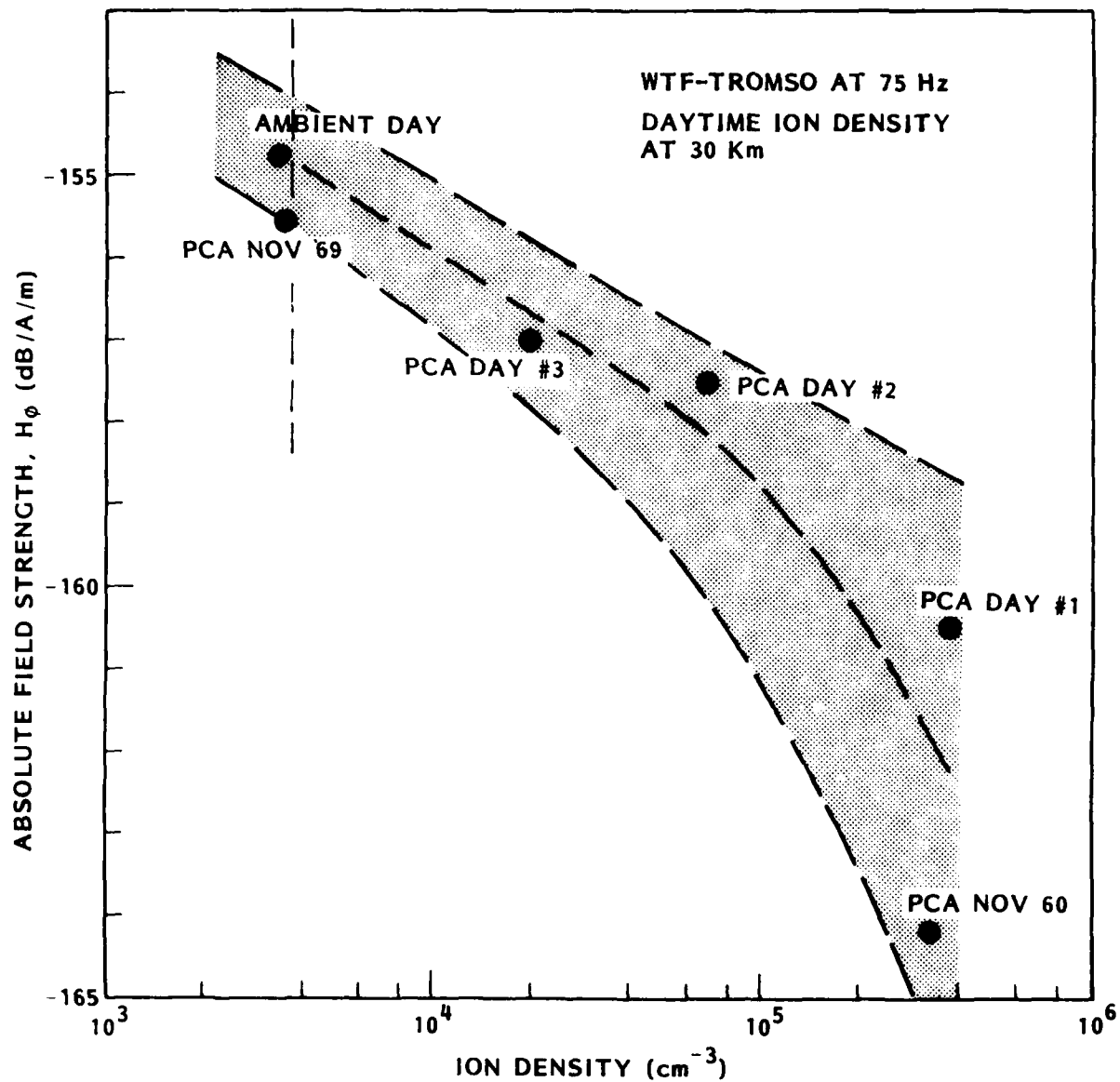
Figure 5.9  Absolute field strength for the WTF to Tromso path versus ion
            density at 30 km altitude for three PCA daytime test cases
            (Section 5.1), for the PCA's of Nov 60 and Nov 69, and for
            standard ambient daytime.

LOCKHEED PALO ALTO RESEARCH LABORATORY
LOCKHEED   MISSILES   &   SPACE   COMPANY,   INC

## 6.0 COMPARISON OF PCA SIMULATION RESULTS

The PCA profiles shown in Figures 5.1 and 5.2 were used in an inter-comparison of ELF calculations over the WTF to Tromso path by three laboratories: LMSC, Naval Ocean Systems Center (NOSC) and Pacific Sierra Research (PSR). The results show a measure of agreement in some cases but more often significant disagreements; see Table 6.1

Table 6.1   Computed change in ELF field strength in going from ambient day and ambient night conditions to PCA conditions. The calculations refer to transmission from WTF to Tromso at 75 Hz.

|              | LMSC     | NOSC     | PSR      |
|--------------|----------|----------|----------|
| PCA Day #1   | -5.7 dB  | -3.8 dB  | -5.6 dB  |
| #2           | -2.8     | -1.0     | -3.9     |
| #3           | -2.3     | -1.3     | -3.7     |
| PCA Night #1 | -6.4     | -6.8     | --       |
| #2           | -7.9     | -6.2     | --       |

The differences may be due to several factors:

- In running a code with elaborate segmentation of the path it is difficult to avoid introducing differences, e.g.:
  - the actual number of segments used may differ
  - the positions and lengths of the individual segments may vary
  - values of the ground conductivities may be chosen differently because of lack of agreement as to their correct values.
  - the size assumed for the WTF area may not be exactly the same
  - the $N_e$, $N^+$ profiles supplied by LMSC needed some extrapolation to

6-1

F region altitudes (PCA night #2) and to very low altitudes. These extrapolations may introduce minor differences.

It appears probably that a major item involves the different sizes of the WTF region used by LMSC and NOSC, which are 200 km and 500 km, respectively. The WTF transmitter region has low ground conductivity at 75 Hz: $3.2 \times 10^{-4}$ mho/m. The extent of this region is taken to be 200 km in our segmentation of the ELF paths. W. Moler, NOSC, used 500 km for the transmitter region. However, at a distance of 500 km from WTF part of Lake Superior ($\sigma \approx 4$ ohm/m) should be included. Thus the analyst faces a dilemma in choosing the size of the first segment.

One run was made for PCA night #2 for which we extended the first segment out to 900 km. The results were:

> PCA night #2 (Segment 1 size 200 km) - 162.6 dB

> PCA night #2 (Segment 1 size 900 km) - 161.5 dB

It is thus obvious that the size of the segments for the WTF area is of importance, especially when one tries to compare results from various codes in absolute terms.

## 7.0 EFFECTS OF CHANGE IN SOLAR ZENITH ANGLE ALONG THE PROPAGATION PATH

Over a long propagation path the solar zenith angle ($\chi$) will change according to the local time, as will the ionospheric conditions since the effective recombination rates for free electrons are dependent upon time of day. Thus, even during a PCA when the ionization can be assumed to be constant over the whole disturbed polar cap region, the electron density height profile will vary with position.

In order to estimate the magnitude of this effect during a PCA the 4 Aug 72 1144 UT- ionization profile was used to calculate the $N_e$ profiles at different solar zenith angles, of Figure 7.1. No change was assumed to take place in the $N^+$ profile. Waveguide calculations were made for several simulated "seasons", as exemplified in Table 7.1 for a spring equinox situation (21 March 2200 UT) with propagation from day conditions over the transmitter ($\chi = 68.5°$) into night with $\chi = 110°$ at the receiver (Tromso, Norway). Runs were also made with either day or night conditions over the complete path. The results are shown in Table 7.2, and indicate that for more accurate estimates of signal strength for a path like WTF to Tromso the effect of the solar zenith angle variation should be included.

Table 7.1 Approximate conditions along the transmission path from WTF to Tromso on 21 March at 2200 UT.

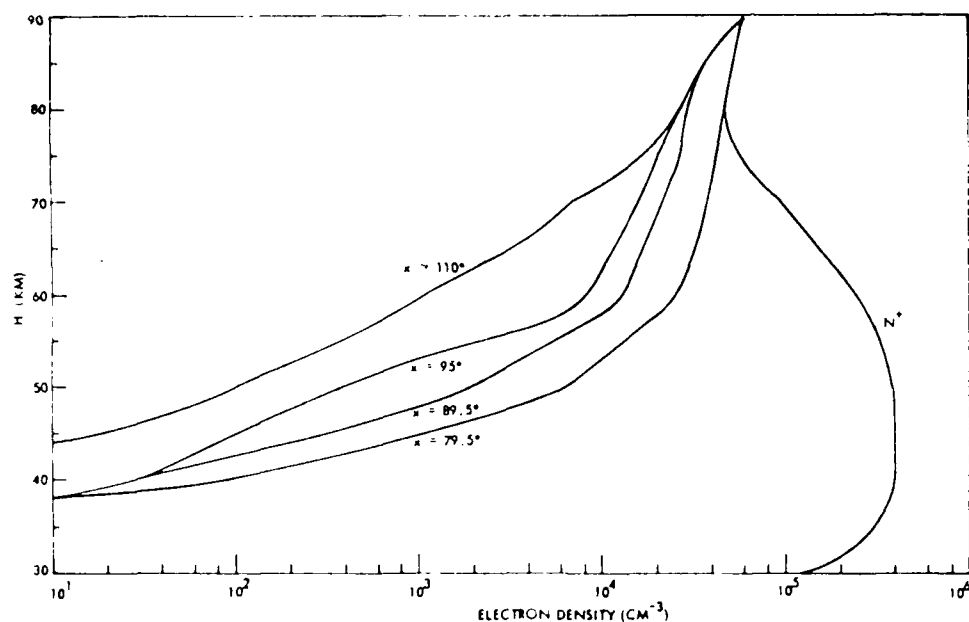| Segment | Range from WTF (km) | Latitude North | Longitude East | Solar Zenith Angle |
|---------|---------------------|----------------|----------------|--------------------|
| 1 | 0 – 200 | $48°$ | $271°$ | $68.5°$ |
| 2 | 200 – 1000 | $52°$ | $274°$ | $72°$ |
| 3 | 1000 – 1800 | $57°$ | $279°$ | $77°$ |
| 4 | 1800 – 2900 | $64°$ | $290°$ | $83°$ |
| 5 | 2900 – 3300 | $68°$ | $302°$ | $89.5°$ |
| 6 | 3300 – 4400 | $71°$ | $318°$ | $94°$ |
| 7 | 4400 – 5800 | $72°$ | $355°$ | $104°$ |
| 8 | 5800 – 6000 | $69°$ | $18°$ | $110°$ |

ELECTRON DENSITY (CM⁻³)

Figure 7.1  Electron density profiles for the 4 Aug 72 (1144 UT) solar
particle event at the four indicated solar zenith angles.  The
positive ion density, taken to be independent of solar zenith
angle, is also shown.

Table 7.2  Calculated field strengths WTF - Norway for SPE of 4 Aug 72.
Variations in electron density with solar zenith angle.

| Solar Zenith | Path Segment | Calculated Field Strength (75 Hz (dB wrt 1A/m) | Calculated Change from Ambient Night (dB wrt 1 A/m) |
|---|---|---|---|
| 79.5° | Whole path | - 156.6 | - 1.9 |
| 110.° | Whole path | - 159.6 | - 4.9 |
| 79.5° | 0 - 2900 km | | |
| 89.5° | 2900 - 3300 | } -158.1 | - 3.4 |
| 95° | 3300 - 4400 | | |
| 110° | 4400 - 6000 | | |

7-2

## 8.0  ELF PROPAGATION CHARACTERISTICS - PHYSICAL INTERPRETATION

As described in Section 2 important recent works have shed light on
the physical understanding of the ELF propagation (Pappert, 1978; Greifinger
and Greifinger, 1978, 1979; Booker, 1980).  In this section we shall describe
the Greifinger and Greifinger (1978 and 1979) work which lends itself
easily to improved understanding of the ionospheric parameters which are
important for ELF propagation.

### 8.1  The Greifinger and Greifinger Approach

Figures 8.1 and 8.2 (Greifinger and Greifinger, 1978) show the relation-
ship between the two heights $h_o$ and $h_1$ (see Section 2), and the variation
of the ELF wave fields and the Joule heating height profiles, respectively.
The two corresponding scale heights $G_o$ and $G_1$ refer to the scale heights at
these heights of the conductivity profile and refractive index, respectively.
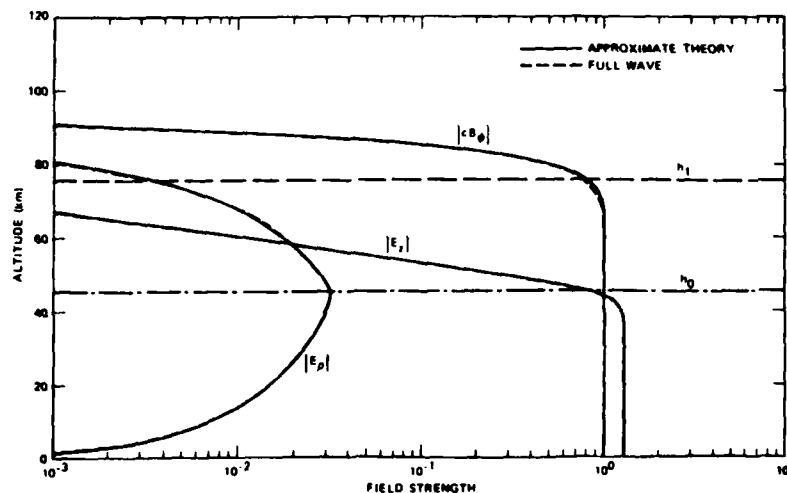


Figure 8.1  Field strength as a function of altitude at a frequency of 50 Hz
for an exponential profile with $h_o$ = 45 km, $G_o$ = 3 km.  The fields
are normalized to $|cB\phi|$ = 1 at the ground (Greifinger and
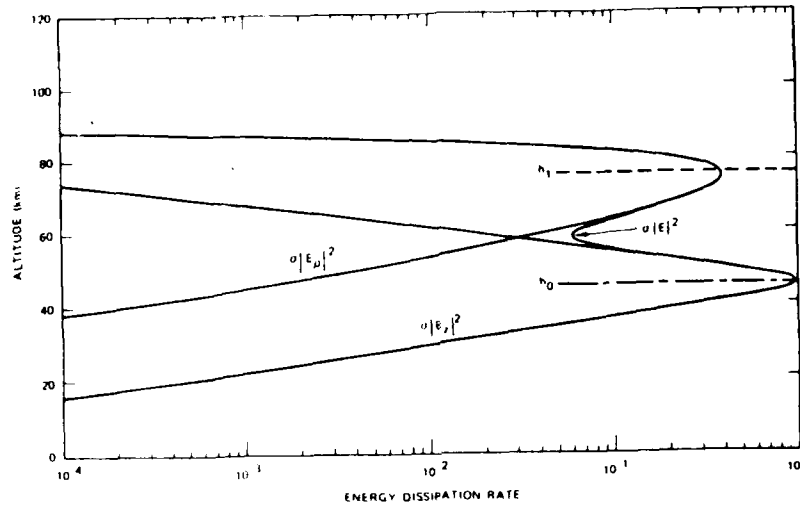Greifinger, 1978).

Figure 8.2  Total and partial energy dissipation rates as a function of 50 Hz for an exponential profile with $h_O = 45$ km, $G_O = 3$ km. The rates are normalized to $|\sigma E|^2 = 1$ at the altitude of maximum dissipation (Greifinger and Griefinger, 1978).

It is noticed that the ohmic heating maximizes at two heights: $h_O$ and slightly below $h_1$. The ELF wavefields rapidly become very small above $h_1$, which may then be regarded as a "practical" upper boundary of the ionosphere as far as ELF propagation is concerned.

Greifinger and Greifinger (1978) give on the basis of their theory the following simple expressions for the ELF propagation parameters:

$$S \approx \left(\frac{h_1}{h_O}\right)^{\frac{1}{2}} \left[ 1 + \frac{i\pi}{4} \left(\frac{G_O}{h_O} + \frac{G_1}{h_1}\right)\right]$$

$$\frac{v}{c} = \frac{1}{\mathrm{Re}(S)} \approx \left(\frac{h_O}{h_1}\right)^{\frac{1}{2}}$$

$$\alpha \approx \left(\frac{h_1}{h_O}\right)^{\frac{1}{2}} \left(\frac{G_O}{h_O} + \frac{G_1}{h_1}\right)$$

where S is the eigenvalue parameter, $v/c$ is the relative wave phase velocity $\alpha$ is the wave attenuation coefficient. This theory applies to cases where there is no significant penetration of the electromagnetic field to altitudes where anisotropy due to the earth's magnetic field must be taken into account.

In their 1979 paper Greifinger and Greifinger extend the 1978 work to include the effects of anisotropy, assuming for simplicity a vertical terrestrial magnetic field. The validity is thus limited to higher magnetic latitudes. The parameters which determine the propagation constant differ for daytime and nighttime ionospheric conditions. In both cases, two parameters which enter are the frequency-dependent altitude $h_o$, at which the conduction current parallel to the magnetic field becomes equal to the displacement current, and the local scale height of the parallel conductivity, $\sigma_o$.

Under daytime conditions, two additional pairs of altitudes (frequency dependent) and scale heights appear as parameters. One pair is the altitude at which the local reciprocal wave number for vertically propagating O wave becomes equal to the local scale height of the refractive index, and the scale height of this refractive index. The other pair is the corresponding quantities for vertically propagating X (whistler) waves. It is assumed in this paper that these altitudes are attained in a region of the ionosphere where $|\sigma_H| > |\sigma_P|$, $\sigma_H$ being the Hall conductivity and $\sigma_P$ the Pedersen conductivity. Under these conditions, which apply over a substantial altitude range, the two pairs of parameters become identical, and the analysis is somewhat simpler. The vicinity of the single altitude $h_1$

8-3

is in this case a region of reflection rather than of significant heating, as was the case for the isotropic ionosphere. The O wave undergoes nearly total reflection at this altitude, but some of the X wave energy leaks out of the waveguide, thereby contributing to the attenuation.

For typical nighttime conditions, a sharp reflecting E-region bottom may be encountered before the local reciprocal wave number becomes equal to the local scale height. Under such circumstances the altitude of the E-region bottom replaces $h_1$ as a parameter, and the refractive index scale height is replaced by the local wavelength on the E-region side of the bottom. Approximate expressions for the propagation parameters are derived similar in form to those given above for the 1978 theory.

These theories have been coded and have been satisfactorily tested at 50 Hz using the exponential conductivity profiles for which results are given in the two papers. In addition calculations made at LMSC with the NOSC full wave code using the exponential conductivity profile specified in the 1979 paper yield results in agreement with those obtained by William Moler of NOSC, which are given in that paper.

In Figures 8.3 through 8.7, some results of calculations applying the Greifinger and Greifinger theory to five of our test profiles are given.

Altitude profiles are shown of electron and ion densities, and electron and ion conductivities and wavelength in the ionized medium at 75 Hz.

In Section 9 we shall give some comparison between fullwave results using the NOSC code and values based upon the theory described here.
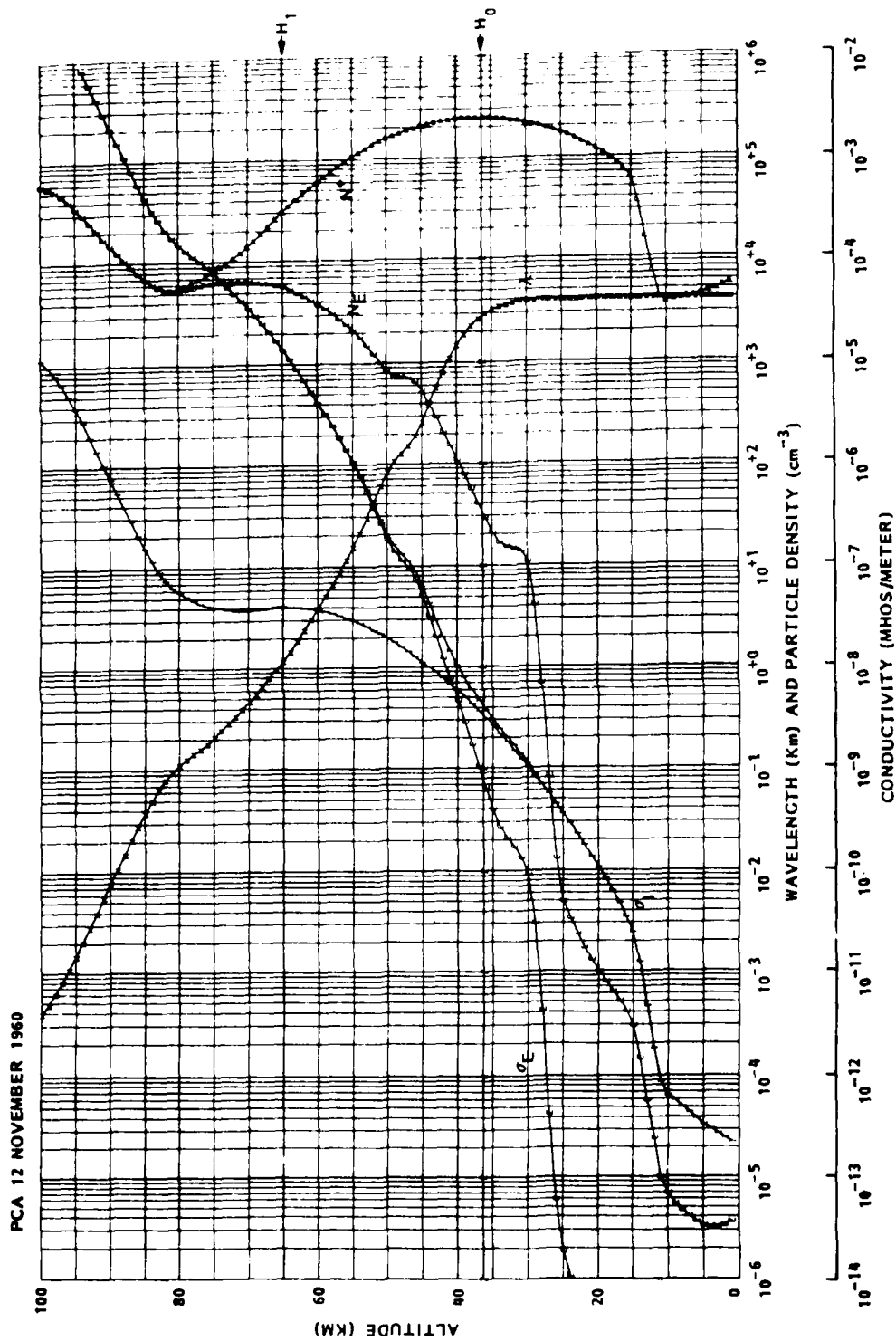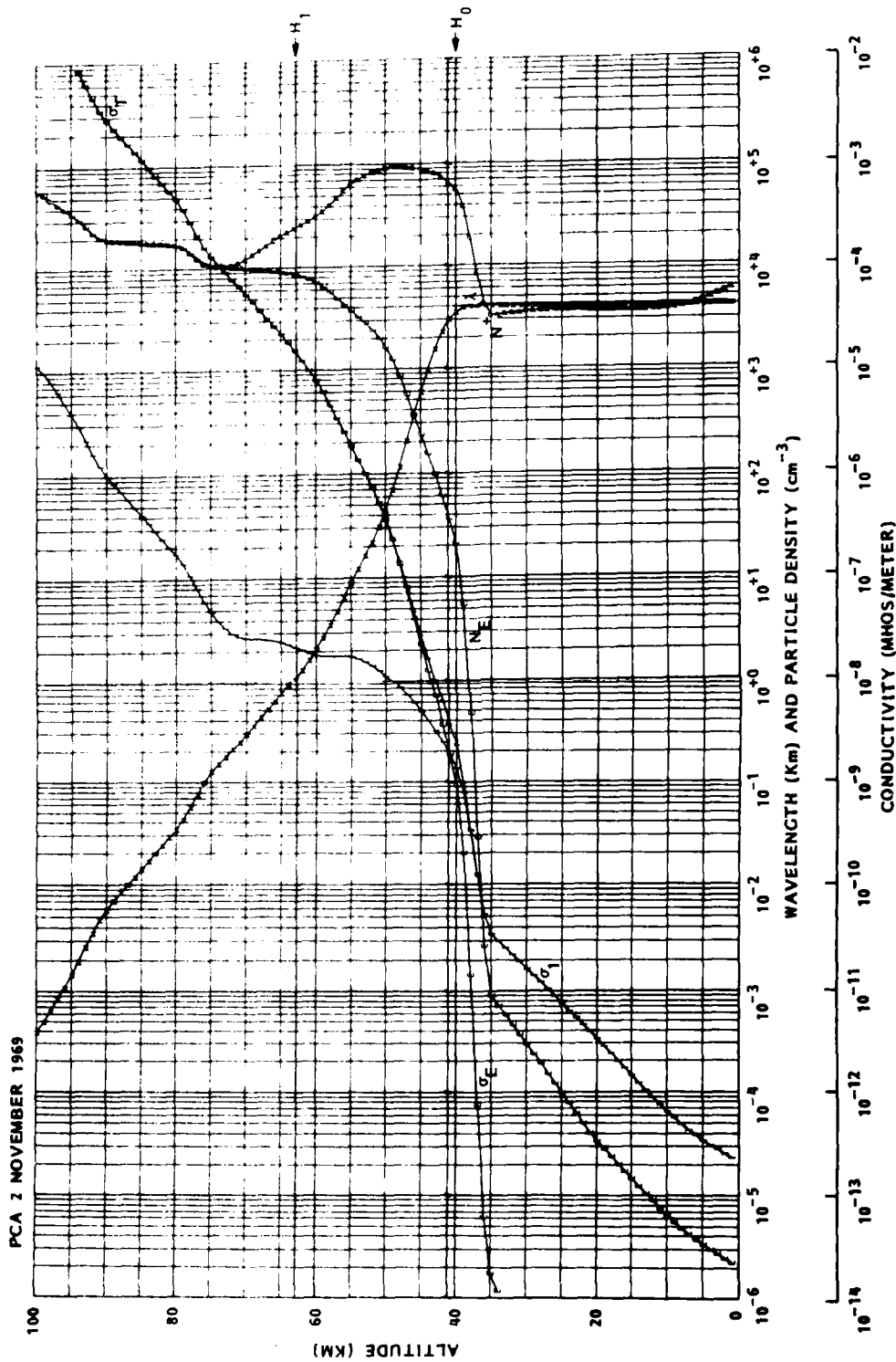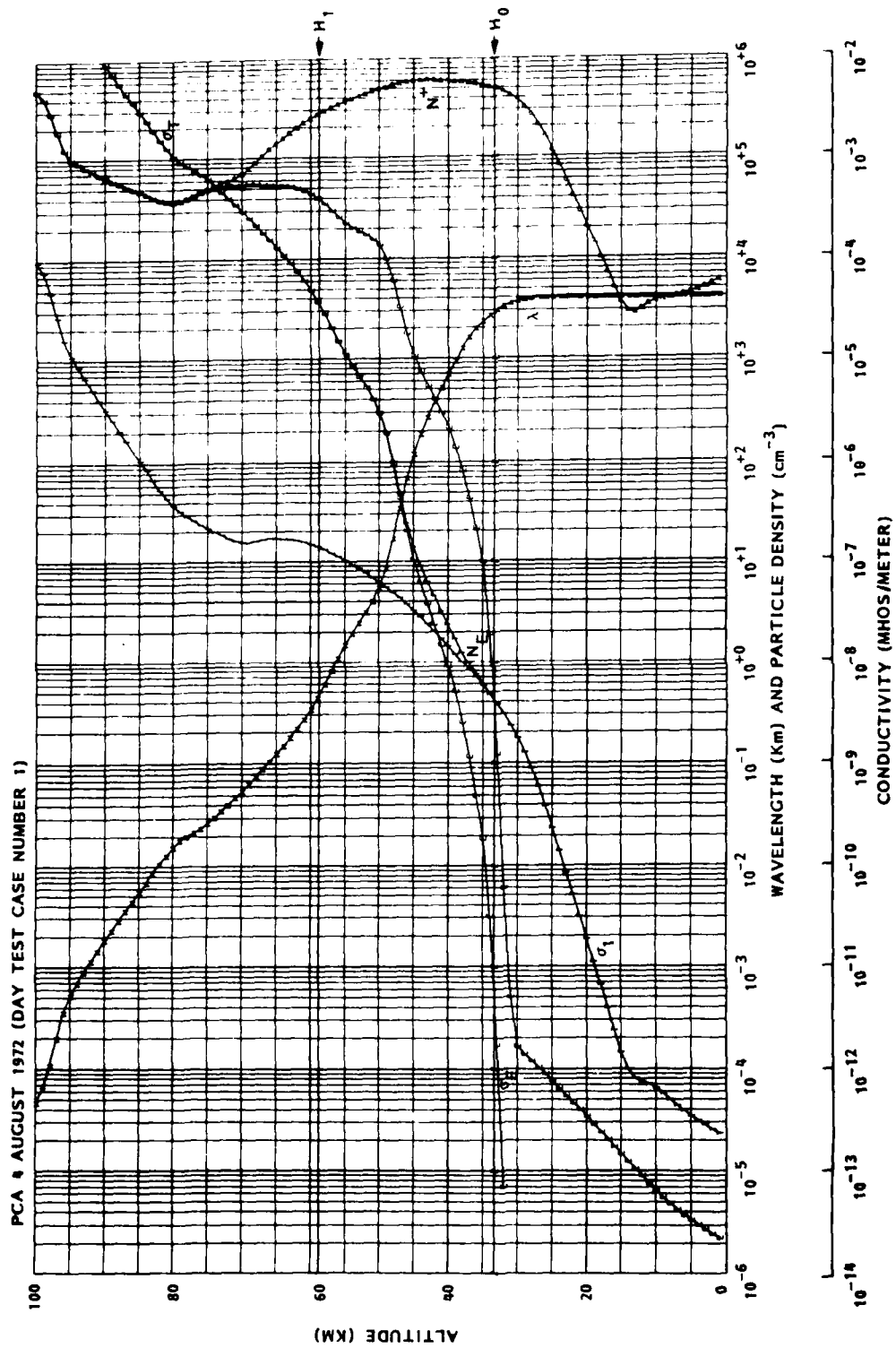
Figure 8.3 Altitude profiles of electron and positive ion densities ($N_E$, $N^+$) in $cm^{-3}$, electron, ion and total conductivities ($\sigma_E$, $\sigma_I$, $\sigma_T$) and wavelength in the medium ($\lambda$) in meters at 75 Hz for the PCA of 12 November 1960.

**LOCKHEED PALO ALTO RESEARCH LABORATORY**
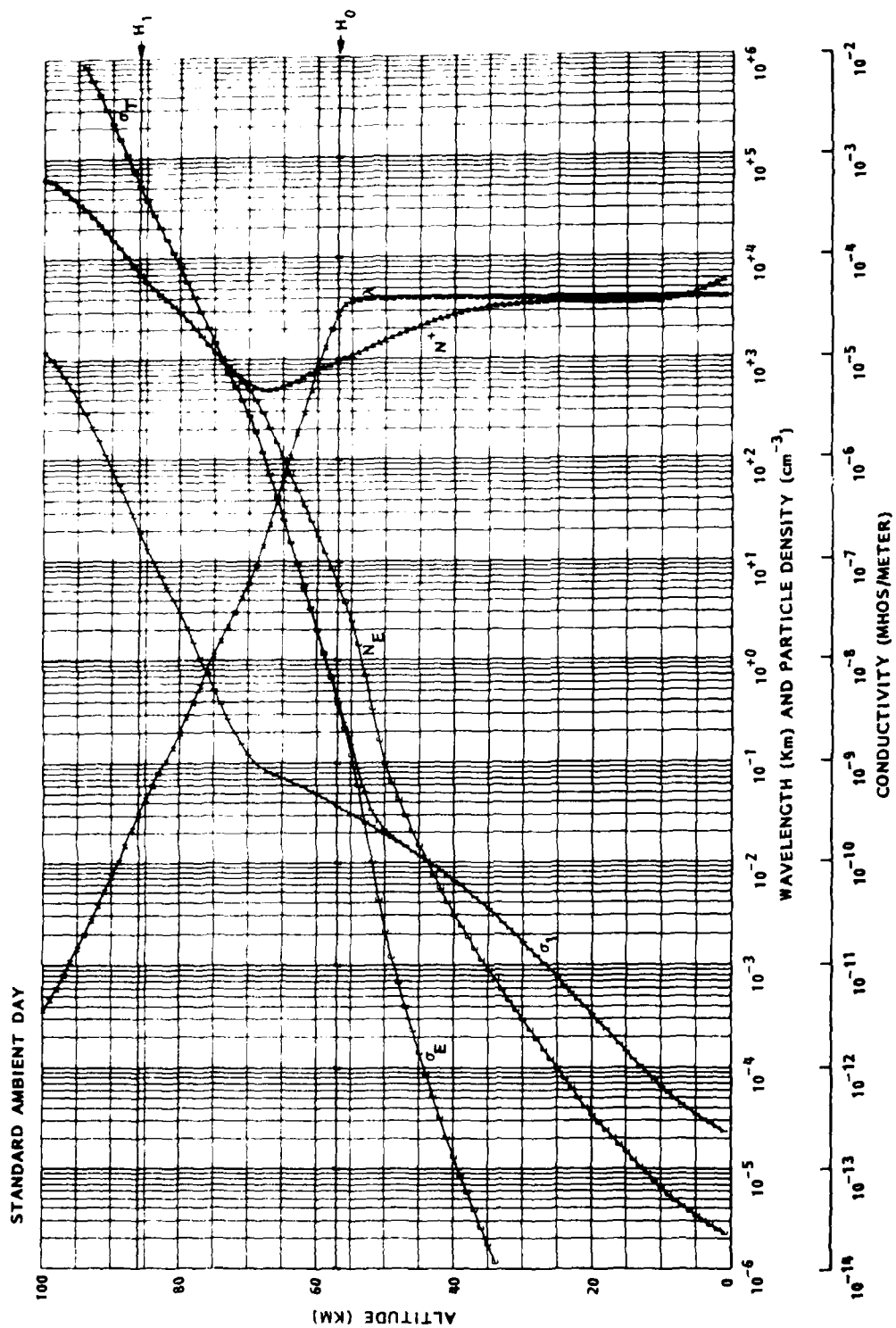
LOCKHEED     MISSILES     &     SPACE     COMPANY     INC

Figure 8.4 Altitude profiles of electron and positive ion densities ($N_E$, $N^+$) in $cm^{-3}$, electron, ion and total conductivities ($\sigma_E$, $\sigma_I$, $\sigma_T$), and wavelength in the medium ($\lambda$) in meters at 75 Hz for the PCA of 2 November 1969.
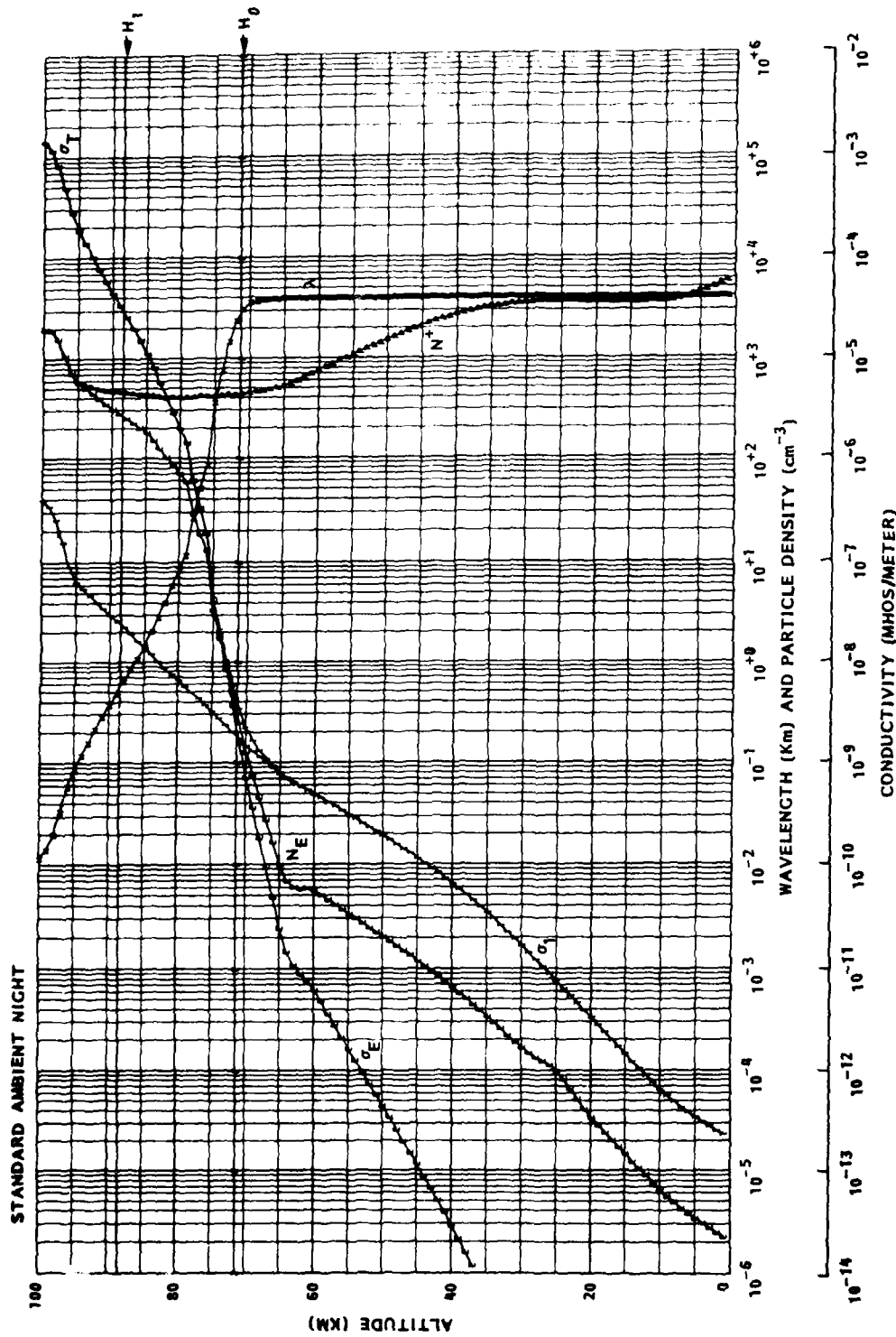
Figure 8.5  Altitude profiles of electron and positive ion densities ($N_E$, $N^+$) in $cm^{-3}$, electron, ion and total conductivities ($\sigma_E$, $\sigma_I$, $\sigma_T$), and wavelength in the medium ($\lambda$) in meters at 75 Hz for the PCA day test case number 1.

Figure 8.6 Altitude profiles of electron and positive ion densities $(N_E, N^+)$ in $cm^{-3}$, electron, ion and total conductivities $(\sigma_E, \sigma_I, \sigma_T)$, and wavelength in the medium $(\lambda)$ in meters at 75 Hz for standard ambient day.

Figure 8.7 Altitude profiles of electron and positive ion densities ($N_E$, $N^+$) in $cm^{-3}$, electron, ion and total conductivities ($\sigma_E$, $\sigma_I$, $\sigma_T$), and wavelength in the medium ($\lambda$) in meters at 75 Hz for standard ambient night.

8-9

## 8.2 Absorption and Reflection of ELF Waves

Using the PCA day and nighttime test cases supplied by LMSC, W. Moler
at NOSC has calculated Joule heating as well as the altitude variations of
the integrated absorption and the reflection density of the downgoing wave
for these conditions. When compared with the actual electron and ion density
variation with height, the variations of the above entities reveal interesting
characteristics of ELF propagation.

As an example, in Figures 8.8 and 8.9 we have plotted the profiles
for the PCA day test case #1 for 75 Hz. Figure 8.8 clearly shows the
importance of the enhanced ion concentration, peaking approximately at 40 km.
The relative heating loss (dotted curve) indicates that the maximum Joule
heating occurs at 35 km. Integrated absorption in dB/1000 km (dash-dotted
curve) furthermore shows that approximately 1.3 dB out of the total 2.1
dB/1000 km can be associated with this layer. The free electrons cause
Joule heating mainly at higher altitudes, maximizing around 60 km. In
Figure 8.4 the reflection density profile of the downgoing wave (dash-
dotted curve) indicates that the region between 50 and 80 km is the main
reflecting region during the PCA conditions.

Similar curves have been obtained for other $N_e$ and $N^+$ profiles. In
the case of quiet ambient nighttime conditions, the ELF fields penetrate
to greater heights before reflection takes place. In this case the Joule
heating, essentially due to electrons, occurs within quite a narrow altitude
interval between 65 and 75 km, whereas the ions cause another maximum at
around 110 km. Also, in this case there is only an insignificant contribution
to the attenuation from Joule heating below 40 km. Significant contributions
to the $H_\phi$ field (at ground level) are coming from altitudes between 100-120 km
but altitudes up to about 160 km do contribute.

8-10

**LOCKHEED PALO ALTO RESEARCH LABORATORY**
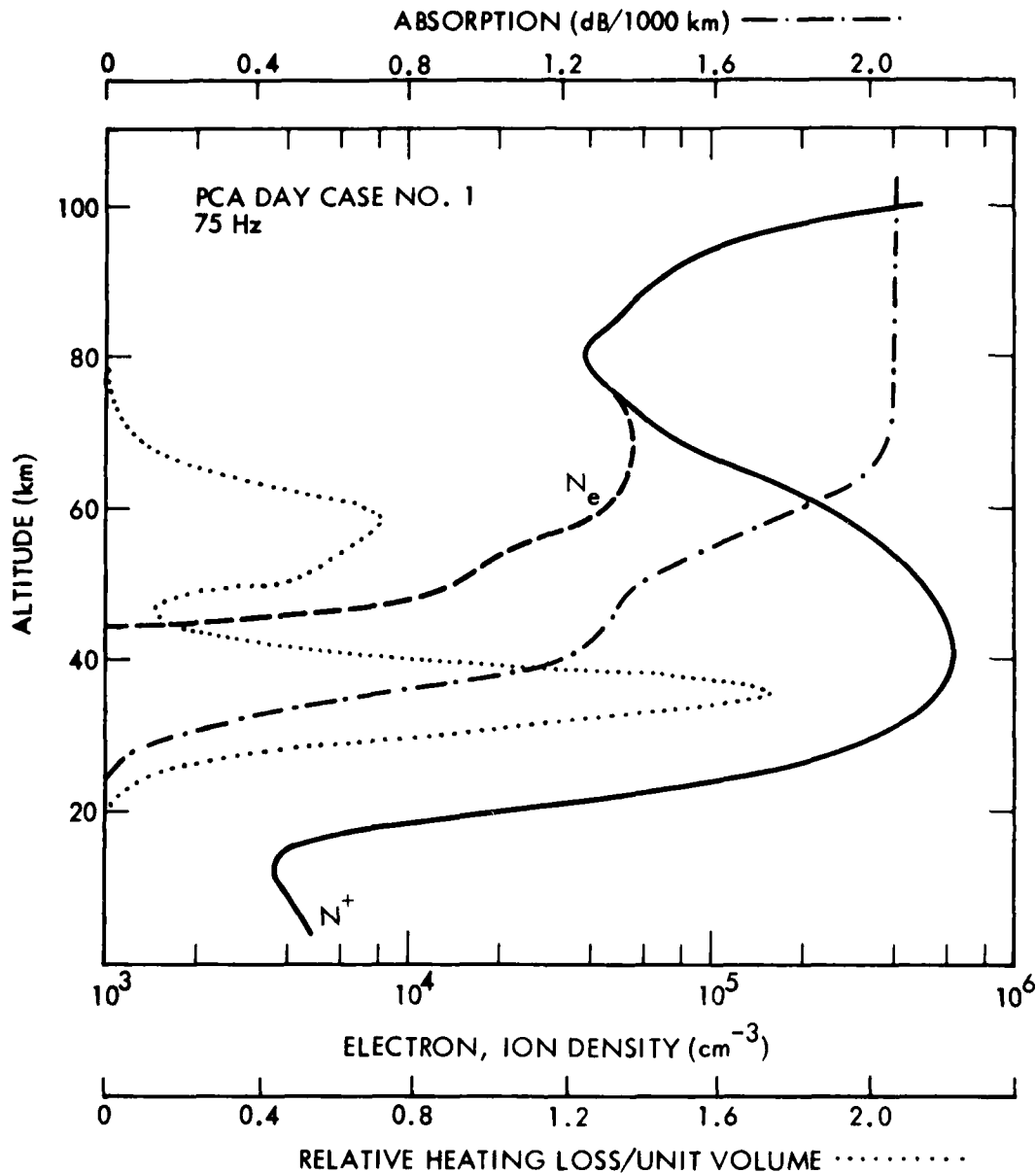LOCKHEED MISSILES & SPACE COMPANY INC

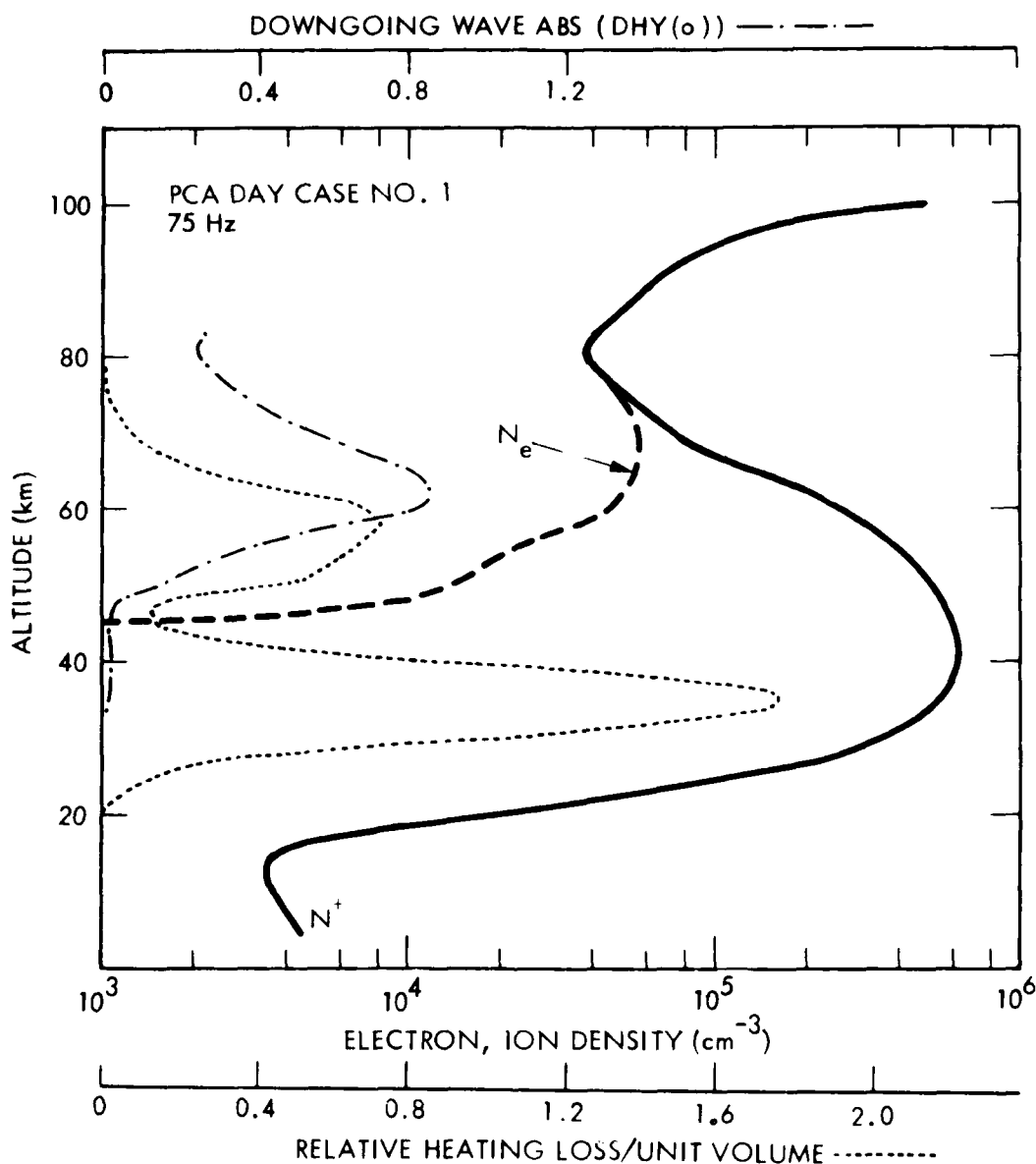Figure 8.8  Altitude variation of ionospheric and ELF characteristics
for PCA daytime conditions (test case #1).

- $N_+$, ion density (heavy, solid curve)
- $N_e$, electron density (heavy, dashed curve)
- Relative heating loss/unit volume (dotted curve)
- Integrated Absorption (dB/1000 km) (dash-dotted curve)

The last two curves were computed by W. Moler, NOSC, for a frequency

of 75 Hz for the pictures $N_+$ and $N_e$ profiles (Moler, 1978).

8-11

DOWNGOING WAVE ABS (DHY(o)) —·—·—



Figure 8.9  Altitude variation of ionospheric and ELF charact.  . 'es for
           PCA daytime conditions (test case #1).

o  N+, ion density (heavy, solid curve)
o  Ne, electron density (heavy, dashed curve)
o  Relative heating loss/unit volume (dotted curve)
o  Reflection density of downgoing wave (Hy)

The last two curves were computed by W. Moler, NOSC for a frequency of 75 Hz
for the pictured N+ and Ne profiles (Moler, 1978).  For further explanation
of the last two curves see Pappert and Shockey (1977).

8-12

## 9.0 ACCURACY ASSESSMENT OF ELF CALCULATIONS

In discussing the accuracy of the ELF calculations one should keep in mind the distinction between accuracies (or inaccuracies) inherent in the actual mathematical treatment of the propagation problem and effects due to less than complete knowledge of the propagation medium and its spatial and temporal irregularities, the ionospheric conductivity profile etc. In an actual ELF calculation, however, it may not be possible to make a sharp distinction between these two classes of possible errors.

As as example we show in Table 9.1 an intercomparison of predicted ELF field strengths for ambient and disturbed condtions based upon use of the identical mathematical computer code (the NOSC code). The discrepancies (in most cases less than 1 dB) are attributed to slightly different ways of segmenting the propagation path, different values for ground conductivities, or other small differences in organizing the computer code run.

Table 9.1 Comparison between ELF absolute field strength calculations at 75 Hz for the path WTF to Tromso.

| Condition | LMSC dB/1A/m | NOSC dB/1A/m |
|---|---|---|
| Day, ambient | −154.7 | −155.4 |
| Night, ambient | −154.7 | −154.6 |
| Day PCA #1 | −160.4 | −159.2 |
| Day PCA #2 | −157.5 | −156.4 |
| Day PCA #3 | −157.0 | −156.7 |
| Night PCA #1 | −161.1 | −161.4 |
| Night PCA #2 | −162.6 | −160.8 |

* The NOSC data supplied by W. Moler have been adjusted by −1.6dB due to a different value used for the soil conductivity under the WTF transmitter (NOSC data were actually computed for $\sigma = 2.2 \cdot 10^{-4}$ mho/m, whereas the field strength values in the table are normalized to $\sigma = 3.2 \cdot 10^{-4}$ mho/m, which is used by LMSC).

Different mathematical approaches to the propagation problem may yield results with less than perfect agreement. As an example, the results of a comparison between altitude profiles of the Joule heating calculated by E. C. Field and by W. Moler for PCA day test case #1 is given in Figure 9.1. The curves have been normalized to provide equal values at the lower maximum in the 30-35 km altitude regime and they indicate that a reasonable agreement exists between two approaches. Both calculations show that the largest attenuation of 75 Hz waves occurs between approximately 25 to 40 km with a secondary maximum around 60 km. The former maximum may be linked with high ion densities, whereas the latter maximum is mainly due to the free electrons.

Such differences may indicate the uncertainty inherent in the various theoretical approaches.

A further example of this point is provided in Table 9.2, where we compare results obtained for a variety of electron/ion profiles by use of the full wave method and the Greifinger and Greifinger approach discussed in Sections 2 and 8. It is noticed that some differences are present, but the remarkable agreement between the full wave method and a simplified theory is striking. In consideration of Table 9.2, it should be noted that under highly disturbed conditions the approach used in the Greifinger and Greifinger (1978) theory is preferred as stated in their 1979 paper.
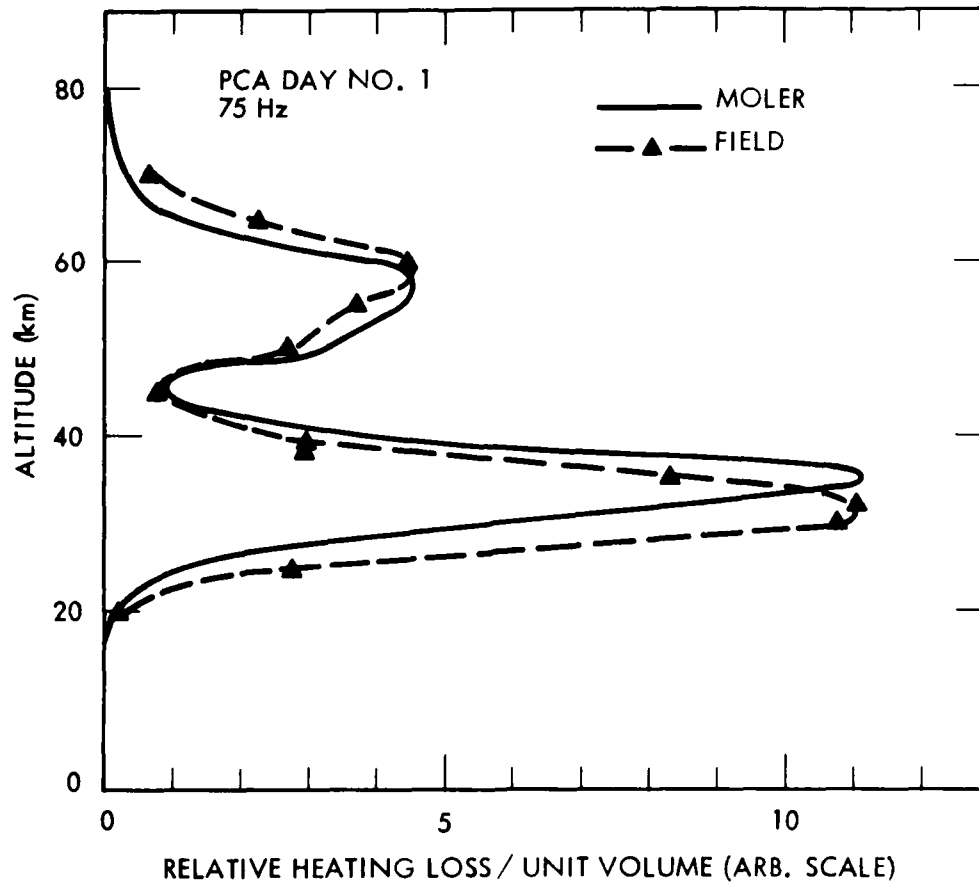
Figure 9.1  Comparison of Joule heating for PCA day test case #1
by E. C. Field (PSR) and W. Moler (NOSC).  The curves
have been normalized to give equal values at the lower maxi-
mum.

**LOCKHEED PALO ALTO RESEARCH LABORATORY**

L O C K H E E D    M I S S I L E S    &    S P A C E    C O M P A N Y    I N C

Table 9.2  Comparison of calculation of ELF relative phase velocity and
attenuation rate at 75 Hz using the full wave method (LMSC) and the
approximate theory of Greifinger & Greifinger (1978, 1979).  LMSC
values are given for the WTF area and the Norwegian Sea.

| Profile | | | $v/c$ | $\alpha$ (dB/Mm) | $h_0$ (km) | $G_0$ (km) | $h_1$ (km) | $G_1$ (km) |
|---|---|---|---|---|---|---|---|---|
| PCA Day | LMSC | | 0.74 | 2.61 | – | – | – | – |
| Test Case | | | 0.75 | 2.35 | | | | |
| #1 | G&G | 78 | 0.77 | 2.68 | 33.4 | 4.3 | 58.7 | 3.4 |
| | | 79 | 0.77 | 2.71 | 33.4 | 4.3 | 58.7 | 3.6 |
| PCA | LMSC | | 0.75 | 1.80 | – | – | – | – |
| 2 Nov 69 | | | 0.79 | 1.51 | | | | |
| | G&G | 78 | 0.81 | 1.71 | 41.3 | 2.1 | 63.4 | 5.2 |
| | | 79 | 0.80 | 1.84 | 41.3 | 2.1 | 62.7 | 5.9 |
| PCA | LMSC | | 0.73 | 3.04 | – | – | – | – |
| 12 Nov 60 | | | 0.73 | 2.94 | | | | |
| | G&G | 78 | 0.76 | 2.80 | 36.4 | 4.3 | 66.0 | 5.2 |
| | | 79 | 0.75 | 3.21 | 36.4 | 4.3 | 65.0 | 7.3 |
| Ambient | LMSC | | 0.82 | 1.37 | – | – | – | – |
| Day | | | 0.83 | 1.19 | | | | |
| | G&G | 78 | 0.85 | 0.90 | 56.7 | 1.6 | 78.4 | 3.0 |
| | | 79 | 0.84 | 1.40 | 56.7 | 1.6 | 80.2 | 6.2 |
| Ambient | LMSC | | 0.84 | 1.17 | | | | |
| Night | | | 0.85 | 0.98 | | | | |
| | G&G | 78 | 0.90 | 0.84 | 71.3 | 1.9 | 88.4 | 3.8 |
| | | 79 | 0.81 | 1.85 | 71.3 | 1.9 | 93.0* | |

\*  Altitude of E-region bottom

LOCKHEED PALO ALTO RESEARCH LABORATORY

LOCKHEED   MISSILES   &   SPACE   COMPANY   INC

## 10.0 AMBIENT PROFILES OF ELECTRON AND ION DENSITY

### 10.1 Introduction

Although our studies of ELF propagation are mostly concerned with the ionosphere perturbed by precipitating particles it has been necessary to use ambient profiles of electron and ion density. Our long path calculations, e.g. from WTF to Tromso, are segmented following ground conductivity variations and frequently one or more segments, such as the first one at the WTF transmitter are considered to have ambient ionospheric conditions. For comparison purposes, calculations have also been performed in which all segments of the long parth are given the same ambient profile. The profiles were typically those used by Pappert and Moler and colleagues (e.g. Pappert and Moler, 1974). These profiles, shown in Fig. 3.2, have come to be called the "standard" ambient day and night profiles.

For modeling the ionosphere realistically over a long segmented path, taking into account the variations along the path in local time as well as atmospheric density and temperature, a good ion chemistry model is needed. Ideally, the model should compute accurately ambient as well as disturbed conditions. Our model has been adjusted to fit PCA daytime disturbed conditions during the 2 November 1969 and 4 August 1972 events. The model has been used in an effort to make realistic calculations of those events including ambient conditions over the WTF transmitter. Ambient calculations for ⊃ 1972 event are shown in Figure 10.1. The figure compares the standard ambient day profiles with those calculated for WTF at one time during the actual event and during a simulated event such as the 4 August 1972 event but shifted in season to the winter solstice. It may
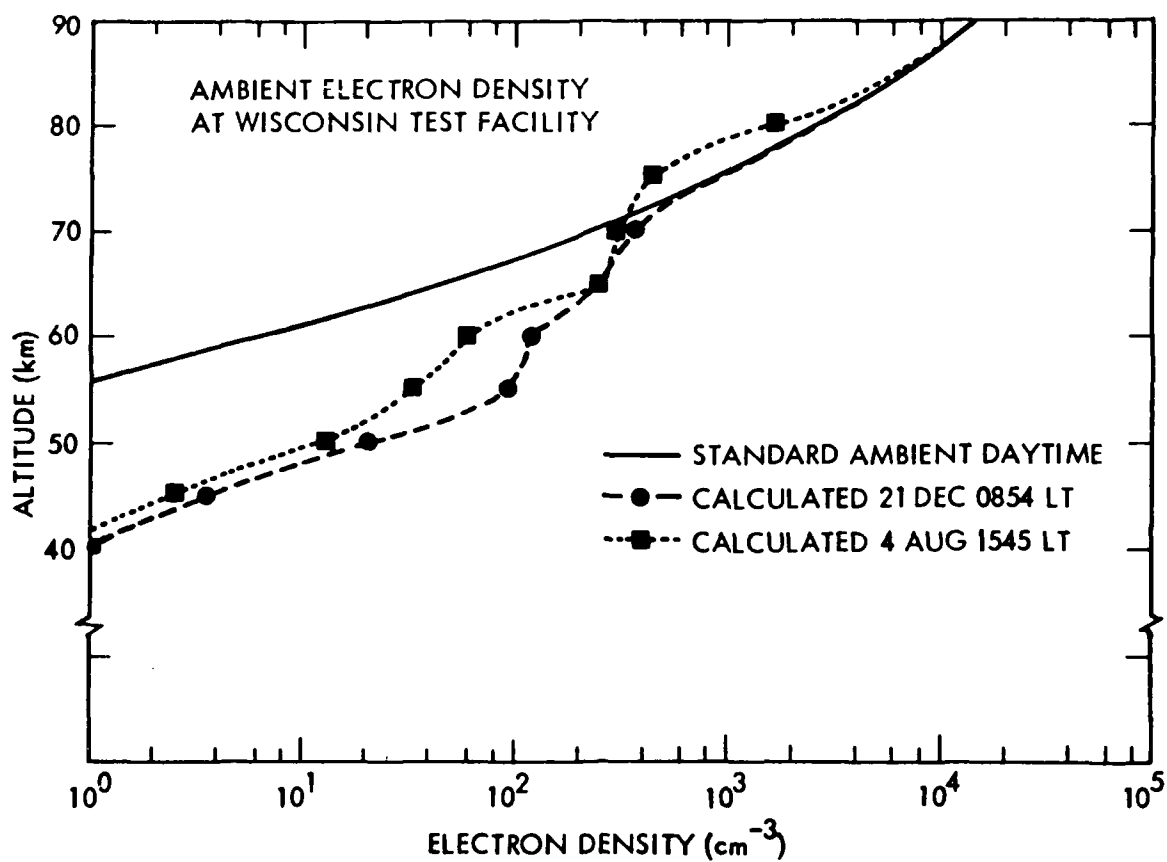
Figure 10.1  Comparison of ambient daytime electron density profiles at WTF
for the two seasons and times of day with the standard ambient
daytime profile discussed earlier in Section 3.

10-2

be noted that these calculated profiles differ from the standard profile,
having larger electron densities at the lower altitudes. As will be shown
later, recent daytime measurements of ambient profiles tend to confirm such
larger densities. These larger densities are significant, leading to a
weakening of the ELF signal at 75hz over the WTF to Tromso path by 0.7 dB
relative to standard ambient day used over the WTF segment.

There have been many measurements of electron and ion density profiles
since the "standard" profiles of Figure 3.2 were generated, particularly
during daytime. There are fewer nighttime measurements and because of their
scatter it would be difficult to improve the present standard night
profiles. Also the present nighttime profile, used in NOSC code calculations
for the WTF to Connecticut path yielded good agreement with measurements
made over the path (Imhof et al., 1976). The purpose of this section is to
propose a new standard daytime profile based on recent measurements.

## 10.2 Proposed New Standard Ambient Profile

In developing this profile considerable use was made of the work of
Keefer (1975) who assembled some representative measured ambient profiles.
Several daytime profiles are shown in Figure 10.2 along with the present
standard daytime profile. All of the experimental profiles are based on
mid-latitude measurements made at a solar zenith angle near $\chi = 60^{\circ}$. Each
of the three profiles within the range 60 to 160 km represents a concensus
by the authors of a number of measurements. The E region profile of Maeda
(1972) was based on winter, low solar activity conditions and differs very
little from the standard ambient day model. The Mechtly et al. (1972) curve
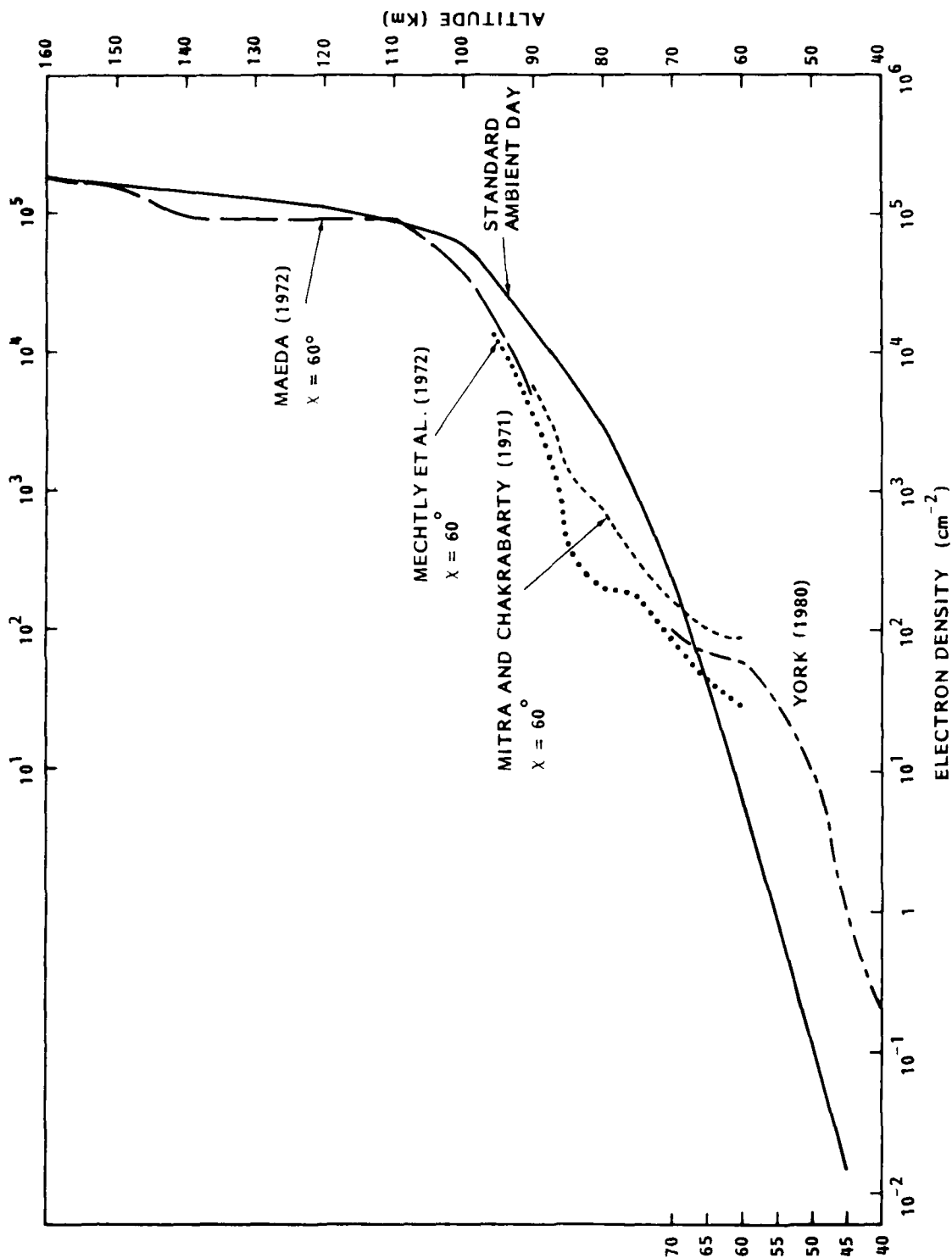
10-3

Figure 10.2  Altitude profiles of some recent daytime measurements of electron density compared with the present standard ambient daytime profile.

10-4

is a mean of quiet sun measurements. The curve of Mitra and Chakrabarty
(1971) is a concensus of measurements made by a number of different methods
in the 65-90 km range. The lower altitude profile is based on the work of
York (e.g., 1980) who has been reevaluating rocket-borne probing techniques
for measuring electron densities, among them the blunt probe (York, 1979).
This re-analysis leads to considerably larger electron densities below 60 km
than specified by the present standard ambient day profile. We have based
the profile shown between 40 and 70 km on measurements reported by York (1980)
made at White Sands in October at a solar zenith angle near $60^{\circ}$.

These more recent results, as shown in Figure 10.2, suggest that the
present daytime standard ambient profile is considerably low at altitudes
below 60 km, is somewhat too high between 60 and 100 km, and above 100 km is
reasonably good. We suggest that the new composite ambient profile shown in
Figure 10.3 be used for comparison purposes to represent daytime conditions
in future ELF propagation studies. Of course, ambient electron density profiles
depend on solar zenith angle, latitude, season and solar activity and no single
profile can represent all of these conditons. Also shown in Figure 10.3
are the present standard profile and a profile ($\chi = 75^{\circ}$) used by Booker (1980).

Figure 10.3 also suggests a positive ion ambient profile to be used with
the new electron profile. It was calculated using relations from simple lumped
parameter ionization theory:

$$N^{+} = N_{e} + N^{-}, \tag{1}$$

specifying charge neutrality, and

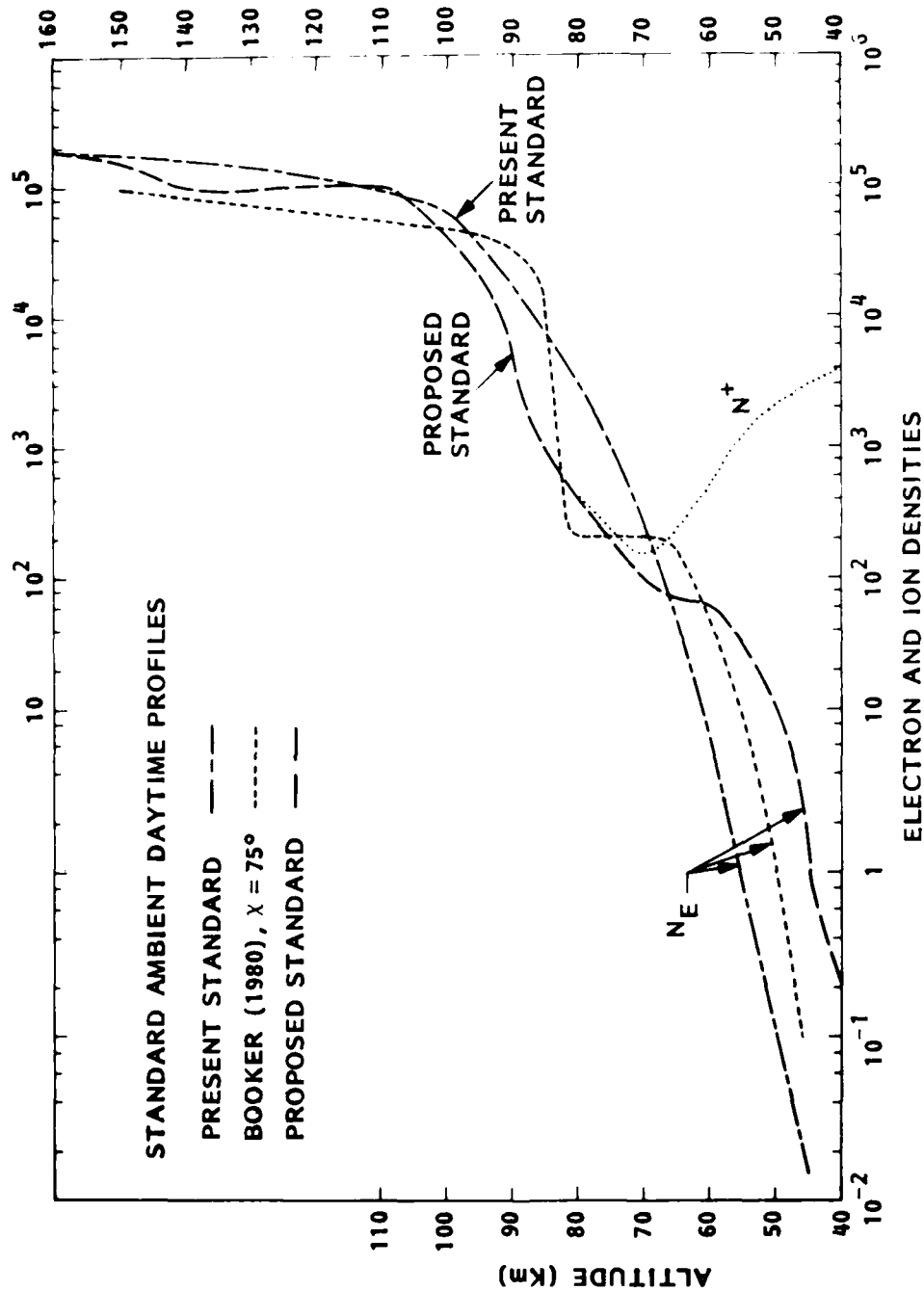$$Q = \alpha_{D} N^{+} N_{e} + \alpha_{I} N^{+} N^{-} \tag{2}$$

10-5

Figure 10.3  Proposed new standard altitude profiles of electron and ion density compared with the present standard profile and one used by Booker (1980).

10-6

the steady state equation for positive ions, where Q is the ion pair production rate, $\alpha_D$ is the electron-ion recombination rate, and $\alpha_I$ is the ion neutralization rate. Equations (1) and (2) may be combined to yield

$$N^+ = (\sqrt{x^2 + y} - x)/2 \tag{3}$$

where $x = N_e (\alpha_D/\alpha_I - 1)$ and $y = 4 Q/\alpha_I$. The value $3 \times 10^{-6}$ $cm^3$ $sec^{-1}$ was assumed for $\alpha_D$ and the values of $\alpha_I$ are those of Table 5.1  The values of Q, galactic cosmic ray (GCR) production rates, are calculated from the formula of Heaps (1978) for average solar conditions and a magnetic latitude of $57^0$ N corresponding approximately to the Wisconsin Test Facility location. The GCR Q rates were augmented with Lyman alpha production rates above 70 km.

Calculations have been made of ELF propagation at 75 Hz from WTF to Tromso using the suggested new profiles supplemented by the old standard values below  40 km for comparison with similar calculations for the old standard. Of course the segmentation and ground conductivities were identical. The resulting  calculated overall signal attenuation is 1.0 dB larger over the 6000 km path, a significant change. This change is due to the larger electron densities in the new profile near 50 km. The effect of the new profile is to produce larger excitation factors which tend to increase the received signal but larger attenuations which reduce it to produce the net effect at the receiver of signal strength 1 dB smaller.

11.0 ION CHEMISTRY MODEL IMPROVEMENT

11.1 Introduction

Because of the strong dependence of ELF propagation on ionospheric conditions demonstrated in this and other studies is it very important to have the capability of making accurate predictions of electron and ion density profiles, given altitude profiles of ion pair production rates derived from satellite or rocket measurements of energetic particle precipitation. This is particularly important for disturbed conditions such as those occurring in polar cap absorption events because of the potentially large effects in reducing ELF signals transmitted through the polar regions.

The theory of ELF propagation in the earth-ionosphere waveguide has been advanced as discussed earlier in this report to the point where Booker (1980) states that "at present, and probably for a long time to come, overall error in such calculations* is likely to be controlled by imperfect knowledge concerning worldwide behavior of the ionosphere". The pertinent available data on the ionosphere should be used to improve the predictive capability of ionospheric models. A good model will be needed when a field campaign is conducted to test ELF propagation theory during a PCA event. In order to validate ELF propagation theory, over long test paths, ionospheric prediction will be needed to extend the ionospheric measurements which can, as a practice matter, be made only over limited time spans and limited spatial extents.

One of our present objectives is to use more of the electron density data measured during the 4 August 1972 solar particle or PCA event by the SRI Chatanika radar than has been done in our previous modeling efforts. As discussed in our previous report (Imhof et al. 1980) previous modeling has

---

*Calculations such as those made by Booker (1980) and by use of the NOSC code (Pappert and Moler 1974, 1978).

been based on data at some 28 points in time.  The ion chemistry model des-
cribed in that earlier report agrees reasonably well with the daytime data
from the August 1972 event, and also with measurements made during the
2 November 1969 PCA (Swider et al. 1978).  These results are shown in Figures
11.1 and 11.2.  There was however, a lack of agreement in magnitude with the
measurement  made at one time at 60 km altitude in deep twilight near midnight
August 4/5 1972; the model predicted a significantly smaller value.  The data
from the 1969 event measured during sunrise show a time lag in the rise of
electron density relative to that predicted by our model and by the model of
Swider et al. (1978).  We have devoted our attention particularly to these
twilight modeling problems during the present effort.  Accurate modeling of
twilight effects is important for prediction of ELF propagation through twi-
light regions near the solar terminator.


11.2 The SRI Data

These data, made available by R. Vondrak of SRI International, consist of
raw electron densities measured by the Chatanika incoherent scatter radar in
the time period 3-7 August 1972 UT including the main peak of the event on
4 August.  The data are based on 10 minute averages of the received signal and
are available typically for over 100 of the 144 such periods during the day.
The data has been interpolated between the actual altitudes of measurement to
altitudes from 50 to 80 km separated by 5 km.  The data provided was not fully
corrected for receiver recovery and a second correction has been applied
following the analysis of Watt (1975).  The data for 70, 60 and 50 km on 4 and
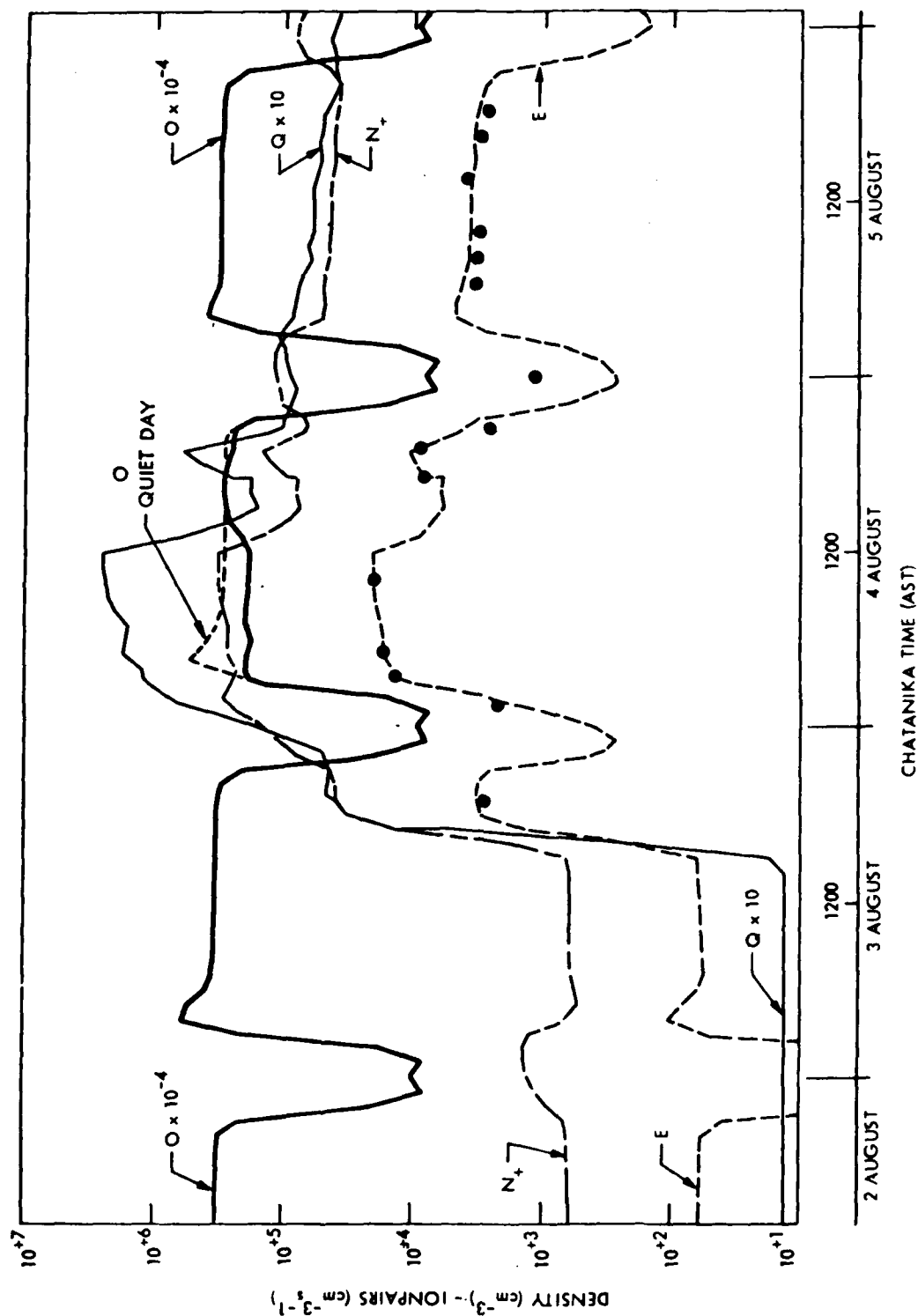5 August 1972 UT are presented in Figures  11.3 to 11.5.  The 60 and 70 km data are

11-2

Figure 11.1  Plot of experimental ion pair production rate and calculated electron density, positive ion density, O atom density vs time at 60 km altitude during SPE72.  The dots are the experimental electron density data from Chatanika radar measurements.
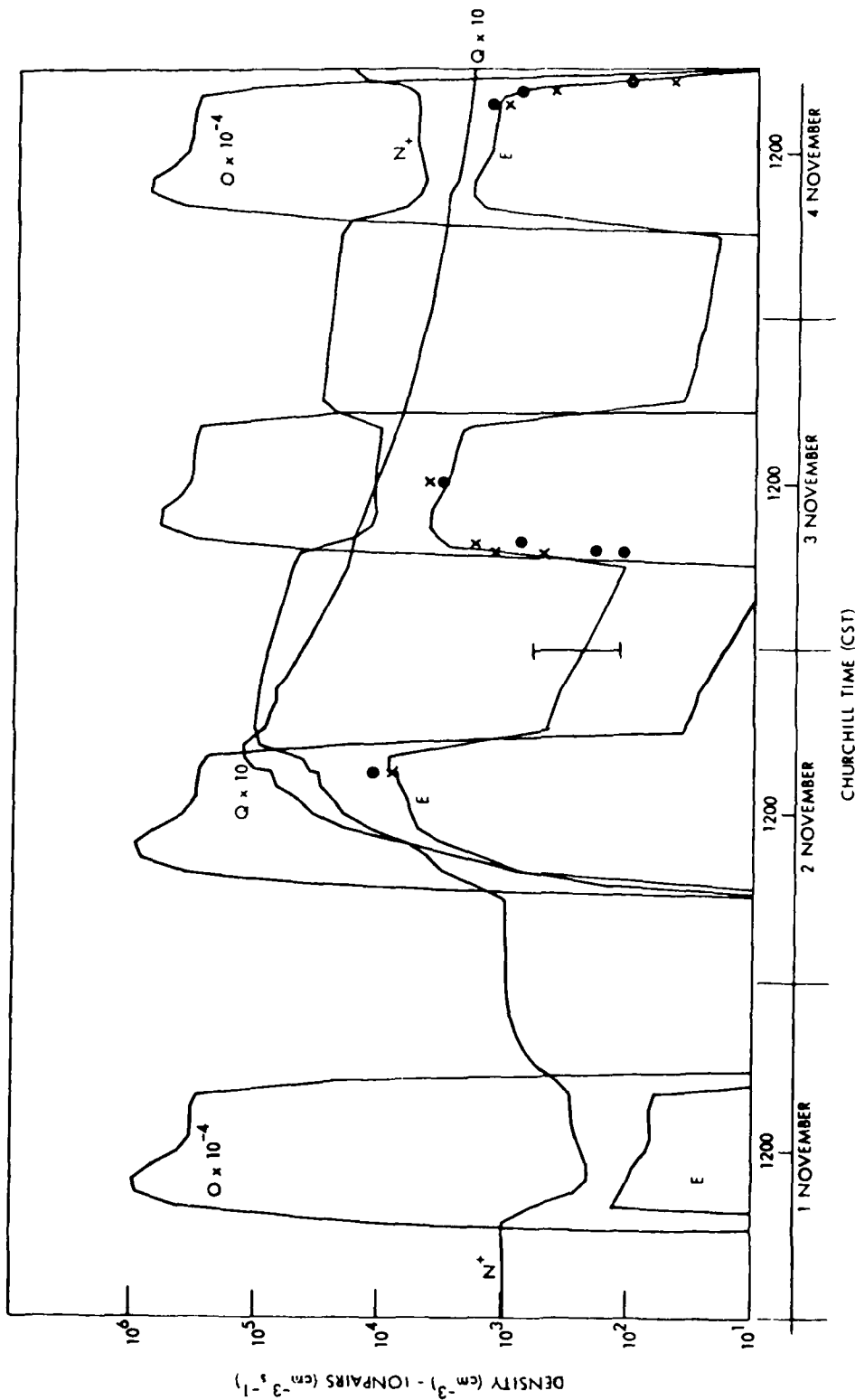
Figure 11.2  Plot of experimental ion pair production rate and calculated electron density, positive ion density, O atom density vs time at 60 km altitude during PCA69. The dots are experimental electron densities and the crosses are calculated electron densities from Swider et al. (1978).  The data range indicated at 0005 Cst 3 November is based on measurements reported by Ulwick (1972).

11-4
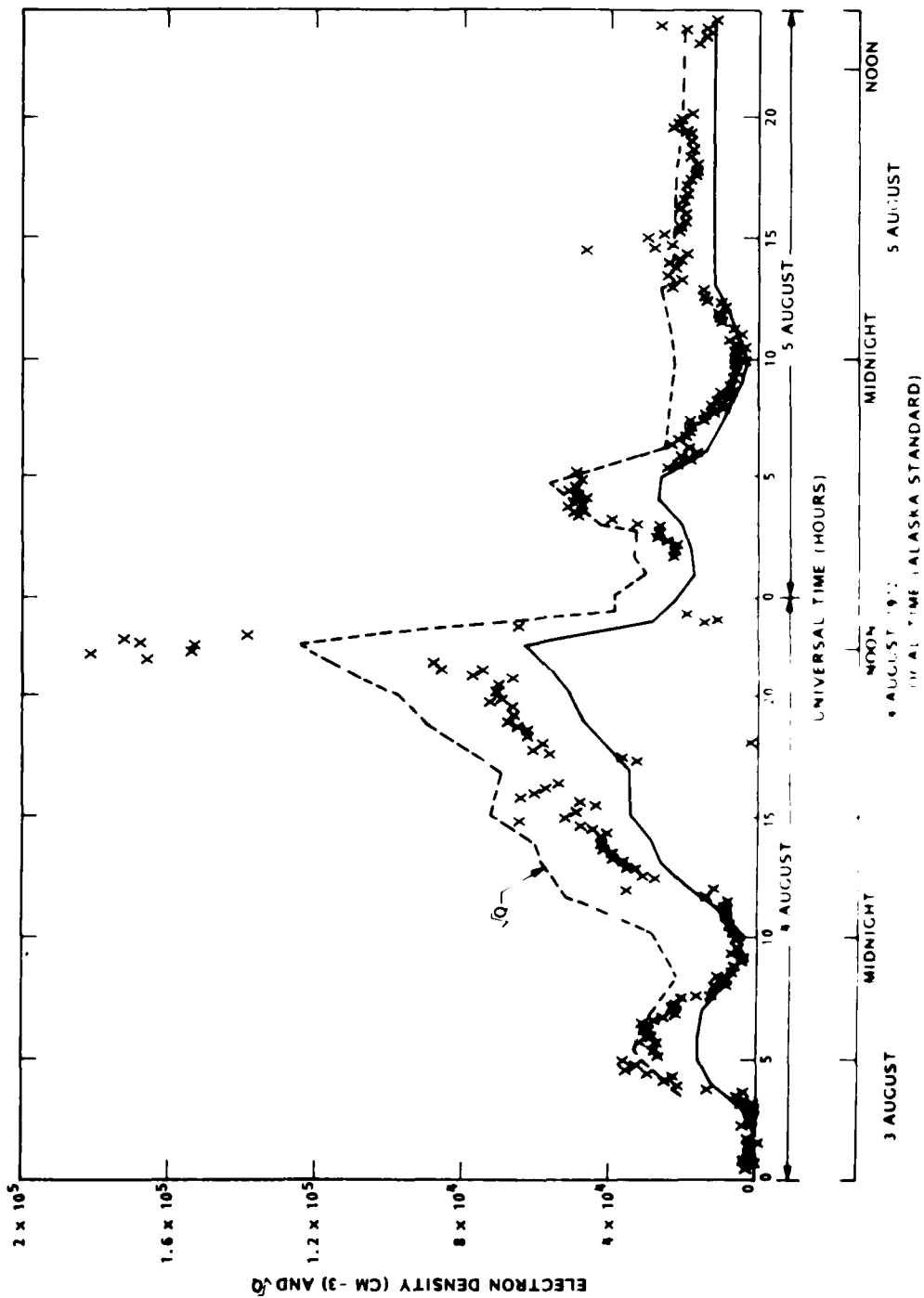
Figure 11.3  Electron density . . . . . . . . . . the SRI Chatanika
incoherent . . . . . . . . . . . 197.. The broken
line is . . . . . . . . . . . . . The solid line represents
electron density . . . . . . . . . . . . See test for further
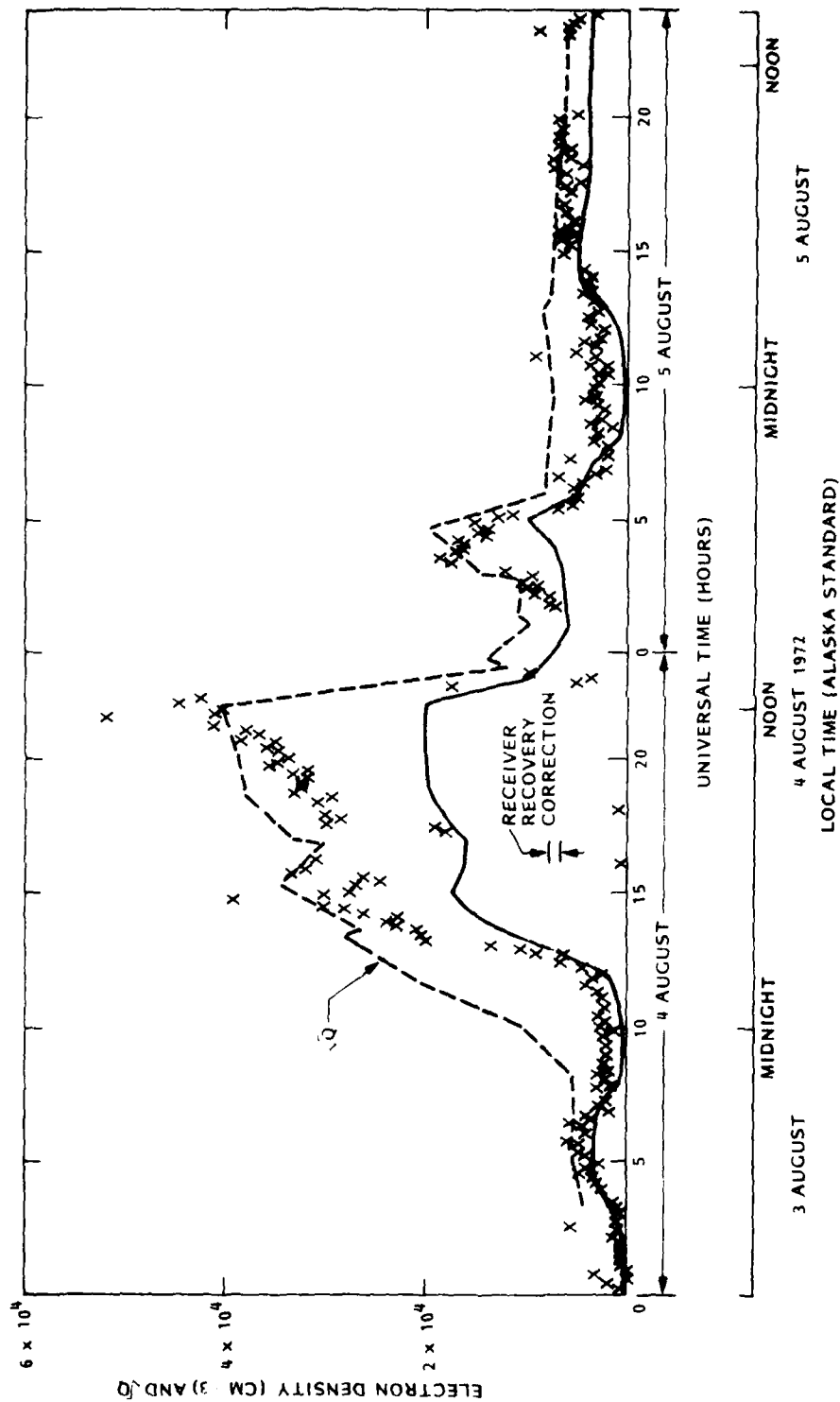explanation

Figure 11.4 Electron density vs. time at 60 km from measurements by the SRI Chatanika incoherent scatter radar during the SPE of 4 August 1972. The broken line is $\sqrt{Q}$ multiplied by a normalizing factor. The solid line represents electron density calculated by our ion chemistry model. See test for further explanation. The receiver recovery correction deduced by Watt (1975) is shown.
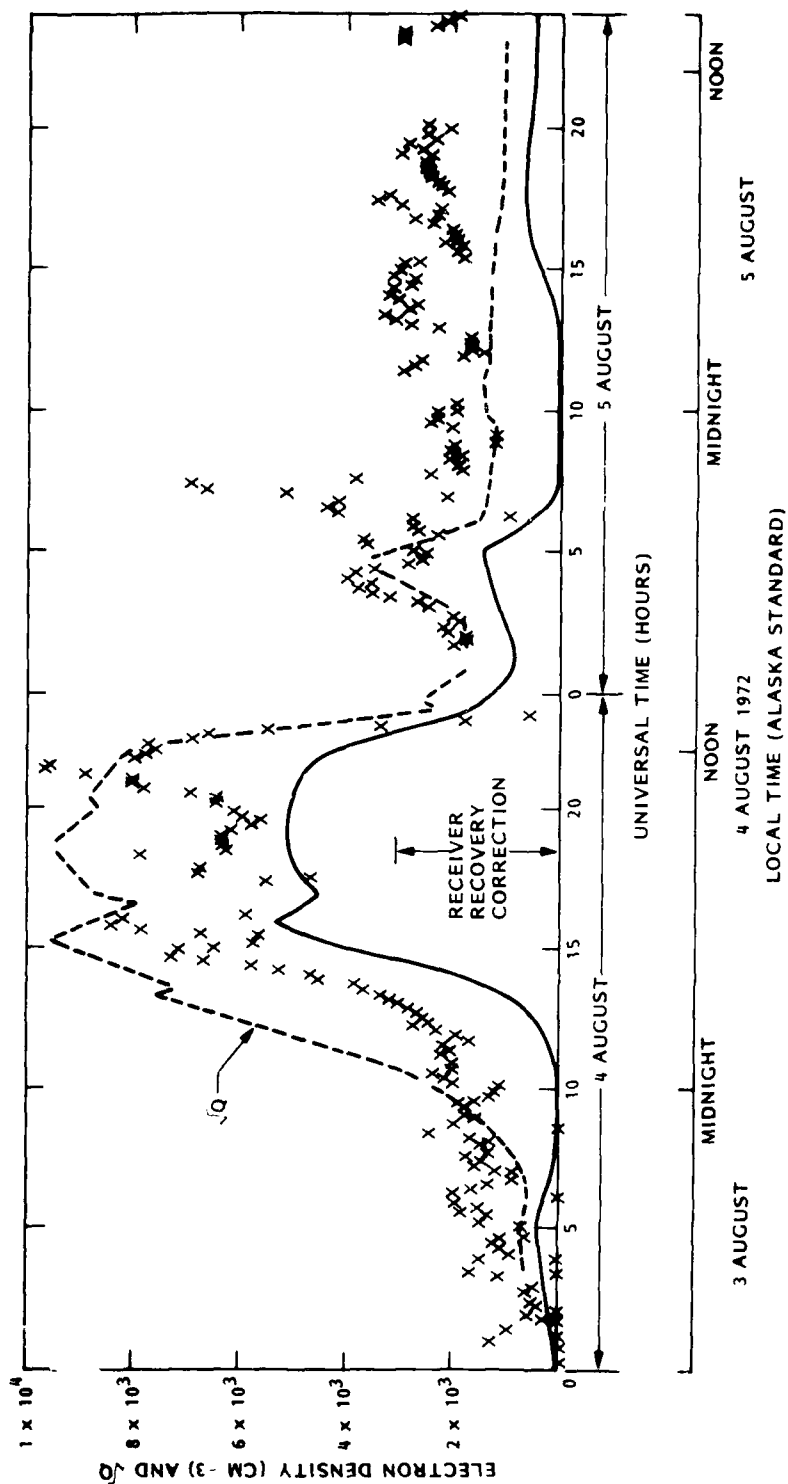
11-6

Figure 11.5  Electron density vs. time at 50 km from measurements by the SRI Chatanika
incoherent scatter radar during the SPE of 4 August 1972.  The broken line
is $\sqrt{Q}$ multiplied by a normalizing factor.  The solid line represents electron
density calculated by our ion chemistry model.  See test for further explanation
The receiver recovery correction deduced by Watt (1975) is shown.

10 minute averages and the 50 km data, because of the large scatter have been converted essentially to 30 minute averages by averaging each original point where possible with its neighbors. The experimental electron density data have not been corrected for the presence of negative ions. The effect of negative ions is to require a reduction of the electron densities by a factor ranging between one and two, depending on the negative ion-electron density ratio as discussed in our previous report (Imhof et al., 1980). The result of this correction is to reduce nearly all of the data at 50 and 60 km by a factor of two and to significantly reduce the values at 70 km. There is also plotted on each figure values of the square root of the ion pair production rates, $\sqrt{Q}$, derived from measurements of precipitating proton fluxes and energies made by Lockheed instrumentation on polar-orbiting satellite 1971-089A (Reagan et al., 1980). The values of $\sqrt{Q}$ have been multiplied by a normalizing factor, different for each altitude so as to make them comparable to the electron densities.

The rationale behind such use of the $\sqrt{Q}$ is based on the expression sometimes used in ionospheric analyses:

$$Q = \alpha_{eff} N_e^2$$

where $\alpha_{eff}$ is an effective loss coefficient for electrons. Then the electron density may be expressed as

$$N_e = \sqrt{Q/\alpha_{eff}}$$

11-8

so that if $\alpha_{eff}$ were constant the time dependences of $N_e$ and $\sqrt{Q}$ would be the same. Expressed in terms of lumped parameters

$$\alpha_{eff} = (1+\lambda)(\alpha_D + \lambda\alpha_I)$$

where $\lambda$ is $N^-/N_e$, the negative ion to electron ratio, $\alpha_D$ is the effective electron-positive ion dissociative recombination coefficient, and $\alpha_I$ is the effective positive ion-negative neutralization coefficient. As implied a lumping together of all the positive ions and of all the negative ions is implied by this simplified expression. Although $\alpha_I$ is thought to be relatively constant, $\alpha_D$ and particularly $\lambda$ vary with minor species concentrations and with photoeffects and are thus time dependent. Thus $N_e$ is not expected to show the same time dependence as $\sqrt{Q}$. However, a comparison of the two does show, for example that the main peak of the event probably is larger than the Q values would indicate. The Q values are grouped in pairs separated by about 1.6 hours, the satellite orbital period.

The electron densities computed by our ion chemistry model (Imhof et al., 1980) are also plotted on the figures. That model, computes the diurnal variation of minor neutral species such as O, $O_2(^1\Delta)$, $O_3$, NO, and $NO_2$ which have important influences on the ion chemistry. The ion chemistry model which is coupled to the neutral chemistry is a simplified model. In this simplification, for example, all of the hydrated protons $H^+(H_3O)_n$ (n>0) are lumped into one species, as are the hydrates of $NO^+$. There are four negative ions: $O_2^-$, $X^-$, $Y^-$, $Z^-$. $X^-$ represents a lumping of $O_4^-$ and $CO_4^-$; $Y^-$ represents $O^-$, $O_3^-$ and $CO_3^-$; and $Z^-$ represents $O_2^-\cdot NO$, $NO_2^-$ and $NO_3^-$. The negative ion reac-

tion scheme is illustrated in Figures 11.6 and 11.7. The diurnal variations of the photocoefficient are computed in advance by a separate code. The model computes one altitude at a time, i.e. it is a box model.

## 11.3 The Twilight Problems

In Figure 11.4 showing the SRI data for 60 km, the time of particular interest is the twilight period around midnight 4/5 August local (Alaska Standard) time. At the latitude of Chatanika, Alaska (65.1°N) at 60 km altitude on 4 August the sun does not set completely at midnight, the solar zenith angle becomes no larger than about 98°. That altitude is still illuminated by visible light; most of the UV has been absorbed in the atmosphere. It will be noted in the figure that Q is relatively constant at this time. The SRI data near midnight have a mean value several times larger than the model (refer also to Figure 11.1) and thus there is a discrepancy. It also is evident that the data and the model have different time dependences at sunrise: the data appear to rise more slowly. The corresponding time dependence at the immediately preceding sunset is not clear partly because of the rapid drop in Q in the early evening which may have influenced the minor neutral species and hence the ion chemistry. There is a question of how well the subtraction of the receiver recovery correction from the raw data has been done. It may be noted at the beginning of the 60 km plot before the start of the event, experimental values of $N_e$ tend toward zero on this plot as would be expected for near ambient conditions.

Examination of the 50 km data in Figure 11.5 during the same time period around midnight 4/5 August local time shows a larger discrepancy between data
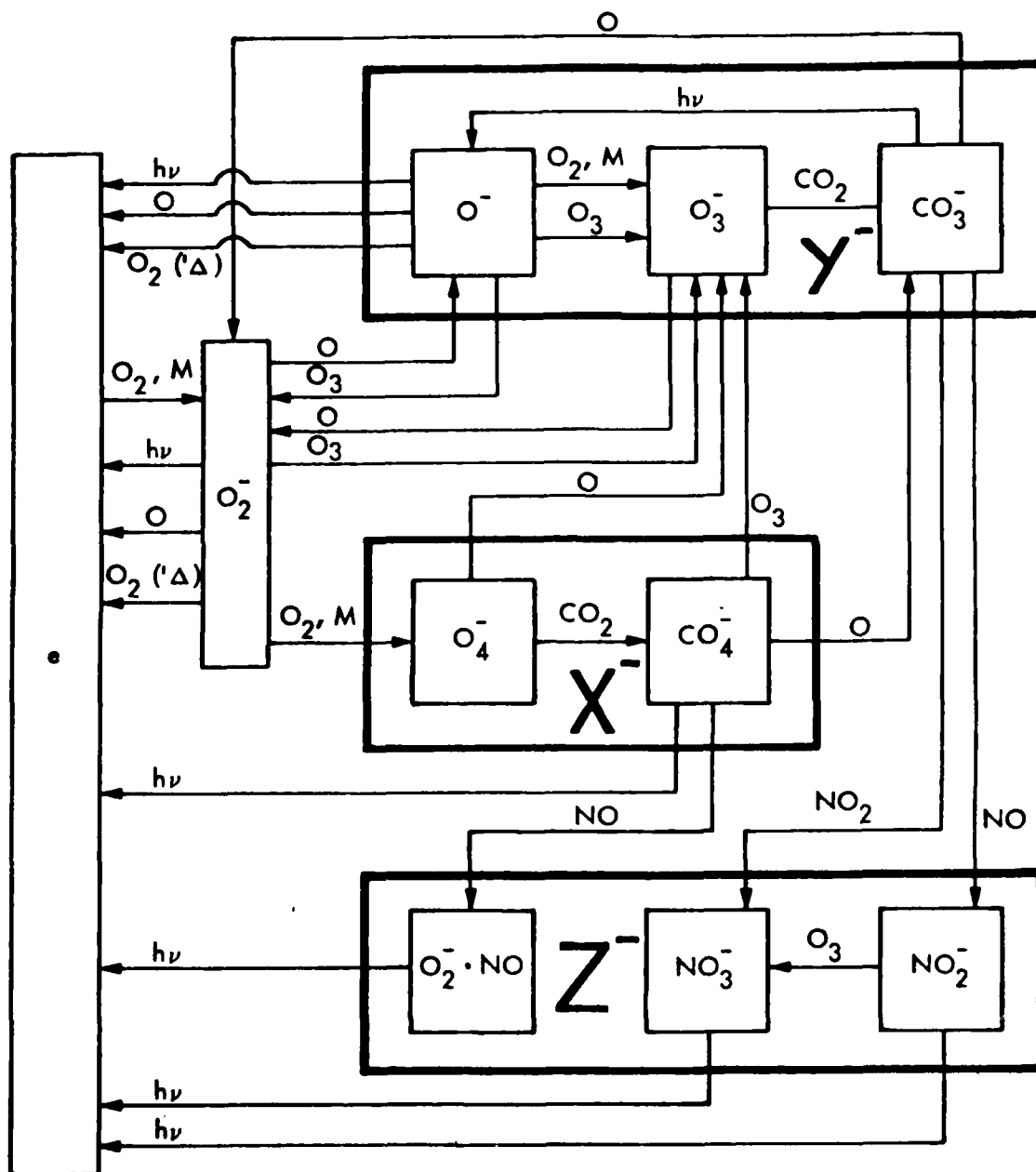
Figure 11.6  Schematic of part of the known negative ion reaction scheme showing the lumping together of ions used in the simplified scheme.
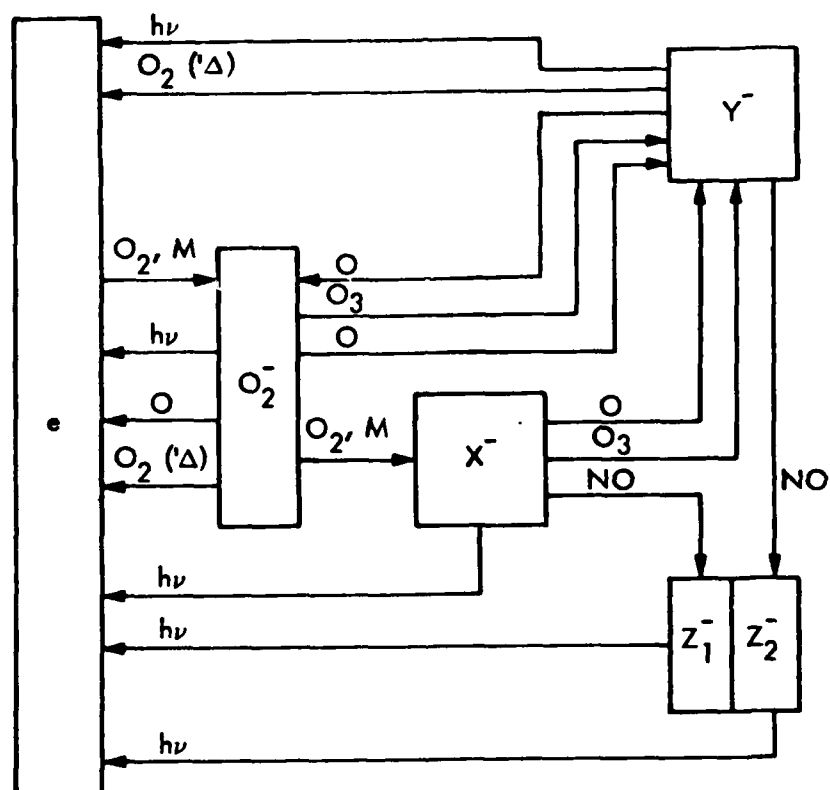
Figure 11.7. Schematic of simplified negative ion reaction model.

and model. The receiver recovery correction made at 50 km is larger and may be a source of some error. The scatter of the 50 km data, even with 30 minute averaging, is too large to permit a comparison of time dependences.

There is evidence about the twilight time dependence of $N_e$ from an earlier investigation by Reid (1961) of enhanced ionization produced by solar proton bombardment during PCA events. Measurements were made by riometers during several PCA events of the vertical absorption of 30 and 60 Mhz cosmic noise. The absorption was large during daytime when electron densities were large but decreased at night only by a factor of about 4 indicating qualitatively that electron densities had decreased in approximately the same ratio.

Reid used balloon measurements of the precipitating protons to deduce ion pair production altitude profiles, and, assuming constant spatially uniform proton fluxes computed differential absorption (db/Km) altitude profiles at the riometer frequencies. The absorption at 30 Mhz had a fairly definite peak at an altitude of about 58 km although the whole region from 35 to 80 km was effective.

To try to explain the measured time dependence of the riometer absorption at sunset and sunrise and to explain the residual nighttime absorption, Reid set up a simple ion chemistry model which included electron-ion recombination, attachment to form $O_2^-$, photodetachment and collisional detachment from $O_2^-$, and ionic recombination. Good data were available for ionic recombination and for the attachment to and photodetachment from $O_2^-$ which is due largely to light in the visible. The estimated electron-ion recombination rate was $3 \times 10^{-8}$ $cm^3$ $sec^{-1}$. In order to maintain the electron density necessary to provide the observed nighttime absorption it was necessary to assume a rate of collisional detachment, e.g. $O_2^- + M \rightarrow O_2 + e + M$ of about $10^{-17}$ $cm^3$ $sec^{-1}$. The rate of

11-13

such a reaction is known to be several orders of magnitude smaller, and there does not appear to be according to current knowledge, any detachment process which can provide the explanation for the small day-night absorption ratio.

The observed twilight time dependence of the riometer absorption also did not match the model. The decrease of absorption at sunset started at an earlier solar zenith angle ($\chi \sim 88°$) than did the model ($\chi \sim 92°$) and at sunrise the rise of absorption ended even later ($\chi \sim 85°$) than the onset of sunset, suggesting an asymmetry between sunset and sunrise. The suggestion was offered that the time dependences might be explained by detachment from an unknown ion by UV radiation.

Although we know much more about mesospheric negative ion chemistry today than was known in 1961 we still cannot answer in detail the questions raised by this interesting work of Reid.

Measurements made at night during a PCA event on 18 November 1968 over Churchill, Canada at 0200 CST have been advanced by Swider et al. (1971) as evidence that nighttime electron densities can be explained by a model in which there is no nighttime detachment. They cite data measured during a nighttime nuclear event (Whitten et al. 1965) as further evidence for this point of view. Also, some data measured during the PCA of 2 November 1969 (Ulwick, 1972) fits our model as indicated in Figure 11.2. Our model has no nighttime detachment mechanism at that time of year.

In summary, there is evidence from the riometer measurements analyzed by Reid (1961) that there may be a detachment process effective in the dark polar night during a PCA event. There is evidence from the SRI Chatanika radar measurements made during the August 1972 event in deep twilight that

visible light photodetachment or some other process may be occurring. On
the other hand, measurements made at night during the November 1969 PCA
event apparently show no detachment. We have been unable to find any way
of resolving these differences.

There is a lack of agreement between measured time dependences of
electron density at twilight during PCA events and the results of current
and earlier models. It may however be possible to shed some light on this
question as discussed in the next section.

## 11.4   The Twilight Time Dependence

Swider et al. (1978) present sunset and sunrise electron density
measurements (made by rocket) during the PCA event of November 1969. The
results clearly show a sunset-sunrise hysteresis at 60 and 70 km altitude
i.e. the rise of the electron density at sunrise is not symmetrical and
occurs later than would be expected if it were symmetrical around midnight
with sunset. Also presented are results from a time-dependent ion chemistry
model which agree quite well with the sunset measurements but shows no
hysteresis, i.e. the modeled sunrise electron densities rise more rapidly
than the measured values. The model includes much of the currently known
chemistry of negative ions in the D region. It appears that detachment in
the model is probably largely photodetachment rather than chemical detachment
by O atoms or excited $O_2(^1\Delta)$ molecules.

Our box model described above when applied to either the November 1969
PCA event or the August 1972 event during the twilight period around midnight
4/5 August, also shows little or no hysteresis and tends at 60 km to be
dominated by photodetachment in the early stages of sunrise e.g. at 0300

11-15

local time.  Later in sunrise detachment from $O_2^-$ by O atoms and $O_2(^1\Delta)$ molecules becomes commensurate with photodetachment.

The time dependence given to all of the photodetachment processes in the box model, for lack of further information, usually has been that computed for $O^-$ using the solar flux in the 3000-8000 Å range.  This tends to cause the electron density at sunrise to rise too early and too rapidly compared with measurements.  When the photodetachment in the model from ions other than $O_2^-$ are given the same time dependence as the photodissociation process.

$$O_3 + h\nu \rightarrow O(^1D) + O_2(^1\Delta) \tag{1}$$
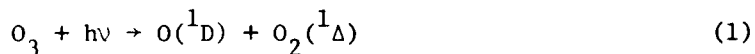
which occurs for wavelengths shorter than about 3100 Å, photodetachment starts later than does the $O^-$ photodetachment but rises too rapidly.

For the box model, the photocoefficients and their time dependences are computed in advance using a separate code having selected but fixed altitude profiles of the absorbing species $O_2$ and $O_3$.  In reality the $O_3$ profile is time-varying during twilight and thus consideration should properly be given to the effect which the temporal dependence of the ozone may have on the photodetachment coefficients.

We have made a preliminary study of this question by making use of a one-dimensional (1-D) neutral chemistry model developed several years ago on another project for the purpose of finding the variations of minor species densities in the mesosphere during the August 1972 PCA event.  It computes a neutral chemistry similar to that of the box model simultaneously at 41 equally spaced altitudes between 40 and 120 km.  The photocoefficients are updated at selected times using the changing $O_3$ profile.

11-16

The 1-D code was first run through several complete ambient days with atmospheric densities and temperatures approximating those of Chatanika, Alaska ($\sim$65°N) in August. Then it was used to model approximately the August 1972 event up to noon on 5 August. Ion pair production altitude profiles varying with time were used to augment the odd nitrogen species by adding 1.5 N atoms per ion pair, and the odd hydrogen production accompanying $H^+ (H_2O)_n$ ion formation and removal was simulated by adding one H atom and one HO radical for each ion pair produced, the upper limit. In addition there is some production of O atoms accompanying the ionization

The results at 60 km showed that despite the changing ozone used in the coupled photocoefficient code the coefficients for the processes (1) above,

$$O_3 + h\nu \rightarrow O + O_2 \qquad \lambda > 3100 \text{ A}^0 \, , \tag{2}$$

and

$$O_2 + h\nu \rightarrow O + O \quad , \tag{3}$$
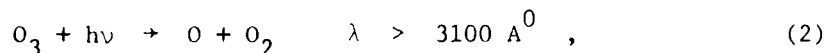
showed very little hysteresis. The time dependences of these processes were slightly different from those of the box model, although the photocodes used in the two models are identical. The differences must be due to the differing ozone profiles input to the photocodes. The fact that the photodissociation processes show little or no hysteresis probably indicates that photodetachment processes involving UV also do not.

The most interesting result was that a pronounced hysteresis appeared in the O atom density at 60 km as shown in Figure 11.8. The sunrise lag in the rise of O atoms may be understood by considering qualitatively some
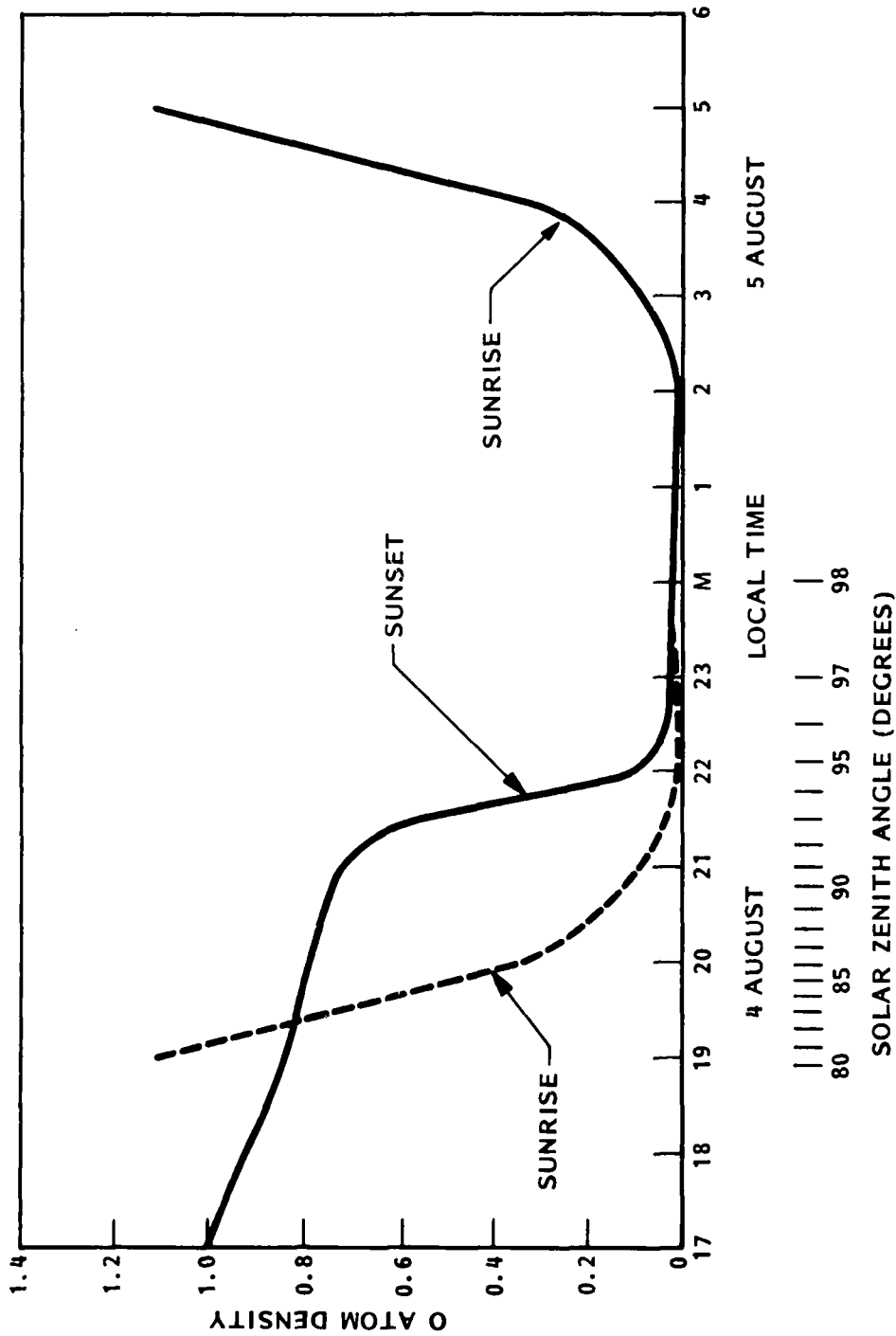
Figure 11.8  Twilight O atom densities at 60 km altitude computed by a
1-D neutral chemistry model for the August 1972 PCA. They
are normalized to unity at 1700 hours on 4 August where the
value is 2.5 x 10$^9$ cm$^{-3}$. The sunrise curve is also shown
mirrored around midnight.

features of the odd oxygen (O, $O_3$) chemistry. From a daytime high the O atom density and also the ozone density tend to fall with the decrease during sunset in the rate of photodissociation of $O_2$, process (3). As the rate of process (1) begins a rapid decrease, O atoms decrease to a low level, reacting with $O_2$ to form $O_3$ which increases to a nocturnal peak. Throughout the night the ozone is slowly removed by catalytic reactions involving odd nitrogen, odd hydrogen species, and a few O atoms. At sunrise, the nocturnal ozone has been depleted and because of the reduced amount of $O_3$ the production of O atoms by processes (1) and (2) is slow enough to cause the hysteresis or relative lag in the rise of O atom density. Although not specifically calculated in the 1-D model, there must be a closely related hysteresis in $O_2(^1\Delta)$ time dependence.

Similar O atom hysteresis was also found to occur for ambient twilight conditions at 60 km in the 1-D model and might also be expected to occur in the box model. In fact, such an effect does occur at 60 km in the box model, but much smaller in magnitude than in the 1-D model, not large enough to have an appreciable effect on the electron density time dependence.

The measured twilight electron densities at 60 km around midnight 4/5 August, shown in Figure 11.4, were analyzed using a lumped parameter approach to find the time dependence of detachment. Such an analysis was necessary to remove the effect of the changing ion pair production rate during this time period. The results in Figure 11.9 do tend to show a slow rise of detachment at sunrise which occurs at approximately the same times as the O atom rise in Figure 11.8. The computed detachment shows a much smaller hysteresis effect than do the O atoms in the 1-D calculation.
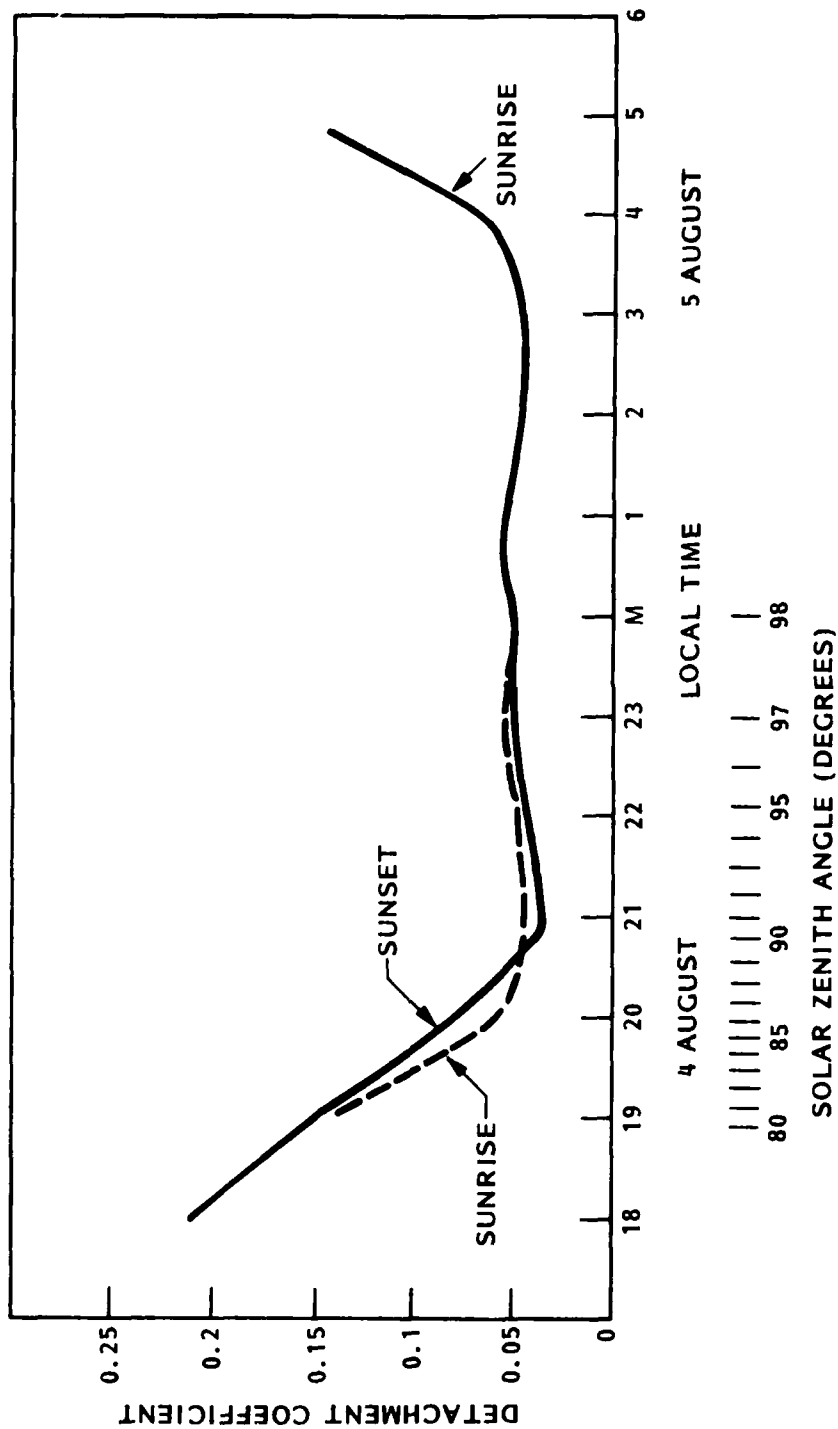
Figure 11.9  Detachment coefficients at 60 km altitude calculated from the data of Figure 11.4.  The sunrise curve is also shown mirrored around midnight.

These results at 60 km based on measurements and modeling of the August 1972 event suggest that the twilight behavior of electron density may be dominated by the minor species, O atoms and $O_2(^1\Delta)$ molecules, rather than by photodetachment which is prominent or dominant in current negative ion models. If this concept can be verified by further study of all the available experimental evidence, reconsideration of present ion chemistry models will be necessary.

## 12.0 THE MASS DISTRIBUTION OF IONS IN THE LOWER STRATOSPHERE AND UPPER TROPOSPHERE

The mass distribution of ions is needed to determine the mobilities and hence the conductivities in the stratosphere. During undisturbed conditions, the ionic mobilities and conductivities can and have been measured directly. Unfortunately, as pointed out by Meyerott, Reagan and Joiner (1980) some of the mobilities and conductivities measured above 10 km on rocket platforms maybe in error due to the high electric fields employed in the measurements. The masses derived from the mobilities measured on rocket platforms appear too small. The small masses may be the result of fragmentation of larger ions broken up during the sampling process. Hence, for quiet conditions improved values of the ion masses or mobilities are required to provide an adequate measure of the conductivities in the stratosphere.

During disturbed conditions, the mass distribution may change depending on the intensity of the disturbance. A higher ion production rate leads to higher ion densities. Since the recombination rate varies as the square of the ion density, the ions have shorter lifetimes during intense disturbances and may not have time to build the larger complex ions that may be present in quiet times. A measurement of the mass distribution can form a basis for the theoretical modeling of the ion mass distributions that may permit one to predict the ionic mass distributions as a function of the ion production rates.

The ionic masses have been measured in the atmosphere at altitudes above 35 km with the use of mass spectrometers. Ionic masses as high as $\sim$ 300 amu, near the upper limit of the spectrometers, have been detected.

No insitu mass spectrometer measurements of ionic masses have been made below $\sim$ 35 km altitude. Mass distributions can be inferred at lower altitudes from measured mobility distributions and a knowledge of the mobility-mass dispersion relationship. In this section the mass distributions determined from the measurement of mobility distributions made in the laboratory by Hoppel (1970) and at $\sim$ 5 km by Hoppel and Kraakevik (1965) will be compared with the mass spectrometer measurements made at $\sim$ 35 km discussed by Meyerott, Reagan and Joiner (1980). Evidence will be presented for the existance of an appreciable fraction of the ionic mass distribution with masses greater than those measured with the mass spectrometers.

If g(m) dm is the fractional number of ions having masses between m and m + dm and f(k) dk is the corresponding number of ions of having mobilities between k and k + dk, then

$$g(m) \ dm = f(k) \ dk \tag{1}$$

$$\text{and} \quad \int_0^\infty g(m) \ dm = \int_0^\infty f(k) \ dk = 1. \tag{2}$$

Consequently,

$$g(m) = f(k) \ (dk/dm). \tag{3}$$

The quantity dk/dm can be derived from the mass-mobility relationship given by Kilpatric (1971), reproduced in Figure 2 of Meyerott, Reagan and Joiner (1980)

The mobility distribution of atmospheric ions in a laboratory simulation has been measured by Hoppel (1970). The mobility distribution

of ions in the atmosphere above the exchange layer at altitudes of 3.05, 4.27 and 5.18 km has been measured by Hoppel and Kraakevik (1965). In Figure 12.1 are shown the mass distributions derived from the mobility distributions of positive and negative ions measured by Hoppel in the laboratory with dry air and the negative ions in moist air. It can be seen in Figure 12.1 that the mass distribution of the negative ions is shifted to the higher masses as the water content of the air is increased. In Figure 12.2 is shown the fraction of the ions having masses greater than m,

$$G(m) = \int_m^\infty g(m) \, dm \qquad (4)$$

plotted against m. It can be seen in Figure 12.2 that in dry laboratory air, 1/2 of the negative ions have masses greater than 70 amu while those in moist air have masses greater than 130 amu. The mass distribution of the positive ions in dry air is weighted toward higher masses than the negative ions with 1/2 of the ions having masses greater than 190 AMU. According to Hoppel, the addition of moisture to the dry air produced no appreciable change in the positive ion distribution.

Laboratory studies of the nature of atmospheric ions have been reported by Mohnen, Del Santo, and Kadlecek (1980). In their experiments ions produced in an ion source are conducted through a drift tube at atmospheric pressure and the masses and mobilities of the emerging ions are measured. An electric quadrupole mass spectrometer is used to identify the ions whose mobilities are measured. In hydrocarbon free air with a $H_2O$ content
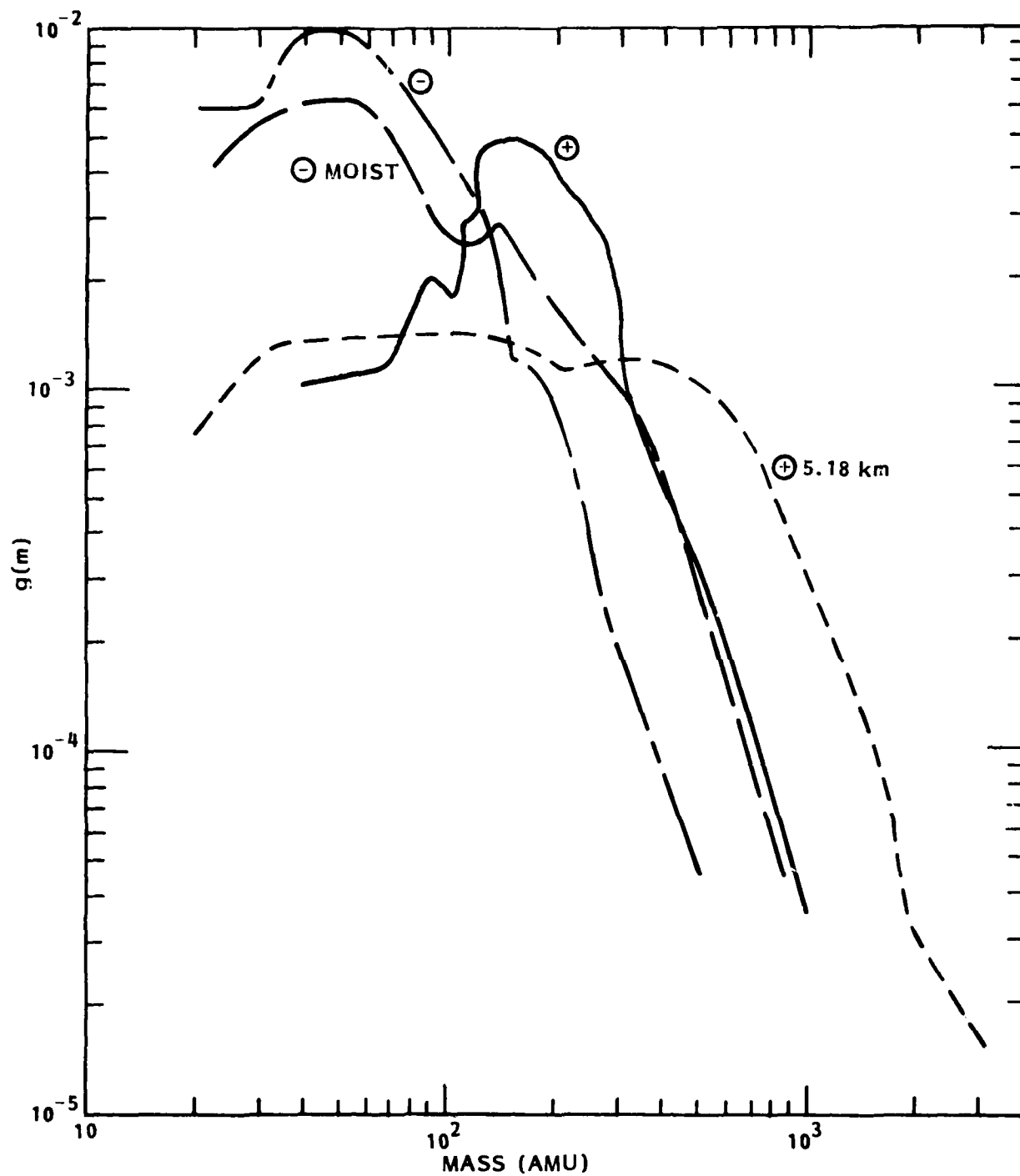
Figure 12.1. Mass distributions of laboratory positive ions (+), and negative
ions (-), in dry air, of negative ions in moist air (- moist),
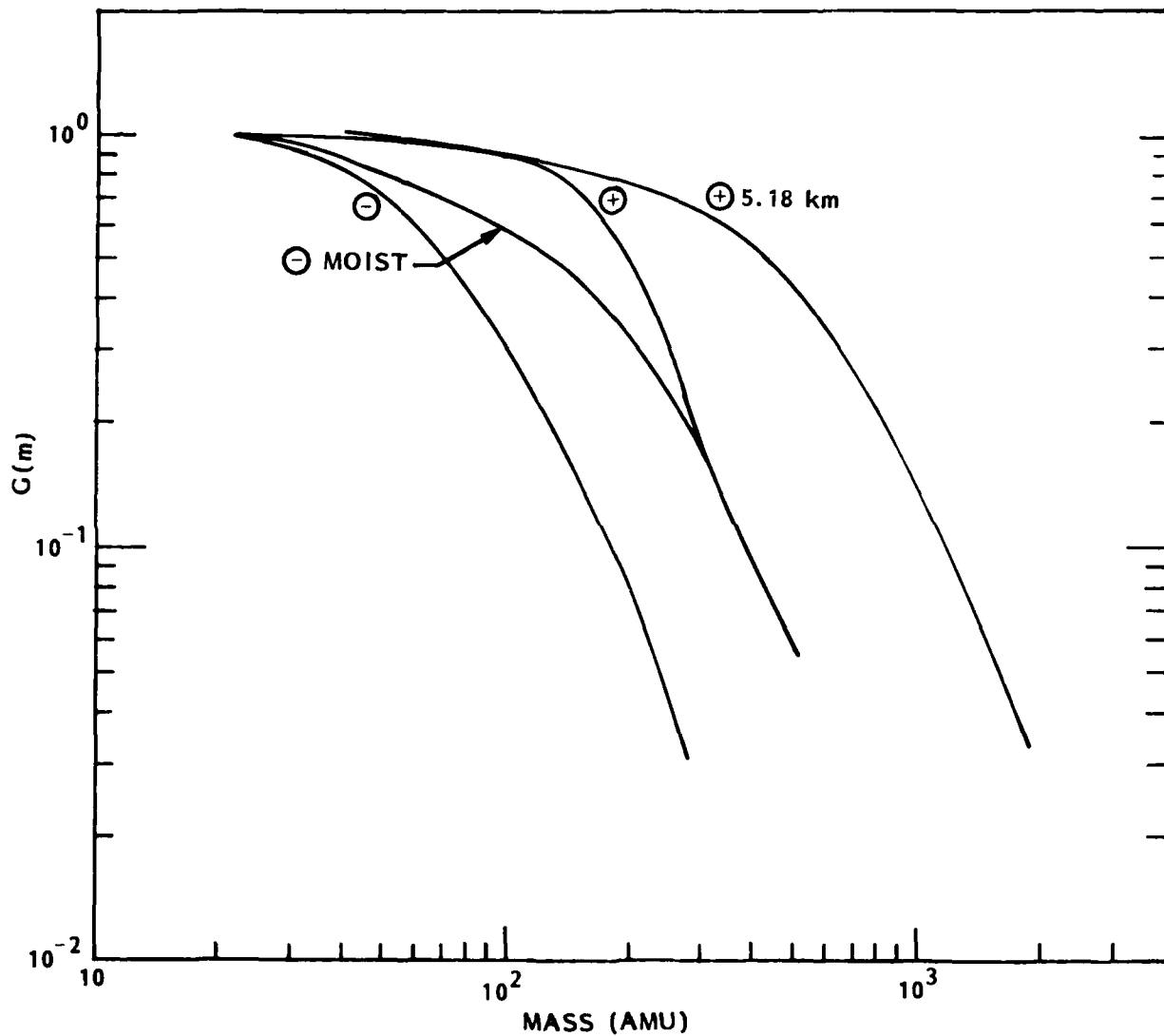and of atmospheric positive ions at 5.18 km (+ 5.18 km).

12-4

Figure 12.2. Fraction of ions having masses greater than  m  for the mass
distributions shown in Figure 12.1.

of $\sim$ 2 ppm, the predominant negative ion is $O_2^- \cdot (H_2O)_2$ mass 68 amu.

$CO_3^-$, 60 amu, $CO_4^- \cdot (H_2O)$, 94 amu, $CO_3 \cdot (H_2O)_1$, 78 amu, $CO_4^-$, 76 amu, $O_2^- \cdot (H_2O)$,

86 amu, $CO_3^- \cdot (H_2O)_2$, 96 amu, and $O_2^- \cdot (H_2O)_1$, 50 amu, in order of decreasing

concentrations were also present. With the addition of a $SO_2$ concentration

of 0.14 ppm, the predominant negative ion becomes $SO_4^-$, 96 amu, with

$SO_5^-$, 112 amu, and $SO_4^- \cdot (H_2O)$, 114 amu, also present.

The laboratory air used by Hoppel probably contained $SO_2$ NO, $O_3$ and

perhaps other impurities in concentration of parts per million. Hence,

the negative ion mass distribution might be expected to be broader than

that reported by Mohnen et al. (1980). However, it is interesting to note

that the negative ion distribution for low humidity air reported by Hoppel

peaks between 40 and 60 AMU which is consistent with that measured by

Mohnen et al. for pure air, 60 to 68 amu. This agreement is reasonably

good considering the relative crudeness of the mobility mass determination

and the fact that the mobility-mass dispersion curve used may be less

accurate for masses below $\sim$ 100 amu as can be seen from the scatter in

the points in Figure 2 of Meyerott et al. (1980).

The positive ion mass distribution derived from the mobility

distribution measured by Hoppel and Kraakevik (1965) in the atmosphere at

5.18 km is also shown in Figure 12.1. It can be seen that the mass distribution

is weighted more toward the higher masses than those of the laboratory

mass distributions. From Figure 12.2 it can be seen that 1/2 of the ions

have masses greater than 440 amu and that 20% of the ions have masses

greater than 800 amu. The mobility distribution of the negative ions

differs from that of the positive ions by $\sim$ 10% and hence is not shown.

The mass distributions derived from the mobility distributions of Hoppel and Kraakevik (1965) at 5.18 km show that a large fraction of the ions have masses in excess of those measured with mass spectrometers at $\sim$ 35 km altitude by Arnold et al. (1977), Arijs et al. (1978) and Arnold and Henschen (1978). While the average mobility measured by Hoppel and Kraakevik at 5.15 km corresponds to a reduced mobility of 1.14 $cm^2 V^{-1} s^{-1}$ which would correspond to an ionic mass of $\sim$ 300 amu, the average mass derived from the mass distribution function in Figure 1 is $\sim$ 600 amu. While it must be pointed out that the mass distribution function for the high masses derived from the portion of the mobility distribution function which is poorly determined and where $dk/dm$ is large, mobility data still suggests the presence of an appreciable fraction of the positive ions at 5.18 km with masses in excess of 300 amu.

The presence of an appreciable fraction of the positive ions with masses in excess of 300 amu at 5.18 km is not inconsistent with the mass spectrometer measurements made at $\sim$ 35 km since the mass spectrometers were limited to masses $\leq$ 328 amu. One might also expect the mass distribution to be weighted more toward the higher masses at 5 km than at 35 km due to the higher density and, perhaps, higher moisture and impurity content of the air. However, the positive ion mobility measurements of Rieckert (1971) at 20 and 30 km indicated a mean reduced mobility of $\sim$ 0.5 $cm^2 V^{-1} s^{-1}$ which would correspond to a mass of $\sim$ 1000 amu. One is forced to conclude that there is a strong possibility that a considerable fraction of the ions up to 35 km have masses higher than measured by the mass spectrometers. Simultaneous measurements on the same (balloon) platform of the mobility

distribution with Gerdien condensers and the mass distribution with mass

spectrometers would be desirable.

APPENDIX A

SPORADIC E-LAYERS

The term "sporadic E-layer" (or $E_s$) is used to describe a phenomenon of increases in the ion and electron densities occurring within narrow height regions (a few km thick or less) at E region heights in the earth's atmosphere (typically between 100 and 130 km). Figure A.1 shows the altitude profile for an $E_s$ at temperate latitude (Smith and Miller, 1980). In this case the maximum densities increased by nearly two orders of magnitude over the ambient background in a thin 2-3 km slab.

There are different classes of $E_s$ probably having different origins; for the middle latitude $E_s$ the preferred explanation assumes concentration of metallic ions in one or more narrow layers by wind shears. At high latitudes energetic particle precipitation may be the source (Jones and Saksena, 1980). Whitehead (1970) reviews the extensive $E_s$ literature and identifies three main types, equatorial, temperate, and auroral zone $E_s$. Figures A.2 - A.5 (Smith, 1957) show some of the relevant characteristics for the latter two types. It will be noted that in the auroral zones $E_s$ is typically an evening or night-time phenomenon since the occurrence frequency drops markedly during the hours around midday. At temperate latitudes, however, maximum occurrence is observed around the summer solstice with predominance of daytime occurrences (Figure A.3).

However, from the point of investigating possible effects of $E_s$ on ELF propagation important information seems to be lacking or is insufficient for realistic calculations, e.g. little is known of the spatial extent of the $E_s$ layers, some may be 1000 km or more in extent (DeGregorio et al., 1962),

A-1

whereas others may be 100 km or less in horizontal extent (Whitehead, 1970). Quantitative information on homogeniety of ionization, vertical and horizontal movements of the $E_s$, geographical positions at given times, time duration, etc. is furthermore limited.
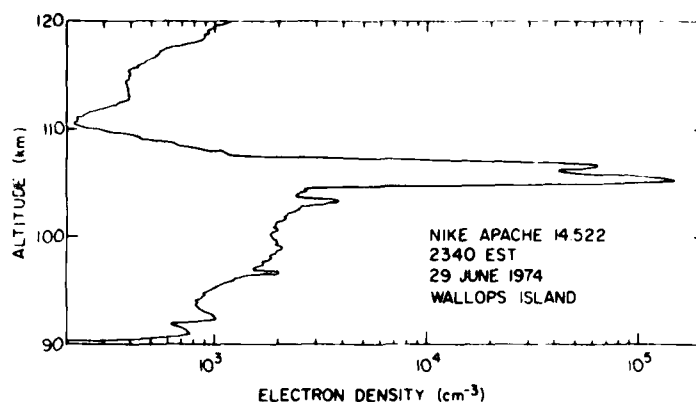
Figure A.1  Double-peaked sporadic E-layer observed near midnight (Smith and Miller, 1980).
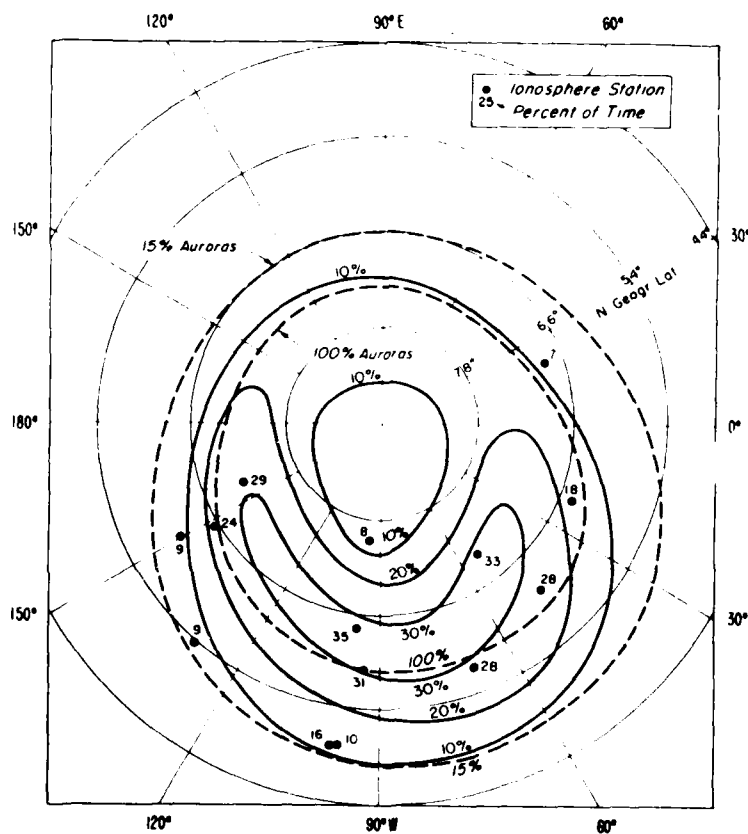


Figure A.2  Mean annual $E_s$ occurrence in the auroral zone $fE_s > 5$ MHz; 1948-1954

A-3

AURORAL ZONE



NARSARSSUAK, GREENLAND
GEOMAG LAT=70 'N

HIGH TEMPERATE ZONE



WASHINGTON, DC
GEOMAG LAT 50 N

LOW TEMPERATE ZONE



ZZZ 10-30% OF THE TIME    50-70% OF THE TIME    GUAM I
30-50% OF THE TIME    70-90% OF THE TIME    GEOMAG LAT=4 N
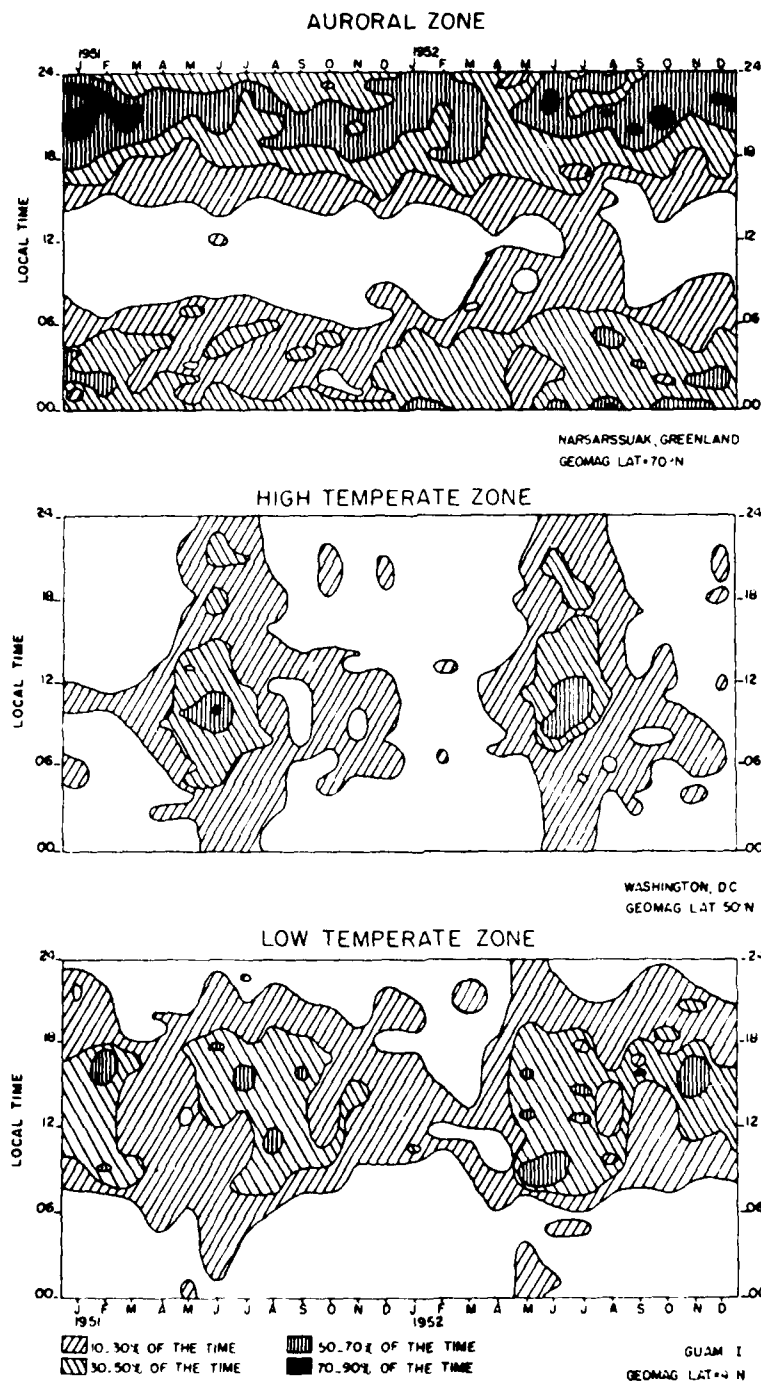
Figure A.3    Comparison:  Auroral zone to temperate zone $E_S$
$fE_S \geq 5$ Mhz

A-4

LOCKHEED PALO ALTO RESEARCH LABORATORY
LOCKHEED    MISSILES    &    SPACE    COMPANY,    INC
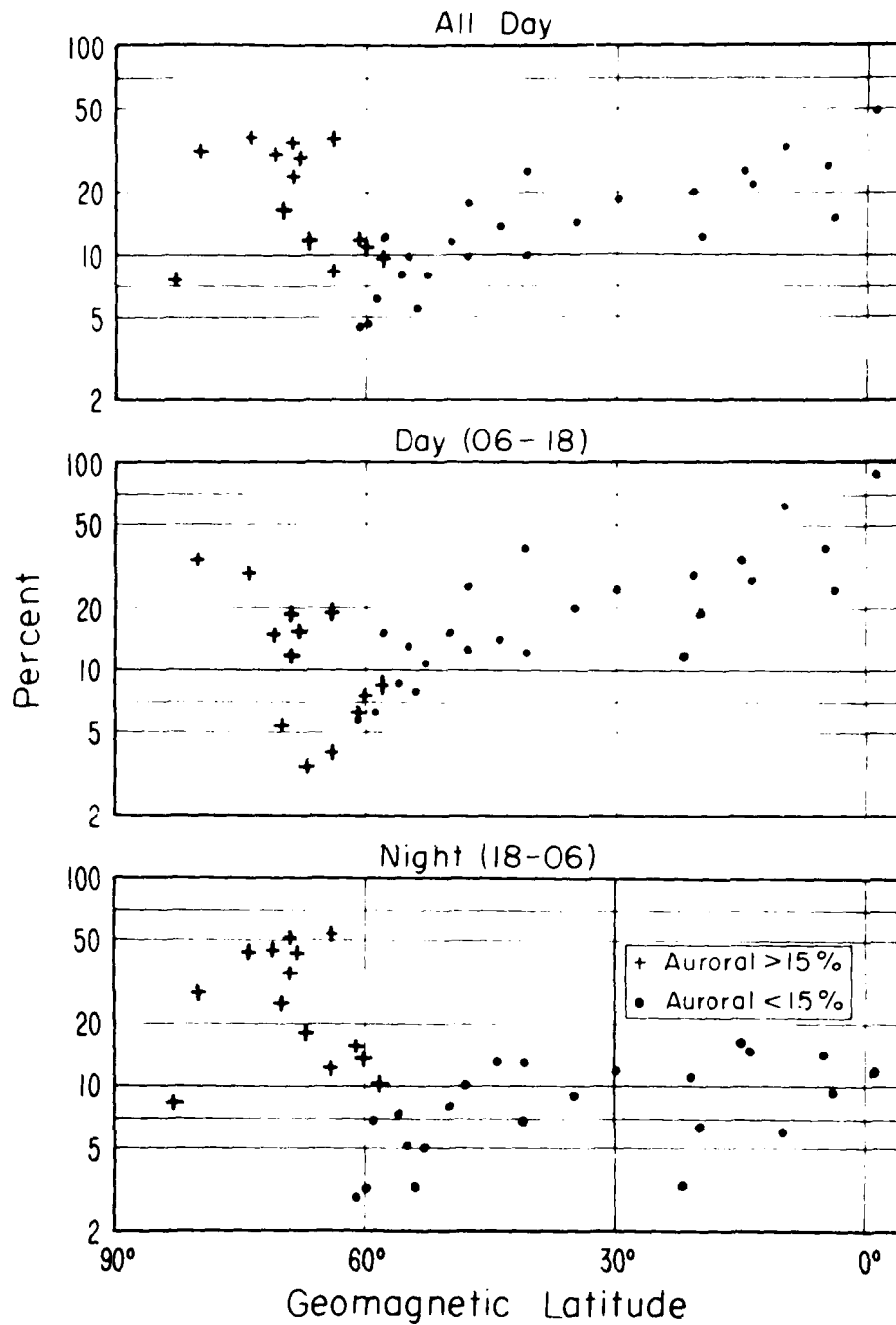
Figure A.4   <u>Occurrence of sporadic  E  in northern hemisphere</u>

<u>fEs > 5 Mhz, 1952</u>

A-5

**LOCKHEED PALO ALTO RESEARCH LABORATORY**

LOCKHEED   MISSILES   &   SPACE   COMPANY,   INC

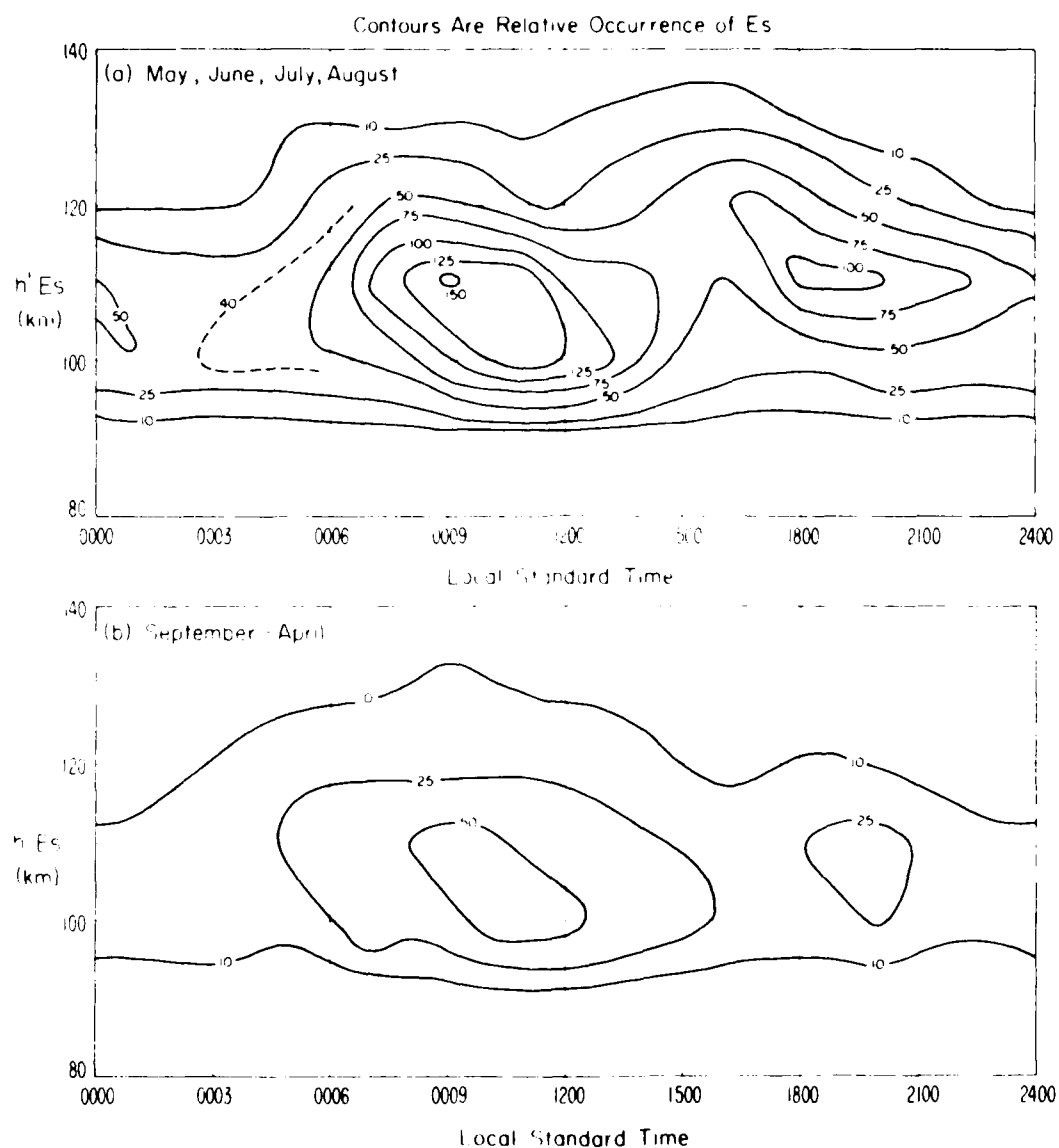Contours Are Relative Occurrence of Es

Figure A.5    E_s height distributions at Washington, DC
              fE_s > 5 MHz 1948-1952

A-6

APPENDIX B

THE EFFECTS OF ENERGETIC-PARTICLE PRECIPITATION ON THE GLOBAL ATMOSPHERIC
ELECTRICAL CIRCUIT

Solar energetic particle precipitation during large solar particle events
(SPE) greatly enhances the conductivity of the atmosphere over extended spa-
tial regions. In addition, for the larger events the electrical current
carried by the solar protons and electrons in the polar caps greatly exceeds
the normal air-earth current that flows between the ionosphere and the ground
at high altitudes. In order to model the effects of the SPE's on the earth's
electrical system, we note that the precipitation is reasonably uniform over
the polar caps whose dimensions are several thousand km. Since the important
perturbation occurs over altitudes below 100 km. the problem is essentially a
plane problem. We have used the SPE's of August 1972 as an example of large
SPE's since the particle precipitation that occurred during that period is
better documented than that for most events.

The electric field in the fair weather regions (no thunder storms present)
can be calculated by assuming that the electrical current density is indepen-
dent of altitude. This assumes quasi-steady state conditions and that cur-
rents are only a function of altitude. The air-earth current density, $J_{AE}$, is
the sum of the current density carried by the precipitating protons, $J_p$, the
current density carried by the precipitating electrons, $J_e$, and the ohmic
current density, $J_\Omega$, i.e.,

$$J_{AE} = J_\Omega + J_p - J_e \qquad (1)$$

B-1

We have used the usual convention that a downward flowing positive charge is a positive current. Since the current carried by the precipitating particles is zero near the earth, $J_{AE}$ is equal to the air-earth current near the earth. From Equation (1) $J_\Omega$ is given by

$$J_\Omega = J_{AE} - J_p + J_e \tag{2}$$

The electric field E(H) at any altitude, H, is given in terms of the conductivity, $\sigma$(H) by

$$E(H) = J_\Omega / E(H) \tag{3}$$

$\sigma$(H) depends on the particle deposition rate and the mobility of the ions.

The conductivity in the polar cap changes during a SPE due to the greatly increased deposition of high energy protons from the SPE and also due to the reduction of galactic cosmic rays known as the Forbush decrease. Changes in the flux of galactic protons at the ground are usually measured by neutron monitors. Figure B.1 is a neutron monitor record taken at the South Pole during the period 3-11 August 1972 from Pomerantz and Duggal (1973). It can be seen in Figure B.1 that the first Forbush decrease (FD) started at ~0300 UT on August 4. At ~1200 UT on August 4 a sharp increase in the neutron counting rate occurred and continued until ~2000 UT. This so-called Ground Level Event (GLE) occurred at the same time as the 10-hour intense solar proton precipitation. Following this GLE, a second FD occurred. This second FD lasted for ~4 days. At ~1500 UT August 7, a second GLE occurred. An
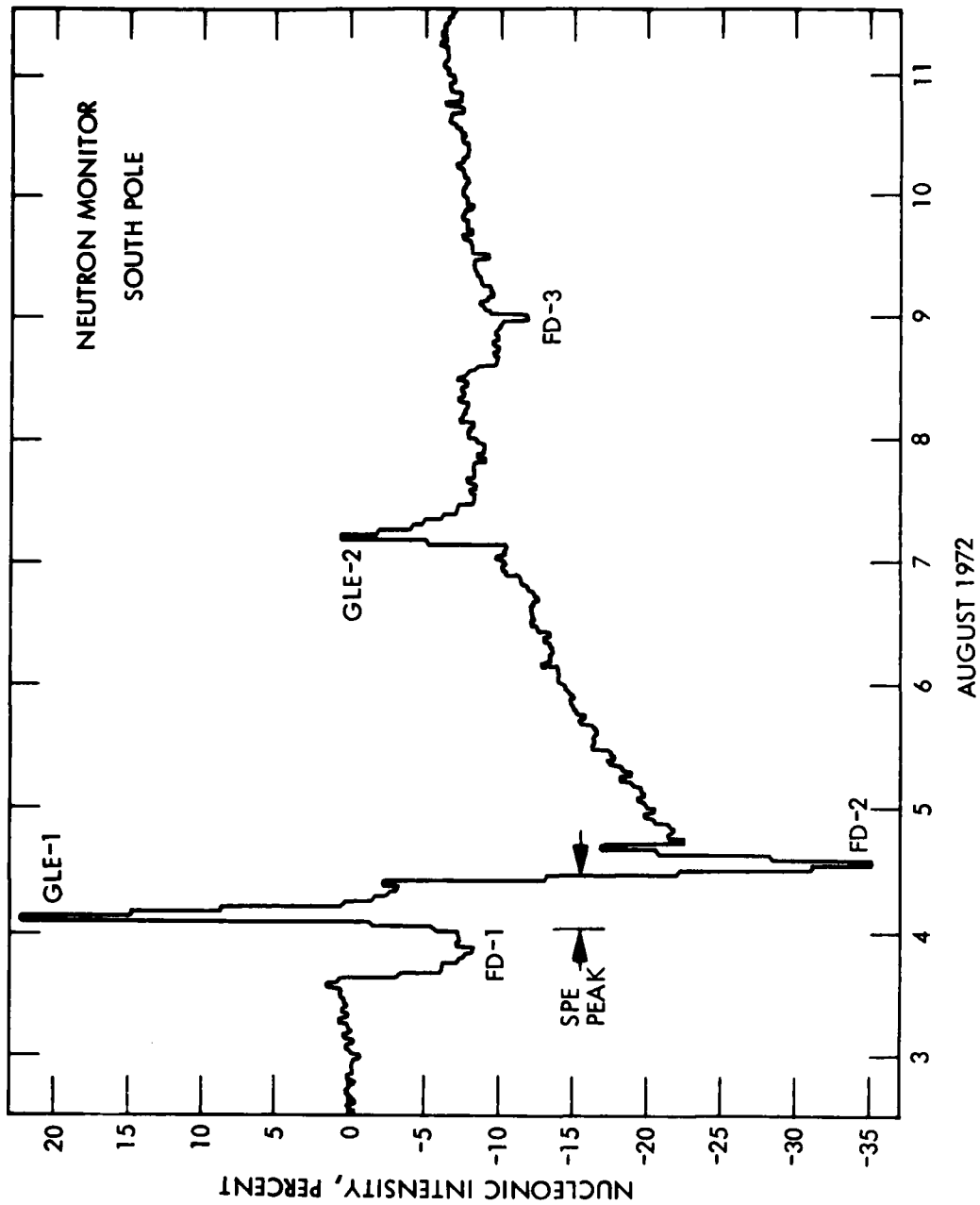
B-2

Figure B.1  Neutron monitor record taken at the South Pole during the period 3-11 August 1972.

increase in solar proton precipitation was also recorded by the satellites at the time of this second GLE.

The ion production rates due to the precipitation of solar cosmic rays and galactic cosmic rays are usually determined by different techniques due to the difference in the spectrum of the precipitating protons. The solar protons have energies ranging from ~1 MeV to ~1 BeV while the galactic primary protons have energies from ~500 MeV to ~100 BeV. The principal energy loss mechanism for protons with energies less than ~500 MeV is ionization loss, while for protons with energies greater than ~500 MeV the principal energy loss mechanism is nuclear collisons. Protons with energies of ~1 BeV or less produce low energy protons and neutrons whose ranges are small compared to the primary protons. Hence, the energy lost by the primaries in nuclear collisions can be considered to produce ionization at the point of the nuclear collision. At proton energies greater than 1 BeV, mesons are produced as well as high energy protons and neutrons. The mesons have ranges much larger than the ranges of the primary protons so that the energy loss by the primary protons cannot be considered as a local deposition. In fact, only about 1% of the ionization at sea level is produced by protons. Mosts of the ionization is produced by mesons.

Ion production rates due to galactic cosmic rays have been extensively measured as a function of altitude, latitude, and solar cycle (Neher, 1971 and references therein). The method used to determine the ion production rates during a Forbush decrease is to reduce the empirical ion production rates determined for a given altitude, latitude, and time of the solar cycle by the square root of the fractional reduction in counting rate of the neutrons monitors from the pre-SPE value.

The ion production rates for the solar protons have been determined in the past at Lockheed PARL from the proton spectrum determined from satellite measurements augmented at the high energy end by balloon measurements (Reagan et al., 1980) through the use of the PROTON deposition code. This spectrum which has been used for the previous studies at LMSC extends from ~1 MeV to ~400 MeV. For the evaluation of the effects of peak proton precipitation during the period ~1200 UT to ~2000 UT August 3, it appeared necessary to extend the solar proton spectrum to higher energies so that there would be a better overlap with the ion production rtes produced by the galactic protons at altitudes below 20 km. The evidence for significant proton flux at energies greater than 400 MeV is evidenced by the first GLE shown in the neutron monitor data in Figure B.1.

The solar proton spectrum for energies greater than ~400 MeV during the first GLE on August 4, 1972 has been determined by Lockhwood et al. (1975) from analysis of the word-wide neutron monitor data taken at that time. We have used the spectrum determined by Lockhwood to extend our previously determined solar proton spectrum for energies greater than 400 MeV. The combined solar proton spectrum for energies greater than 100 MeV for 1508 UT August 4 is shown in Figure B.2. Also shown in Figure B.2 for comparison, is the galactic cosmic ray proton spectrum for 1972 given by Fulks (1975). We have used this solar proton spectrum as representative of the solar proton spectrum for the entire ~10 hour peak irradiation period.

The extension of the solar proton spectrum to include protons with energies above 400 MeV required some modification of the PROTON code to take nuclear collisions into account. This was done by multiplying the proton flux
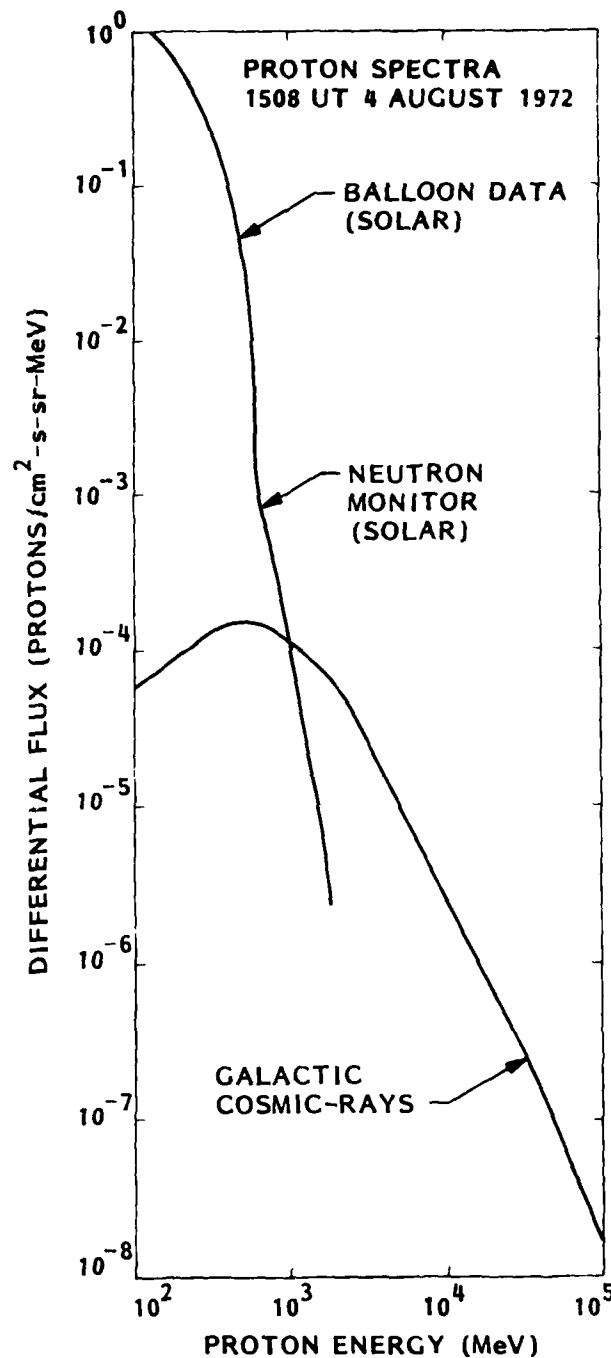
Figure B.2  Solar Proton spectra for energies greater than 100 MeV for
period ∿ 1200 to ∿ 2000 UT 4 August 1972.  Galactic cosmic
ray proton spectrum for 1972.

B-6

of energy E making an angle $\theta$ with the vertical at a height h, $F(E\theta)$, by exp $(-\int_h^\infty \rho(h)dh/\lambda\cos\theta)$, where $\rho(h)$ = atmospheric density at height h and $\lambda$ = mean free path for nuclear reactions. The value of $\lambda$ = 205 $gm/cm^2$ as suggested by Peters (1958) for protons of energy ~400 MeV was used. The energy lost per $cm^3$ through nuclear collisions was assumed to be deposited locally and was added to that lost through ionization at a rate of 35 eV per ion pair.

The PROTON deposition code was also modified so that it would calculate the proton current across a horizontal unit area at any altitude as well as the energy deposited at that altitude. In Figure B.3 is a plot of the proton current density divided by 3.70 x $10^{-12}$ amp.$m^2$ as a function of altitude at 1508 UT August 4, 1972, the most intense period of that SPE. The nominal air-earth current density in the polar cap is 3.70 x $10^{-12}$ amp/$m^2$. It can be seen that the proton current density becomes comparable to the air-earth current at ~30 km and is ~50 times larger than the nominal air-earth current at ~100 km. Also shown in Figure B.3 is the electron current density that was estimated from the measurements made at Chatanika, Alaska. While the proton current density is fairly uniform over the polar cap, the electron current exhibits considerably spatial variation due to auroral activity. Since Chatanika, Alaska is in the auroral zone, the electron current density shown in Figure B.3 is probably an upper limit to the current density in the polar cap.

The ion conductivity, $\sigma_i$, can be calculated from the positive and negative ion concentrations, $N_+$ and $N_-$, and the respective mobilities, $K_+$ and $K_-$, by
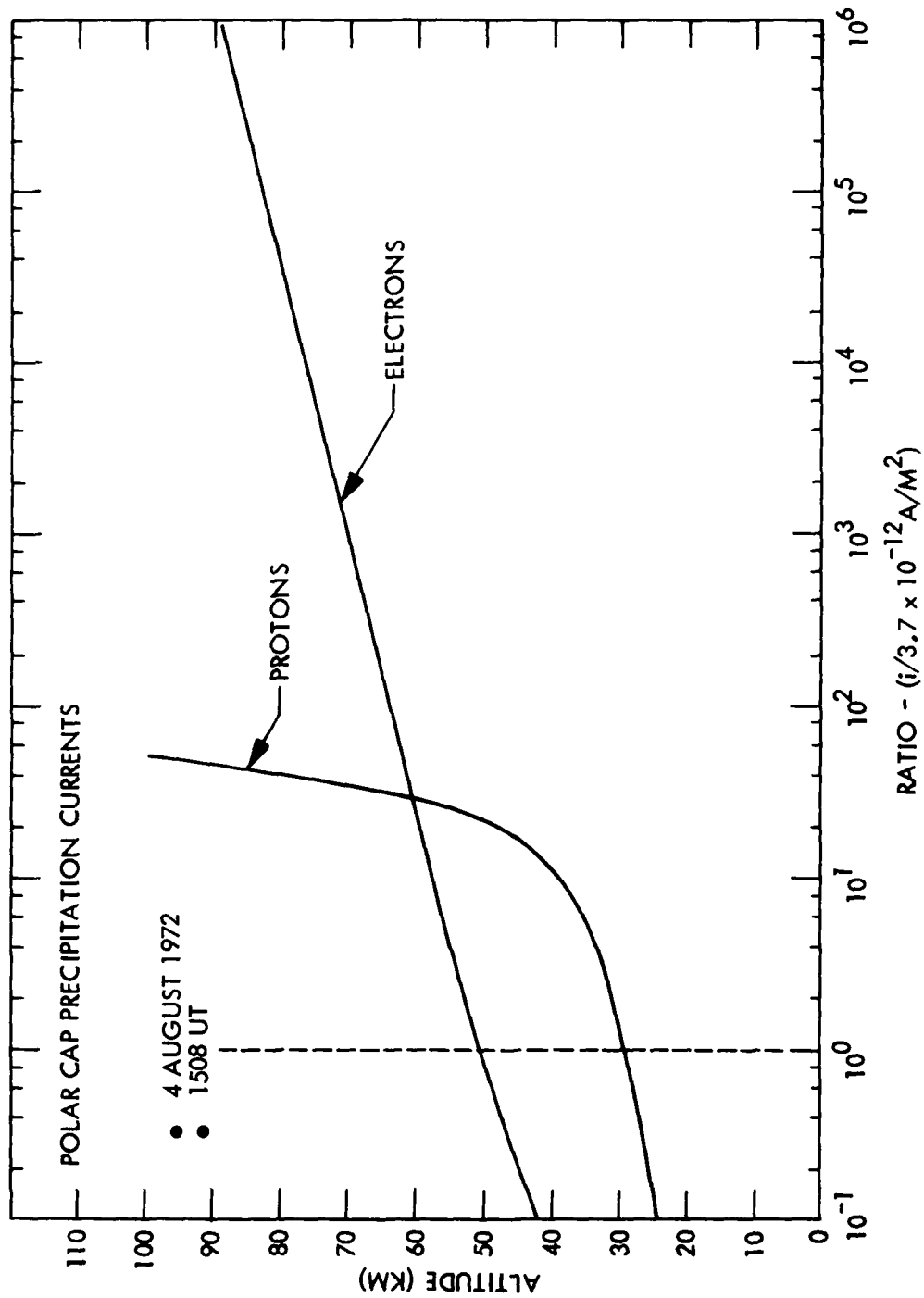
$$\sigma_i = eN_+K_+ + eN_-K_- \tag{4}$$

B-7

Figure B.3  Polar cap currents carried by precipitating solar protons and electrons expressed as the ratio of a typical air-earth current.

In the lower atmosphere, below 50 km, $N_+ \cong N_-$, and $K_+ \cong K_-$ so that

$$\sigma_i = 2eNK \tag{5}$$

When the ion production rates, Q, are known, N is given in terms of the production rates and the ion-ion recombination coefficient, $\alpha_{i,i}$, by

$$N = (Q/\alpha_{i,i})^{1/2} \tag{6}$$

Hence

$$\sigma_i = 2eK(Q/\alpha_{i,i})^{1/2} \tag{7}$$

In Figure B.4 is shown the calculated ion conductivity in the polar cap for quiet periods for 1972. The production rates were assumed to be due to cosmic rays for that period of the solar cycle. Conductivities for three different values of the mobilities corresponding to ions masses of 100, 200, and 1000 AMU are shown. Also shown are conductivity measurements by Kraakevik (1961) for altitudes from 0 to 6 km and by Tanaka et al. (1977) from 20 to 35 km. the derived conductivities of Tanaka et al. were obtained from measurements of the air-earth current and electric fields in the polar caps, with $\sigma = i_{AE}/E$. The conductivity measurements of Kraakevik were made over Greenland in 1954. This is approximately the same relative period in the solar cycle as the August 1972 SPE. The measurements by Tanaka et al. were made over the South Pole in November - December 1972.
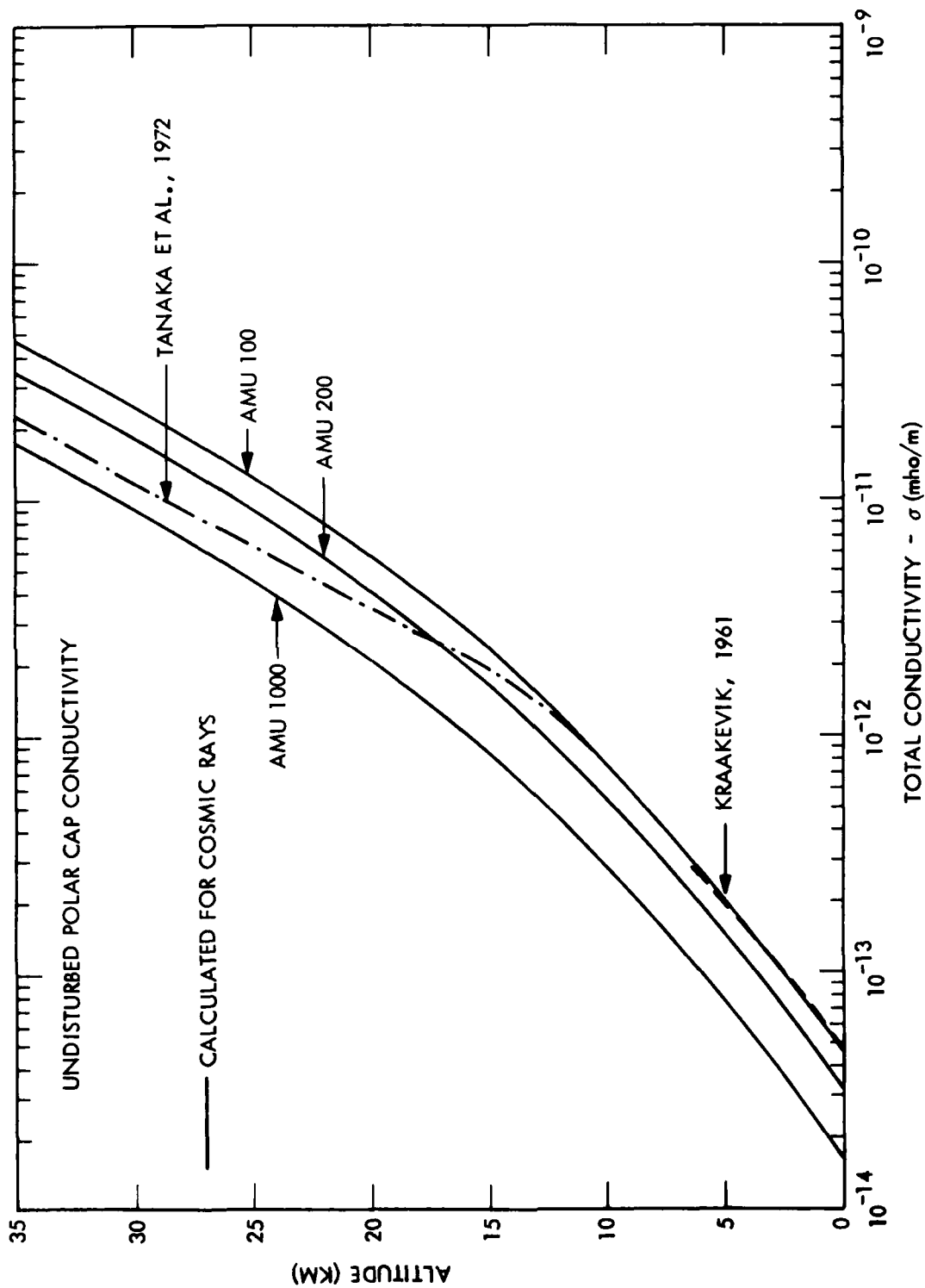
Figure B.4  Calculated undisturbed polar cap conductivities due to cosmic rays for ions having atomic masses of 100, 200 and 1000.  Measured conductivities at high latitudes are also shown.

LOCKHEED PALO ALTO RESEARCH LABORATORY

LOCKHEED  MISSILES  &  SPACE  COMPANY,  INC

It can be seen in Figure B.4 that the conductivities derived from the measurements of Kraakevik fit the calculated conductivity curve for an ion mass of 100 AMU while the measurements of Tanaka et al. fall between the curves for a mass of 200 and 1000 AMU. As discussed by Meyerott, Reagan, and Joiner (1980) the low value of the conductivity at ~30 km may be due either to ion densities at this altitude which are lower than that predicted by the theory or because the masses of the ions at this altitude are greater than 200 AMU.

The quiet time ionic conductivity, $\sigma_{i,u}$, for August 1972 was taken to be the curve shown in Figure B.4 which fits the conductivities derived from the measurements of Kraakevik from 0 to 6 km and those derived from the measurements ot Tanaka et al. at ~30 km. The ionic conductivity disturbed period 1508 UT August 4, $\sigma_{i,d}$, was obtained from the undisturbed ionic conductivity by

$$\sigma_{i,d} = \sigma_{i,u}(Q_d/Q_u)^{1/2} \tag{8}$$

This approach assumes that the mobilities and the recombination coefficients during the disturbance are the same as those during the undisturbed times. The disturbed ion production rates, $Q_d$, were taken to be the sum of the production rates by galactic cosmic rays, $Q_{d,CR}$, and the production rates, $Q_{SPE}$, calculated from the measured proton spectrum from the modified PROTON code as described previously.

$$Q_d = Q_{d,CR} + Q_{SPE} \tag{9}$$

B-11

As can be seen from the neutron monitor data shown in Figure 1 the magnitude of the Forbush decrease during the peak of the event was 8%; hence, $Q_{dCR}$, is given from the undisturbed cosmic ray production rates, $Q_{u,CR}$, by

$$Q_{d,CR} = 0.92 \ Q_{u,CR} \tag{10}$$

In Figure B.5 is shown the conductivity in the polar cap for altitudes up to 35 km for the disturbed period 1508 UT 4 August 1972 and for the undisturbed periods of 1972. Figure B.6 shows the conductivities extended from 35 km to 90 km. It can be seen that the disturbed conductivity is slightly smaller than the undisturbed below ~12km and is much larger than the disturbed for altitudes above 20 km.

The electric field for the disturbed and undisturbed periods can be calculated from Equation (3). For the disturbed period, Equation (3) becomes

$$E(H) = J_{AE}/\sigma_{i,d} - J_p/\sigma_{i,d} + J_e/\sigma_{i,d} \tag{11}$$

In Figure B.7 the vertical electric field for the disturbed and undisturbed case is shown as a function of altitude. It can be seen that the disturbed electric field becomes negative from ~30 km to ~55 km. This is due to the fact that, as is shown in Figure B.3 , the proton current is larger than the air-earth current for altitudes above ~30 km. At ~55 km the electron precipitation current exceeds the proton current and hence the electric field becomes positive above that altitude. Electric field measurements have been
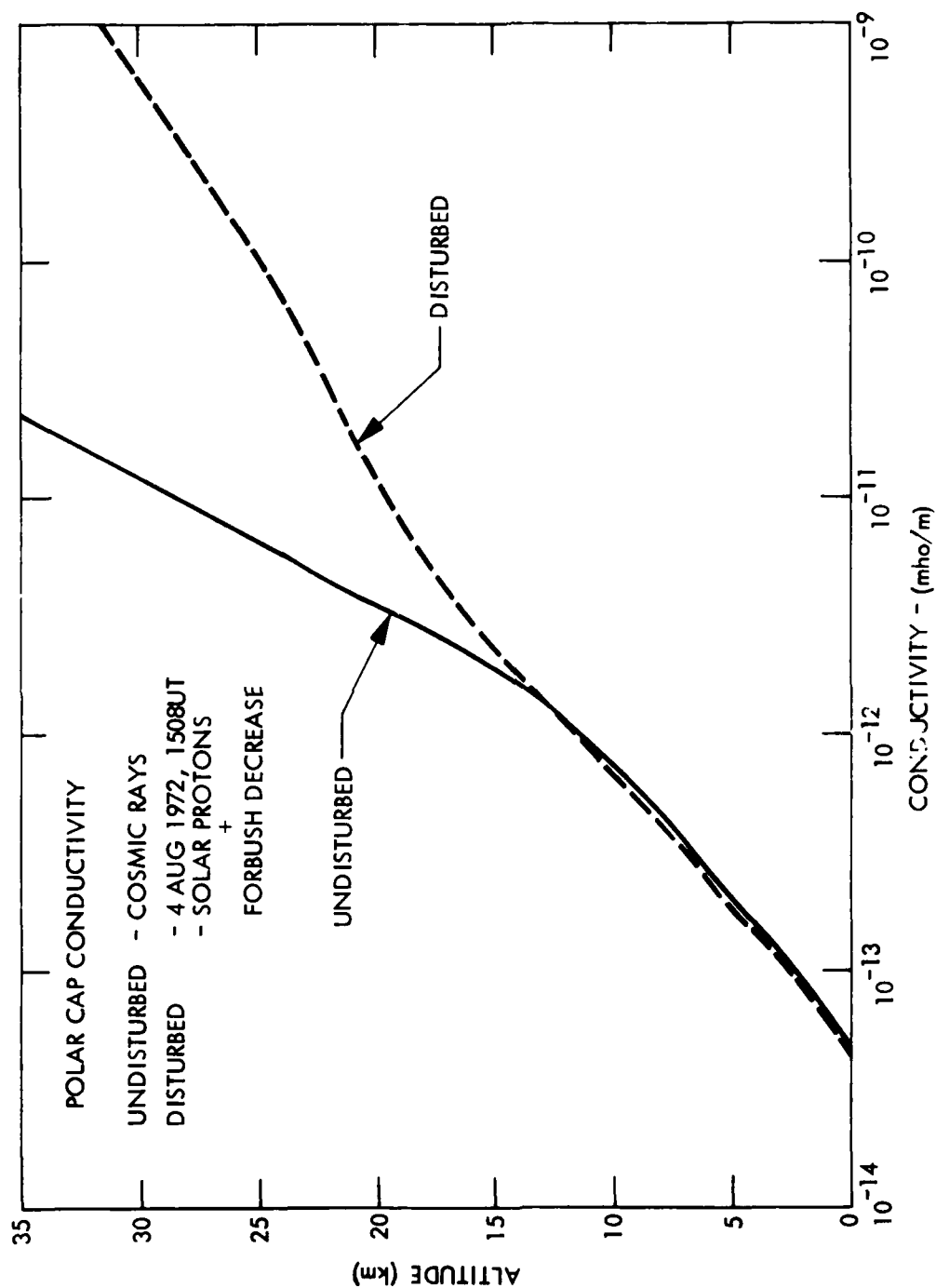
Figure B.5   Calculated conductivity profile during the peak of the SPE as compared to the undisturbed case.

Figure B.6  Calculated undisturbed and SPE disturbed conductivities on 4 August 1972 at Chatanika, Alaska at 0508 local time (1508 UT) during the main peak of the event.

LOCKHEED PALO ALTO RESEARCH LABORATORY

LOCKHEED   MISSILES   &   SPACE   COMPANY.   INC

Figure B.7   Calculated vertical electric field profiles in the polar cap during undisturbed times and at the peak of the August 1972 SPE.

made at 30 km by Holzworth and Mozer (1979) during the 5 August 1972 SPE.
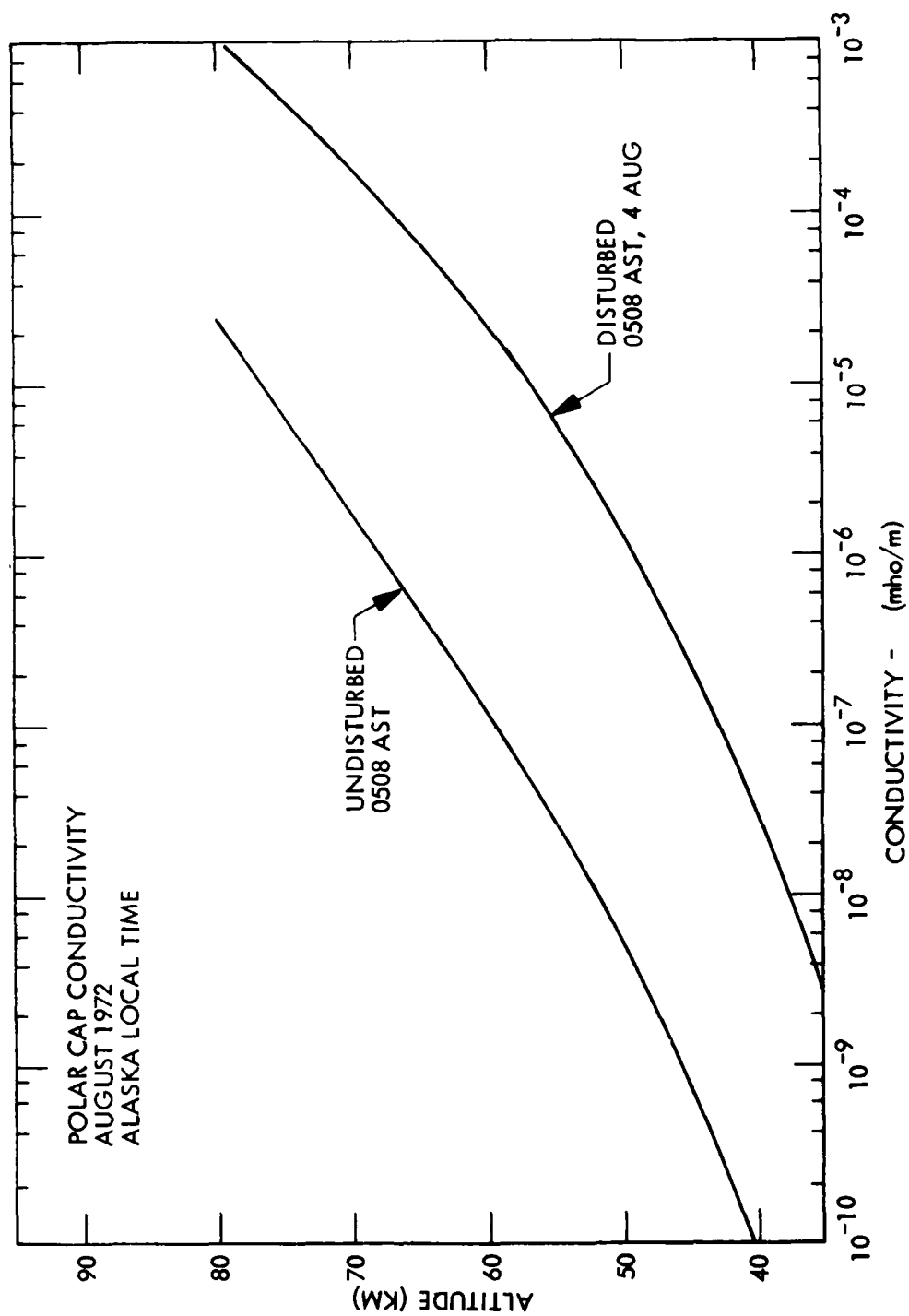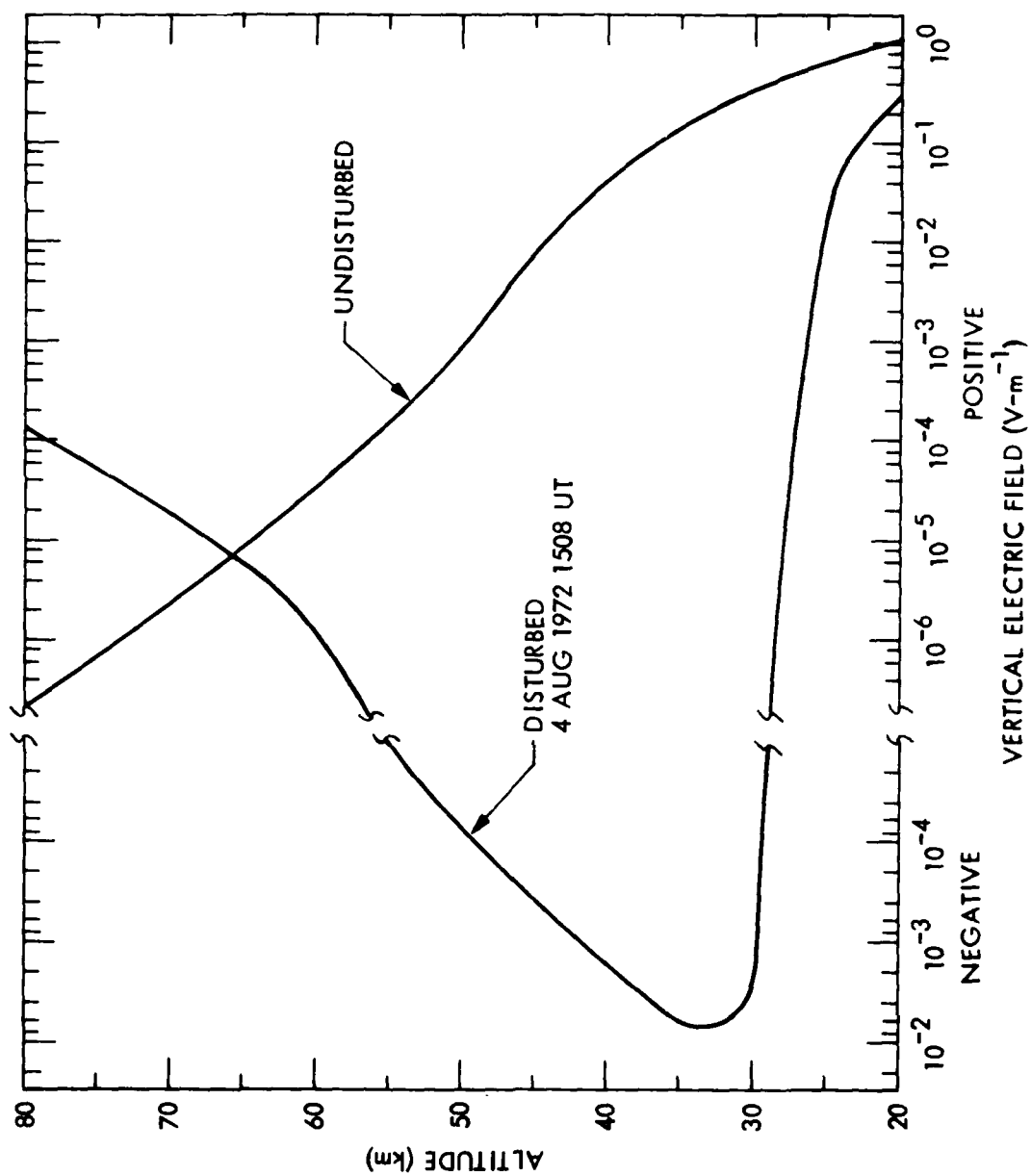They measured a very small electric field at 30 km. Considering the error in
their measurements it is not possible to tell whether the field was positive
or negative.

The implications of the change in conductivities and the large precipi-
tation currents in the polar cap on the potential of the ionosphere can be
inferred by calculating the ionospheric potential inside the polar cap and
just outside the polar cap assuming the same air-earth current at both loca-
tions. Inside the polar cap the electric field is the disturbed field shown
in Figure B.7 . Outside the polar cap the conductivities are the undisturbed
conductivities reduced by the Forbush decrease of ~0.4%. In Figure B.8 is
shown the difference in potential at 1508 UT as a function of altitude between
positions inside ($V_i$) and outside ($V_o$) the polar caps, for an air-earth cur-
rent density of $3.70 \times 10^{-12}$ amp/m$^2$. Since the conductivity both inside and
outside the polar cap is changed by the same amount up to ~10 km due to the
Forbush decrease, the potential up to this altitude remains the same at the
two positions. At 30 km, however, the atmospheric potential at the two loca-
tions differs by almost 10 kilovolts due to the presence of the solar particle
currents and the enhanced conductivities in the polar caps but not outside the
polar caps.

A paper entitled "The Effects of Energetic-Particle Precipitation on the
Global Atmospheric Electric Circuit" based on the work in this report was
presented at the VIth International Conference on Atmospheric Electricity held
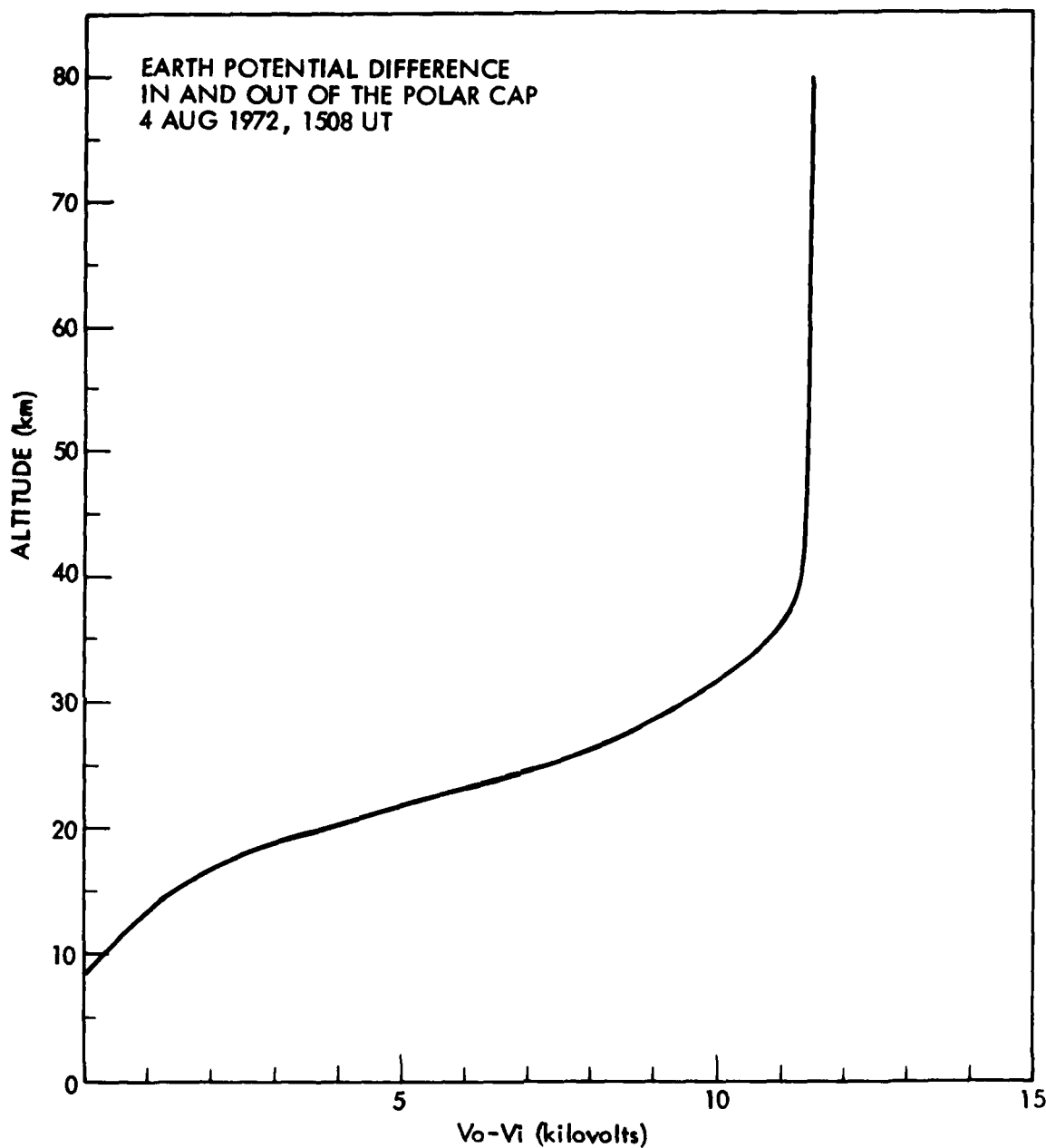in Manchester, England, 28 July to 1 August, 1980.

Figure B.8  Difference in the earth's potential at 1508 UT, 4 August
1972 as a function of altitude between positions inside ($V_i$)
and outside ($V_o$) the polar caps.

**LOCKHEED PALO ALTO RESEARCH LABORATORY**
LOCKHEED   MISSILES   &   SPACE   COMPANY,   INC.

## REFERENCES

Arijs, E., J. Ingels, and D. Nevejans, Mass spectrometric measurements of the positive ion composition of the stratosphere, Nature, 271, 642-644, 1978.

Arnold, F., D. Krankowsky, and K. H. Marien, First mass spectrometric measurements of positive ions in the stratosphere, Nature, 267, 30-32, 1977.

Arnold, F., and G. Henschen, First mass analysis of stratospheric negative ions, Nature, 275, 521-522, 1978.

Bannister, P. R., F. J. Williams, J. R. Katan, and R. J. Ingram, Results of far field measurements made in Connecticut from June 1970 to May 1973, NUSC Technical Report 4617, 1973.

Bannister, P. R., Far field extremely low frequency (ELF) rpopagation measurements, IEEE Transactions on Communication, Vol.COM-22, 468-474, (1974).

Bannister, P. R., and F. J. Williams, NUSC Technical Report 4719, Naval Underwater Systems Center, New London Laboratory, 1974.

Bannister, P. R., F. J. Williams, A. L. Dahlvig, and W. A. Kraimer, Wisconsin Test Facility transmitting antenna pattern and steering measurements, IEEE Trans. Comm., Comm-22, 412, 1974.

Barr, R., The effect of sporadic-E on the nocturnal propagation of ELF radio waves, J. Atmos. Terres. Phys., 39, 1379, 1977.

Booker, H. G., The ionosphere as the secondary conductor of a transformer for ELF, Radio Science, 8, 757, 1973.

Booker, H. G., and F. Lefeuvre, The relation between ionospheric profiles and ELF propagation in the earth-ionosphere transmission line, J. Atmos. Terres. Phys., 39, 1277, 1977.

Booker, H. G., A simplified theory of ELF propagation in the earth-ionosphere transmission line and its worldwide application, ONR Report N00014-78-C-0682-0001, UCSD, La Jolla, California, 31 March 1980.

Budden, K. G., Radio waves in the ionosphere, Cambridge University Press, 1961.

Budden, K.G., and G. J. Daniell, Rays in magnetoionic theory, J. Atmos. Terres. Phys., 27, 3, 395-415, March 1965.

Davis, J. R., ELF propagation irregularities on northern and mid-latitude paths, in ELF-VLF Radio Wave Propagation, J. Holtet, ed., D. Reidel Publ. Company, Dordrecht-Holland, 263-277, 1974.

Davis, J. R., and W. O. Meyers, NRL Report 7924, Naval Research Laboratory, Washington, D.C., 1975.

Davis, J. R., Localized nighttime D-region disturbances and ELF propagation, J. Atmos. Terres. Phys., 38, 1309, 1976.

De Gregorio, J. F., J. W. Finney, K. Kildahl, and E. K. Smith, Recent sporadic-E experimental work in the United States, in Ionospheric Sporadic E, Vol. II, Pergamon Press Ltd., Oxford-London, New York, 1962.

Field, E. C., Measurement of ELf propagation and ionospheric parameters during polar-cap-absorption events (PCA), PSR Note 201, Pacific Sierra Research Corporation, Santa Monica, California, April 1978.

Field, E. C., and R. G. Joiner, An integral-equation approach to long-wave propagation in a nonstratified earth-ionosphere waveguide, Radio Science, 14, 1057, 1979.

Field, E. C., S. J. Gayer, and B. P. D'Ambrosio, ELF propagation in the presence of nonstratified ionospheric disturbances, PSR Report 1013, Pacific Sierra Research Corporation, Santa Monica, California, June 1980.

Fukuyama, K., and W. Kofman, Incoherent scattering of an electromagnetic wave in the mesosphere: a theoretical consideration, Solar Terrestrial Environment Research (Japan), 3, 1979.

Fulks, G. J., Solar modulation of galactic cosmic ray electrons, protons, and alphas, J. Geophys. Res., 80, 1701, 1975.

Greifinger, C., and P. Greifinger, Approximate method for determining ELF eigen values in the earth-ionosphere waveguide, Radio Science, 13, 831, 1978.

Greifinger, C., and P. Greifinger, On the ionospheric parameters which govern high-latitude ELF propagation in the earth-ionosphere waveguide, Radio Science, 14, 889, 1979.

Gunton, R. C., R. E. Meyerott, and J. B. Reagan, Ion and neutral chemistry of the D-region during the intense solar particle event of August 1972, Final Report LSMC-D556351, Lockheed Palo Alto Research Laboratory, January 1977.

Heaps, M. G., Parametrization of the cosmic ray ion-pair production rate above 18 km, Planet. Space Sci., 26, 513, 1978.

Holzworth, R. J., and F. S. Mozer, Direct evidence of solar flare modification of stratospheric electric fields, J. Geophys. Res., 84, 363, 1979.

Hoppel, W. A., and J. H. Kraakevik, The mobility of tropospheric ions above the exchange layer, J. Atmos. Sci., 22, 509-517, 1965.

Hoppel, W. A., Measurement of the mobility distribution of tropospheric ions, Rev. Pure Appl. Geophys., 81, 230-245, 1970.

Imhof, W. L., T. R. Larsen, J. B. Reagan, and E. E. Gaines, Analysis of satellite data on precipitating particles in coordination with ELF propagation anomalies, LMSC-D502063, Lockheed Palo Alto Research Laboratory, Palo Alto, California, 30 April 1976.

Imhof, W. L., T. R. Larsen, J. B. Reagan, and E. E. Gaines, Analysis of satellite data on precipitating particles in coordination with ELF propagation anomalies, LMSC-D560323, Lockheed Palo Alto Research Laboratory, Palo Alto, California, 30 June 1977.

Imhof, W. L., T. R. Larsen, E. E. Gaines, J. B. Reagan, R. C. Gunton, and R. E. Meyerott, Analysis of satellite data of precipitating particles in coordination with ELF propagation anomalies, LMSC-D633266, Lockheed Palo Alto Research Laboratory, Palo Alto, California, 30 November 1978.

Imhof, W. L., R. C. Gunton, T. R Larsen, E. E. Gaines, J. B. Reagan, and R. E. Meyerott, Study of ELF propagation anomalies as related to improved knowledge of electron density profiles produced by energetic particle precipitation, LMSC-D681778, Lockheed Palo Alto Research Laboraotry, 30 January 1980.

Jones, E. S. O., and R.C. Saksena, Synoptic studies of the high-latitude types of sporadic-E, Ann. Geophys., 35, 53, 1979.

Keefer, J. A., Ambient electron density profiles from high altitude nuclear effects chemistry codes, Report DNA 3520T, Mission Research Corporation, Santa Barbara, California, 14 February 1975.

Kilpatric, W. D., An experimental mass-mobility relation for ions in air at atmospheric pressure, Proc. Ann. Conf. Mass Spectrosc. 19th, 3290325M 1971.

Kraakevik, J. H., Measurements of current density in the fair weather Atmosphere, J. Geophys. Res., 66, 3735, 1961.

Larsen, T. R., Preliminary discussion of ELF/VLF propagation data, in ELF-VLF Radio Wave Propagation, 263-77, J. Holtet, ed., D. Reidel Publishing Company, Dordrecht-Holland, 1974.

Larsen, T. R., Effects of D-region ionization on radio wave propagation, Solar-Terrestrial Predictions Proceedings, Vol II. Working group reports and reviews, U. S. Department of Commerce, NOAA/ERL, U. S. Government Printing Office, Washington, D.C. 20402, 1979.

Lockwood, J. A., L. Hsieh, and J. J. Quenby, Some unusual features of the cosmic ray storm in August 1972, J. Geophys. Res., 80, 1725, 1975.

Maeda, K., E region electron density profiles, Space Res., 12, 1229, 1972.

Matthews, J. D., The effect of negative ions on collision-dominated Thomsom scattering, J. Geophys. Res., 83, 505, 1978.

Mechtly, E. A., S. A. Bowhill, and L. G. Smith, Change of lower ionosphere electron concentrations with solar activity, J. Atmos. Terres. Phys., 34, 1899, 1972.

Meyerott, R. E., J. B. Reagan, and R. G. Joiner, The mobility and concentration of ions and the ionic conductivity in the lower stratosphere, J. Geophys. Res., 85, 1273, 1980.

Mitra, A. P., and D. K. Chakrabarty, Models of lower ionosphere electron density profiles, Space Res., 11, 1013, 1971.

Mohnen, V. A., J. J. Del Santo, and J. A. Kadlecek, Nature, mobility and physico-chemical reactivity of ions in the lower atmosphere (less than 40 km), VI International Conference on Atmospheric Electricity, Abstracts, Manchester, England, Session I, Paper 10, 1980.

Moler, W. Letter to DNA, 28 April 1978.

Neher, H. V., Cosmic rays at high latitudes and altitudes covering four solar maxima, J. Geophys. Res., 76, 1637, 1971.

Niles, F. E., Chemistry of atmospheric deionization outside intermediate altitude fireballs, II. 15, 20, and 25 km altitude, BRL Report 1909, Ballistic Research Laboratory, Aberdeen Maryland, August 1976.

Pappert, R. A., Effects of elevation and ground conductivity on horizontal dipole excitation of the earth-ionosphere waveguide, Radio Science, 5, 579-590, March 1970.

Pappert, R. A., and W. F. Moler, Propagation theory and calculations at lower (ELF) extremely low frequencies, IEEE Trans. Comm., COM-22, 4, 438-451, April 1974.

Pappert, R. A., and L. R. Shockey, Ionospheric reflection and absorption properties of normal modes at ELF, Interim Report No. 772, Naval Ocean Systems Center, 15 September 1977.

Pappert, R. A., and W. F. Moler, A theoretical study of ELF normal mode reflection and absorption produced by nighttime ionospheres, J. Atmos. Teres. Phys., 40, 1031, 1978.

Pappert, R. A., Effects of a large patch of sporadic-E on nighttime propagation at lower ELF, J. Atmos. Terres. Phys., 42, 417, 1980.

Peters, B., Cosmic rays, in Handbook of Physics, E. U. Condon and H. Odishaw, eds., McGraw-Hill, New York, 1958.

Pomerantz, M. A., and S. P. Duggal, Remarkable cosmic ray storm and associated solar particle events of August 1972, World Data Center A Report UAG-28, Part II, 430, 1973.

Reagan, J. B., and T. M. Watt, Simultaneous satellite and radar studies of the D-region ionosphere during the intense solar particle events of August 1972, J. Geophys. Res., 81, 4579, 1976.

Reagan, J. B., W. L. Imhof, E. E. Gaines, T. R. Larsen, J. R. Davis, and W. R. Moler, Effects of precipitating energetic particles on an ELF communication link, paper presented at the Symposium on the Effect of the Ionosphere on Space and Terrestrial Systems, sponsored by the Naval Research Laboratory and the Office of Naval Research, Arlington, Virginia, January 1978.

Reagan, J. B., R. E. Meyerott, R. W. Nightingale, R. C. Gunton, R. G. Johnson, J. E. Evans, W. L. Imhof, D. F. Heath, and A. J. Krueger, Effects of the August 1972 solar particle events on stratospheric ozone, J. Geophys. Res., 86, 1473, 1981.

Reid, G. C., A study of the enhanced ionization produced by solar protons during a polar cap absorption event, J. Geophys. Res., 66, 4071, 1961.

Riekert, H., Untersuchungen zur beweglichkeit der kleinionen in der freien atmosphare, Dissertation Eberhard-Karls-Universitat, Tubingen, 1971.

Sheddy, C. H., A general analytic solution for reflection from a sharply bounded anisotropic ionosphere, Radio Science, 3, 792-795, August 1968.

Smith, E. K., Worldwide occurrence of sporadic E, National Bureau of Standards Circular 582, 15 March 1957.

Smith, L. G., and K. Miller, Sporadic-E layers and unstable wind shear, J. Atmos. Terres. Phys., 42, 45, 1980.

Smith, D., and M. J. Church, Ion-ion recombination rates in the earth's atmosphere, Planet. Space Sci., 25, 433, 1977.

Swider, W., R. S. Narcisi, T. J. Keneshea, and J. C. Ulwick, Electron loss during a nighttime PCA event, J. Geophys. Res., 76, 4691, 1971.

Swider, W., Composite PCA '69 Study: Final report, AFCRL-TR-75-0149, Air Force Cambridge Research Laboratory, Bedford, Massachusetts, March 1975.

Swider, W., T. J. Keneshea, and C. I. Foley, An SPE-disturbed D-region model, Planet. Space Sci., 26, 883, 1978.

Tanaka, T., T. Ogawa, and M. Kodama, Stratospheric electric fields and currents measured at Syowa Station, Antarctica-1. The vertical component, J. Atmos. Terres. Phys., 39, 523, 1977.

Ulwick, J. C., Comparison of black brant rocket measurements of charged particle densities during solar particle events, in the Proceedings of the COSPAR Symposium on the Solar Particle Event of November 1969, AFCRL-72-0474, Air Force Cambridge Research Laboratories, Bedford, Massachusetts, p. 395, August 1972.

Watt, T. M., Effective recombination coefficient of the polar D-region under conditions of intense ionizing radiation, DNA 3663T, Stanford Research Institute, Menlo Park, California, July 1975.

Whitehead, J. D., Production and prediction of sporadic E, Rev. Geophys. Space Phys., 8, 65, 1970.

Whitten, R. C., I. G. Popoff, R. S. Edmonds, and W. W. Berning, Effective recombination coefficients in the lower atmosphere, J. Geophys. Res., 70, 1737, 1965.

York, T. M., Measurement of electron densities in the middle atmosphere using rocket borne blunt probes, Report ASL-CR-79-0100-5, U.S. Army Electronics Research and Development Command, Atmospheric Sciences Laboratory, White Sands Missile Range, New Mexico, October 1979.

York, T. M., Comparison of electron densities in the middle atmosphere indicated by rocket borne probing techniques, Report PSU-IRL-IR-69, Ionosphere Research Laboratory, Pennsylvania State University, University Park, Pennsylvania, January 1980.

DISTRIBUTION LIST


Department of Defense

Director
Defense Advanced Research Projects Agency
1400 Wilson Boulevard
Arlington, Virginia  22209

   1 cy   ATTN:  TIO
   1 cy   ATTN:  STO
   1 cy   ATTN:  NRMO

Director
Defense Communications Agency
8th Street and South Courthouse Road
Arlington, Virginia  22204

   3 cys  ATTN:  MEECN Office

Defense Technical Information Center
Cameron Station
Alexandria, Virginia  22314

  12 cys  ATTN:  TC

Director
Defense Nuclear Agency
Washington, D.C.  20305

   1 cy   ATTN:  STTL
   1 cy   ATTN:  DDST
   3 cys  ATTN:  RAAE
   1 cy   ATTN:  RAEV

Joint Chiefs of Staff
Department of Defense
Washington, D.C.  20301

   1 cy   ATTN:  J-6

Director
National Security Agency
Fort George G. Meade, Maryland  20755

   2 cys  ATTN:  Technical Library

-1-

Under Secretary of Defense (Research and Engineering)
Department of Defense
Washington, D.C.  20301

   2 cys  ATTN:  DDS&SS


Department of Commerce

U. S. Department of Commerce
Office of Telecommunications
Institute for Telecommunication Sciences
National Telecommunications and Information
 Administration
Boulder, Colorado  80303

   2 cys  ATTN:  W. F. Utlaut


Department of the Army

Commander/Director
Atmospheric Sciences Laboratory
U. S. Army Electronics Command
White Sands Missile Range, New Mexico  88002

   1 cy   ATTN:  DRSEL-BL-SY-S
                 F. E. Niles

Director
U. S. Army Ballistic Research Laboratories
Aberdeen Proving Grounds, Maryland  21005

   1 cy   ATTN:  George E. Keller

Commander
U. S. Army Foreign Sciences and Technology Center
220 7th Street, N.E.
Charlottesville, Virginia  22901

   1 cy   ATTN:  Robert Jones


Department of the Navy

Chief of Naval Operations
Department of the Navy
Washington, D.C.  20350

   1 cy   ATTN:  NOP 985
   1 cy   ATTN:  NOP 094H

2

Chief of Naval Research
Department of the Navy
800 North Quincy Street
Arlington, Virginia  22217

    1 cy   ATTN:  Code 465, R. G. Joiner
    1 cy   ATTN:  Code 427, H. Mullaney

Commander
Naval Electronic Systems Command
Department of the Navy
Washington, D.C.  20360

    1 cy   ATTN:  PME-117
    1 cy   ATTN:  PME-117T
    1 cy   ATTN:  PME 117-21
    1 cy   ATTN:  PME 117-21A
    1 cy   ATTN:  PME 117-22

Director
Naval Ocean Systems Center
Electromagnetic Propagation Division
271 Catalina Boulevard
San Diego, California  92152

    1 cy   ATTN:  Code 2200, W. F. Moler
    1 cy   ATTN:  Code 2200, John Bickel

Director
Naval Research Laboratory
4555 Overlook Avenue, S.W.
Washington, D.C.  20375

    1 cy   ATTN:  Code 7700, Timothy P. Coffey
    1 cy   ATTN:  Code 7709, Wahab Ali
    2 cys  ATTN:  Code 7750, John Davis
    1 cy   ATTN:  Code 2627

Commander
Naval Surface Weapons Center (White Oak)
Silver Spring, Maryland  20910

    1 cy   ATTN:  Technical Library

Office of Naval Research , Western Regional Office
1030 East Green Street
Pasadena, California  91106

    1 cy

LMSC-D767238

Department of the Air Force

Commander
Air Force Geophysics Laboratory, AFSC
L. G. Hanscom Air Force Base, Massachusetts 01731

  1 cy   ATTN:  OPR,
  1 cy   ATTN:  LKB, W. Swider
  1 cy   ATTN:  LKB, K. Champion

Director
Air Force Technical Applications Center
Patrick Air Force Base, Florida 32920

  1 cy   ATTN:  TD
  1 cy   ATTN:  HQ 1035th TCHOG/TFS


Department of Defense Contractors

General Electric Company
TEMPO - Center for Advanced Studies
816 State Street
Santa Barbara, California 93102

  1 cy   ATTN:  Warren S. Knapp
  1 cy   ATTN:  DASIAC

Lockheed Missiles and Space Company
3251 Hanover Street
Palo Alto, California 94304

  1 cy   ATTN:  J. B. Reagan
  1 cy   ATTN:  W. Imhof
  1 cy   ATTN:  Martin Walt

Mission Research Corporation
735 State Street
Santa Barbara, California 93101

  1 cy   ATTN:  M. Scheibe
  1 cy   ATTN:  D. Sowle

Pacific-Sierra Research Corporation
1456 Cloverfield Boulevard
Santa Monica, California 90404

  1 cy   ATTN:  E. C. Field

Pennsylvania State University
Ionospheric Research Laboratory
College of Engineering
318 Electrical Engineering - East Wing
University Park, Pennsylvania  16802

    1 cy   ATTN:  John S. Nisbet
    1 cy   ATTN:  Les Hale
    1 cy   ATTN:  A. J. Ferraro
    1 cy   ATTN:  H. S. Lee

R&D Associates
4640 Admiralty Way
Marina Del Rey, California  90291

    1 cy   ATTN:  R. Lelevier
    1 cy   ATTN:  F. Gilmore
    1 cy   ATTN:  R. Turco

The Rand Corporation
1700 Main Street
Santa Monica, California  90406

    1 cy   ATTN:  Cullen Crain

Professor Chalmers F. Sechrist
155 Electrical Engineering Building
University of Illinois
Urbana, Illinois  61801

    1 cy   ATTN:  C. Sechrist

Stanford Research Institute
333 Ravenswood Avenue
Menlo Park, California  94025

    1 cy   ATTN:  Allen M. Peterson
    1 cy   ATTN:  Ray L. Leadabrand

Stanford Electronics Laboratory
Stanford  University
Stanford, California 94305

    1 cy   ATTN:  A. Fraser-Smith

Radioscience Laboratory
Department of Electrical Engineering
Stanford University
Stanford, California

    1 cy   ATTN:  R. Helliwell